

GLUTAMATE-ACTIVATED CURRENTS IN UNIPOLAR BRUSH CELLS

By

Carolina Borges-Merjane

A DISSERTATION

Presented to the Neuroscience Graduate Program

and the Oregon Health and Science University

School of Medicine

in partial fulfillment of the requirements for the degree of

Doctor of Philosophy

March 2015

School of Medicine
Oregon Health & Science University

CERTIFICATE OF APPROVAL

This is to certify that the Ph.D. dissertation of
CAROLINA BORGES-MERJANE
has been approved on March 6, 2015

Advisor, Laurence Trussell, Ph.D.

Member and Chair, Craig Jahr, M.D.

Member, Stephen David, Ph.D.

Member, Stephen Smith, Ph.D.

Member, Henrique vonGersdorff, Ph.D.

TABLE OF CONTENTS

ACKNOWLEDGEMENTS.....	iii
ABSTRACT.....	iv
LIST OF FIGURES.....	vi
INTRODUCTION.....	1
CHAPTER 1. ON AND OFF UNIPOLAR BRUSH CELLS TRANSFORM MULTISENSORY INPUTS TO THE AUDITORY SYSTEM.....	19
Abstract.....	20
Introduction.....	21
Methods.....	23
Results.....	30
<i>Identification of DCN UBCs.....</i>	30
<i>UBC populations defined by response to synaptic input.....</i>	30
<i>Characterization of mossy fiber input to ON and OFF UBCs.....</i>	32
<i>ON UBCs are mGluR1α positive.....</i>	35
<i>ON and OFF UBCs of cerebellum.....</i>	37
<i>mGluR2 mediated outward K⁺ current in ON and OFF UBCs.....</i>	39
<i>Correlation of ON and OFF UBC physiology with known UBC subtypes.....</i>	41
<i>Excitability of ON and OFF UBCs.....</i>	42
Discussion.....	44
Acknowledgements.....	50
CHAPTER 2. MAINTENANCE OF INTRINSIC FIRING IN CEREBELLAR UNIPOLAR BRUSH CELLS BY AMBIENT GLUTAMATE.....	78
Abstract.....	79
Introduction.....	80

Methods.....	82
Results.....	87
<i>Identification of ON and OFF UBCs in cerebellum.....</i>	<i>87</i>
<i>Ambient glutamate desensitize AMPAR-mediated baseline current.....</i>	<i>87</i>
<i>mGluRs also mediate glutamate standing currents in UBCs.....</i>	<i>92</i>
<i>Intrinsic firing of UBCs.....</i>	<i>93</i>
<i>Vesicular glutamate contributes to glutamate-mediated standing current.....</i>	<i>95</i>
Discussion.....	98
Acknowledgements.....	104
SUMMARY AND CONCLUSIONS.....	118
REFERENCES.....	123

ACKNOWLEDGEMENTS

I am grateful to many individuals for their support during this work. Firstly, I thank my advisor Larry Trussell, for his mentorship and guidance. Through many discussions, his encouragement to think deeply about experimental design and execution to address specific questions was essential for all I have learned about neurophysiology. His professional guidance also comprised valuable advice beyond the rig, which has shaped my career as a scientist. He was patient during tough times and supportive during critical parts of my graduate career. I feel privileged to have Larry as a mentor.

I thank my dissertation advisory committee for all their helpful comments and advice regarding this work since the beginning. In particular, I would like to thank Craig Jahr for many discussions about this work with Larry and me.

I thank members of the Trussell Lab with whom I interacted during my time in the lab, for making the day-to-day in lab a great environment to be in. In particular, I am thankful to Kevin Bender, who was an excellent teacher during my first year in the lab.

I owe my deepest gratitude to my parents, Jorge and Telma, and my sister Mariana, for their constant support and encouragement.

I am thankful to have met two of my classmates who become two of my dearest friends, Karen Thiebes and Karen Tonsfeldt. Their friendship was crucial and sharing my pursuit of this work side by side as they pursued their own was one of the most joyful experiences I have had.

Finally, I thank Ben Suter. Over the last year and a half his love, unconditional support and encouragement was very meaningful and makes him a big part of this achievement.

ABSTRACT

Unipolar brush cells (UBCs) are glutamatergic interneurons present in cerebellum-like structures. In mammals, they are found in cerebellum and the dorsal cochlear nucleus (DCN). They receive glutamatergic mossy fiber input on an elaborate brush-like dendrite, and relay multisensory signals to granule cells through a feedforward pathway. The first studies characterizing synaptic properties of cerebellar UBCs revealed a slow-decaying biphasic excitatory post-synaptic current (EPSC) that triggered a long train of postsynaptic action potentials. Thus, UBCs seemed to be amplifying multisensory signals from mossy fibers to their target granule cells.

Immunohistochemical studies revealed two distinct UBC populations: calretinin⁺ UBCs and mGluR1 α ⁺ UBCs. Some of their intrinsic electrophysiological properties were characterized in cerebellum, further supporting a model in which the two different UBC subpopulations may have different function.

In chapter 1, we investigated glutamate sensitivity and synaptic transmission from mossy fibers to UBCs in the DCN. We found that the two UBC subtypes may function as ON and OFF cells with respect to their response to glutamatergic input in a manner reminiscent of retinal bipolar cells, due to dual modes of action of glutamate and differential expression levels of glutamate receptor types in the two subtypes. mGluR1 α positive UBCs had an excitatory (ON) response to glutamate, due to high expression of AMPARs and mGluR1 α , and small GIRK currents elicited by mGluR2 activation. mGluR1 α negative UBCs had an inhibitory (OFF) response to glutamate resulting from small AMPAR-mediated currents and large outward K⁺ currents activated by mGluR2. Thus, UBC subtypes may provide distinct parallel processing of multisensory input to

their target granule cells.

Additionally, UBCs fire spontaneously, and this activity is critical for the ON and OFF responses. Chapter 2 describes a role of glutamate receptors in maintaining intrinsic firing of UBCs in response to a standing current generated by background levels of glutamate. I discovered that this action of glutamate is specific to UBCs as opposed to other cell types. Thus, antagonizing glutamate receptors interferes with the background firing frequency of UBCs. Furthermore, my data suggests that the origin of the glutamate mediating this standing current is vesicular.

LIST OF FIGURES

1.1. UBC localization in the DCN.....	51
1.2. ON and OFF responses of UBCs.....	53
1.3. Characteristics of responses of ON and OFF UBCs to mossy fiber input.....	55
1.4. ON UBCs are mGluR1 α ⁺	57
1.5. Cerebellar UBCs also show either ON or OFF subtypes.....	59
1.6. Synaptic activation of mGluR2 receptors in OFF UBCs.....	61
1.7. Correlation of physiology and UBC subtype with immunohistochemistry.....	64
1.8. Intrinsic firing of ON and OFF UBCs.....	66
1.S1. Morphology of UBCs.....	68
1.S2. Minimal stimulation of presynaptic mossy fiber input to ON and OFF UBCs.....	69
1.S3. ON UBCs relay feedforward excitation to granule cells in DCN.....	71
1.S4. mGluR1 α positive and calretinin positive UBCs colocalize with mGluR2.....	73
1.S5. Correlation of physiology and immunohistochemistry for UBC subtypes.....	75
1.S6 Summary diagram.....	77
2.1. UBC identification in cerebellum.....	105
2.2. Outward current in ON UBCs.....	107
2.3. AMPAR-mediated standing current in ON UBCs.....	108
2.4. AMPAR-mediated standing current in OFF UBCs.....	110
2.5. mGluR mediated standing currents.....	112
2.6. ON and OFF responses are intact in cell-attached recordings.....	114
2.7. Decrease of vesicular glutamate concentration decreases standing current.....	116

INTRODUCTION

Understanding the role that specific neurons plays within neural networks is critical for the understanding of how networks process information. Beyond knowing if excitatory or inhibitory transmission is being relayed, we can ask how neurons *transform* information that impacts how signals are relayed and integrated downstream. Unipolar brush cells (UBCs) are glutamatergic interneurons found in cerebellum-like networks, relaying multisensory input for integration with other sensory signals downstream. An intermediary cell in a feedforward pathway should delay transmission of signals. However, UBCs may offer more than a delayed relay of information. On the time scale of neuroanatomical discovery, UBCs are a relatively new cell type and thus very little is known about their physiology. Although they play a key role in transmission of multisensory input, and likely impact integration of signals, how they process this information is still unknown.

Multisensory input function in the dorsal cochlear nucleus and cerebellum

UBCs are found in cerebellum-like networks, neural circuits that resemble the anatomy and circuit organization of the cerebellum. Mammalian cerebellum-like networks are comprised of the cerebellum and the dorsal cochlear nucleus (DCN), located on the brainstem (Bell *et al.*, 2008; Roberts and Portfors, 2008).

The DCN has been suggested to respond to behaviorally relevant sounds in complex auditory scenes, and localize them in space (Oertel and Young, 2004). However, the DCN is the earliest stage of the auditory pathway in which multisensory input is integrated with auditory input. The diversity of multisensory input sources to the DCN

suggests a more intricate integration of signaling by this auditory structure (Fig. 1) (Oertel and Young, 2004; Roberts and Portfors, 2008).

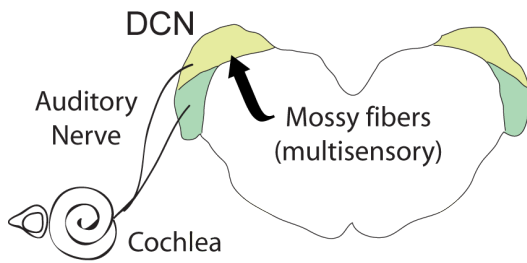


Figure 1: Diagram of a coronal section of brainstem, depicting the cochlear nuclei – ventral in green and dorsal and yellow. The DCN integrates auditory and multisensory input from various other brain regions.

Multisensory fibers projecting to the DCN originate from many regions, and among these are primary and secondary somatic sensory neurons innervating head and neck regions. The secondary sensory nuclei, spinal trigeminal nucleus and dorsal column nuclei, are the main projections ending in mossy fiber

terminals, the main synaptic structure relaying multisensory input to the DCN, while the trigeminal and dorsal root ganglion, the primary sensory nuclei, terminate in small *en passant* boutons. Both primary and secondary sensory inputs are associated with proprioception and light touch or cutaneous sensation (Shore *et al.*, 2000; Shore *et al.*, 2007; Zhou and Shore, 2004; Haenggeli *et al.*, 2005; Itoh *et al.*, 1987; Li and Mizuno, 1997). Additionally, the DCN also receives input from the auditory cortex, inferior colliculus, vestibular nerve root and vestibular nucleus (Oertel and Young, 2004; Burian and Gstoettner, 1988; Bukowska, 2002). Remarkably, trigeminal ganglion stimulation alone, without auditory input, can lead to excitation or inhibition of the principal output neurons of the DCN, fusiform cells. This indicates that multisensory input can modify auditory spike timing depending on the nature or strength of the input stimulus, thus modulating the integration of both input sources by the principal output cells of this nucleus (Koehler *et al.*, 2011; Shore, 2005). Although the DCN has been identified as an important structure for multisensory and auditory input integration, the underlying

cellular mechanisms of multisensory input modulation by this structure is not known. Furthermore, how other modalities of multisensory input are integrated by the DCN is unknown.

In cerebellum, in contrast to the other well-known neuronal types in the circuit, UBCs are not equally distributed across all cerebellar lobes. There are UBCs in regions receiving input from pontine and spinocerebellar nuclei – conveying information from motor and premotor cortices, somatosensory and proprioceptive inputs from spinal cord, as well as visual and auditory information. However, as a general principal, UBCs are primarily concentrated in the vestibulocerebellum of most mammals, although the distribution varies within species, which receives primarily input from vestibular organs and nuclei. (Fig. 2) (Diño *et al.*, 1999). In fact, labeling of single mossy fibers originating in Scarpa’s ganglion of gerbils revealed terminals contacting UBCs in vestibular lobes – the nodulus (X) and the uvula (IX) (Diño *et al.*, 2001), and in cat and rhesus monkey vestibular stimulation induces c-FOS expression in UBCs in the nodulus (Sekerková *et al.*, 2005; Mugnaini *et al.* 2011).

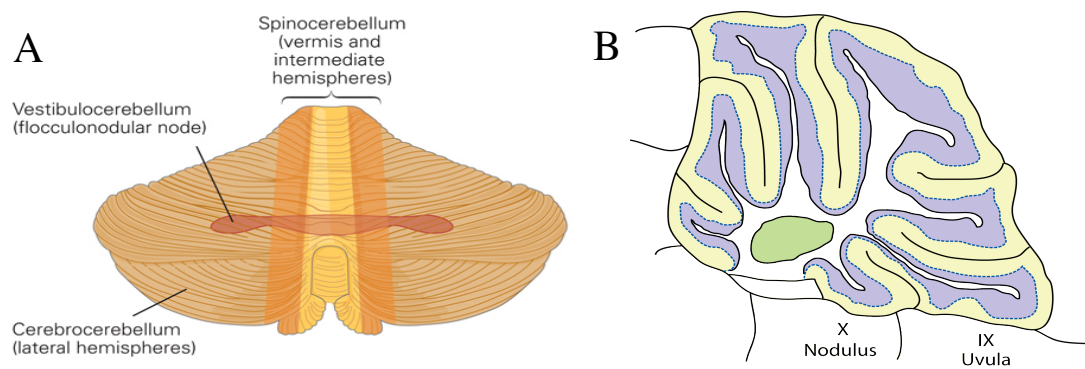


Figure 2. Left panel: Functional regions of the cerebellum (human) (Figure from Kandel *et al.*, 2012). Right panel: diagram of a midline sagittal section of a mouse cerebellum, showing lobes IX (Uvula) and X (Nodulus).

Considering that multisensory input to both DCN and vestibulocerebellum largely comprise sensorimotor processes that modulate body, head and eye position and motion, UBCs likely play an important role in processing this information at very early stages of both auditory and vestibular function. Investigating the physiology of the ultrastructure of UBCs – intrinsically and synaptically – would lead to a better understanding of their function in processing multisensory input to these neural networks.

Anatomy of cerebellum-like networks: dorsal cochlear nucleus and cerebellum

In order to understand UBCs possible function it is necessary to define the UBC microcircuitry. Cerebellum-like networks have two main common features. The first is that they are 3-layered structures, and the second is that their output cells integrate two input modalities (Bell *et al.*, 2008; Roberts and Portfors, 2008), as depicted in Figure 3.

The deep or granule cell layer (L3) receives both input modalities. One of them is multisensory input from various origins, relayed by extrinsic mossy fibers (eMF), which terminate in large presynaptic terminals and contact granule cells (GrC) and UBCs, as well as inhibitory Golgi cells. UBC axons form 2-3 branches, and also terminate in large intrinsic mossy fiber terminals (iMF), contacting granule cells and other UBCs. Granule cell axons then project to the superficial or molecular layer (L1) and form parallel fibers (PF) that contact the apical dendrites of the principal output cells in the cell body layer (L2) – Purkinje cells (PC) in cerebellum and fusiform cells (FC) in DCN. Parallel fibers also contact molecular layer inhibitory interneurons, which also contact the principal cells. The second input modality contacts the principal cells directly. In cerebellum, climbing fiber (CF) relay input from the inferior olivary nucleus, with sensory

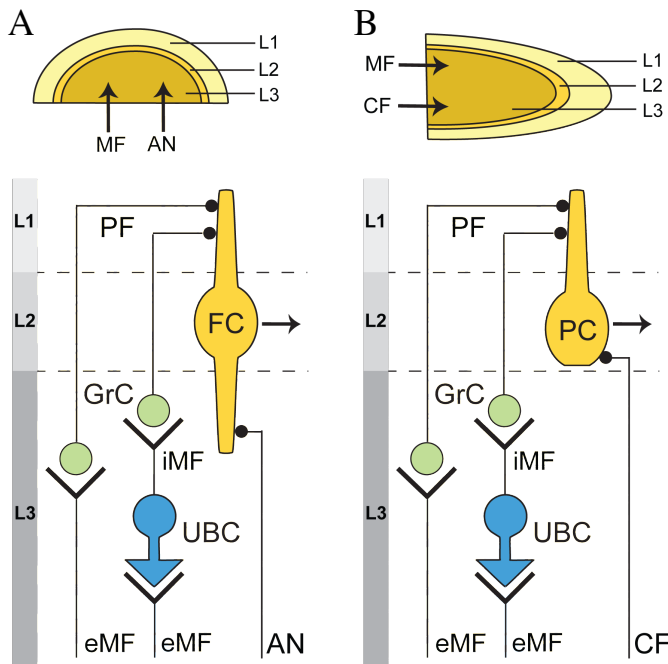


Figure 3. Cerebellum-like circuits. (A) Top panel shows diagram of a coronal section of DCN with layers and inputs. Bottom panel shows simplified DCN circuit. (B) Top panel shows diagram of a sagittal section of a cerebellar lobe. Bottom panel shows simplified cerebellum circuit.

information from the periphery and cortex, depending on the cerebellar lobe. In DCN these are auditory nerve (AN) projections (Oertel and Young, 2004; Ito, 1984).

The electrosensory lateral line lobe in the cerebellum of the mormyrid electric fish is also a cerebellum-like neural circuit that features UBCs, and is often functionally compared to their mammalian counterparts DCN and cerebellum (Bell *et al.*, 2008;

Roberts and Portfors, 2008). This is further discussed later in this session and also in Chapter 1.

Although there are many similarities between cerebellum and DCN, as cerebellum-like circuits, there are a few significant differences. One of them is that the Purkinje cell project outside of the cerebellar lobes, to the deep cerebellar nuclei, and those neurons in turn, project outside of the cerebellum. However in the DCN, the purkinje-like neuron cartwheel cell is actually an interneuron. Cartwheel cells inhibit Fusiform cells which project to the IC. So Fusiform cells, the output cells of the DCN are actually correlated to the deep cerebellar nuclei neurons, rather than to Purkinje cells. A second difference is the contact between climbing fiber-Purkinje cells versus auditory

nerve-Fusiform cell synapses. A Purkinje cell is innervated by a single climbing fiber, while this is not the case for Fusiform cells.

UBC morphology and synapse characterization

The unique morphology of UBCs is critical for synaptic morphology, and thus for synaptic transmission, as described below.



Figure 4: (taken from Diño *et al.*, 2000). Cartoon depicting an UBC dendritic brush being contacted by a mossy fiber terminal.

UBCs are small glutamatergic neurons about 9-12 μm in diameter, with a single short dendrite, that terminates in a brush-like structure with fine dendritic appendages. The dendritic shaft linking the soma to the dendritic brush varies in length and the brush structure also varies in size and can sometimes be as large as the soma (Mugnaini and Floris, 1994; Floris *et al.*, 1994; Rossi *et al.*, 1995). Furthermore, although most neurons in the brain receive at least a few, to several inputs, UBCs belong to a small category of cells that receives only one, and on rare occasions two, glutamatergic input with mossy fiber terminals (Mugnaini and floris, 1994). The calyx of Held is a well-known example of a one-to-one synapse, and as the calyx, UBCs have a very specialized synapse (Mugnaini and Floris, 1994; Berthié and Axelrad, 1994; Rossi *et al.*, 1995; Mugnaini *et al.*, 1997; Nunzi and Mugnaini, 2000; Diño *et al.* 2000).

The dendritic brush interlocks with a presynaptic terminal (Fig 4), forming a large and unique synaptic structure. The synaptic contacts between UBCs and mossy fiber terminals are extensive, with continuous sections of postsynaptic densities, and with large area of synaptic apposition (Fig 5) (Mugnaini *et al.*, 1994; Rossi *et al.*, 1995; Diño and

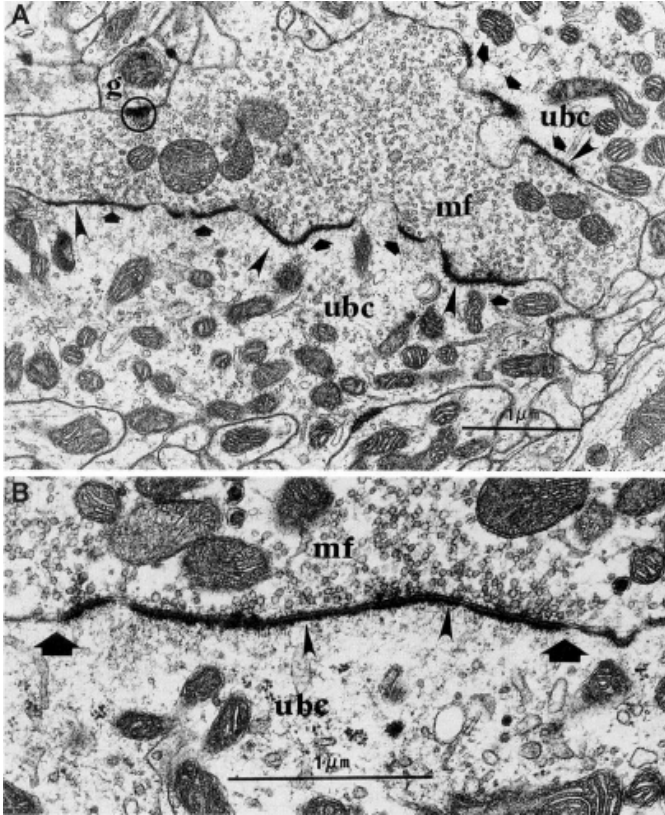


Figure 5. (taken from Rossi *et al.*, 1995) Ultrastructure of MF-UBC synapse. (A) extensive asymmetric MF-UBC synapses (block arrows) involving two branchlets (ubc, bottom and upper right corner). MF rosette (mf) forms a small asymmetric synapse (encircled) with a granule cell dendrite (g). Rosette shows groups of synaptic vesicles crowded at points on presynaptic membrane. UBC branchlets (ubc), however, show nearly continuous postsynaptic densities. Consequently, along the synaptic appositions there are points (arrowheads) at which the postsynaptic densities lack opposing groups of synaptic vesicles. (B) enlargement of asymmetric MF-UBC synapse (between block arrows).

Mugnaini, 2000). Together with the irregular and complex synaptic cleft formed by the mossy terminal and dendritic brush, the ultrastructure of this synapse has important consequences for the dynamics of synaptic transmission.

Brief history of unipolar brush cells

Despite the thorough characterization of cerebellar anatomy and circuitry by well-known anatomists such as Camillo Golgi and Santiago Ramon y Cajal, UBCs were misidentified for decades. The first images known to depict UBCs in electron

micrographs of cat cerebellum were from the late 1960s and early 1970s (Hámori and Szentágothai, 1966; Eccles, *et al.*, 1967; Mugnaini, 1970; Mugnaini, 1972), but they were thought to be unusual Golgi cells. They continued to be mistaken for Golgi cells, atrophied Purkinje cells or other abnormal cell types in cerebellum (Chan-Palay and Palay, 1971; Monteiro, 1986; Mugnaini *et al.*, 1980) and as “mitt” and “chestnut” cells in

the DCN (Hutson and Morest, 1996; Weedman *et al.*, 1996; Josephson and Morest, 2003).

During the 1980's Enrico Mugnaini and colleagues further characterized the circuit anatomy of the cerebellum, as well as of the DCN. His lab officially identified UBCs as a new cell type in the early 1990's (Harris *et al.*, 1993; Mugnaini and Floris, 1994; Berthié and Axelrad, 1994; Mugnaini *et al.* 1994; Floris *et al.*, 1994). In 1995 and 1997, the first physiological studies were published (Rossi *et al.*, 1995; Kinney *et al.*, 1997), characterizing excitatory synaptic transmission to UBCs and also further characterizing their morphology with electron microscopy.

Since then, several studies have characterized molecular markers, intrinsic properties and inhibitory transmission in UBCs. However there has been little further characterization of their excitatory input since 1997, and their functional role in the neural circuits in which they are present remains unknown.

Molecular definition of UBC subtypes

Early studies first identified calretinin⁺ UBCs in both cerebellum and cochlear nucleus of rats (Floris *et al.* 1994) and cerebellum of mice (Abbott and Jacobowitz, 1995), monkeys and cats (Yan and Gary, 1996). Different ionotropic glutamate receptors subunits were detected in cerebellar UBCs of cats and rats. For example, UBCs strongly expressed AMPAR subunits GluR2/3, and moderately expressed KAR subunits GluR5/6/7 and NMDAR subunit NR1, all found at post-synaptic densities located on the dendritic brush (Jaarsma *et al.*, 1998).

Around the same time, several groups showed that UBCs of cerebellum and cochlear nucleus are mGluR2 positive in various mammalian species, including rats, mice, cats, monkeys and primates, and humans (Ohishi *et al.*, 1998; Knoflach and Kemp, 1998; Jaarsma *et al.*, 1998; Spatz, 1999; Spatz, 2000, Nunzi *et al.*, 2001; Spatz, 2001). Further physiology studies showed that, in UBCs, mGluR2 are activating inhibitory G-protein activated inward rectified potassium channels (GIRKs) (Knoflach and Kemp, 1998; Russo *et al.*, 2008).

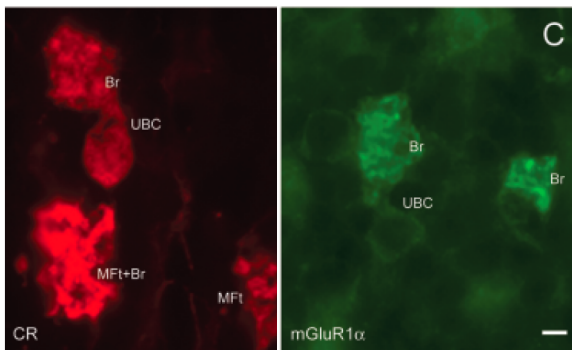


Figure 6: (taken from Nunzi *et al.*, 2002) Immunofluorescence staining showing UBC colocalization with calretinin (red) and mGluR1 α (green). Scale bar 5 μ m.

Wright and colleagues (Wright *et al.*, 1996) were the first to identify UBCs that were positive for mGluR1 α , in the dorsal cochlear nucleus of rats and guinea pigs. Supporting this finding, in 2002, a study showed not only mGluR1 α UBCs, but also a mutually exclusive expression of calretinin and mGluR1 α positive UBCs,

establishing for the first time two subsets of UBCs based on molecular markers, in mouse cerebellum (Nunzi *et al.*, 2002) (Fig 6). This study also demonstrated that both UBC subsets colocalize with glutamate receptors mGluR2, GluR2/3 and NR1. In 2008, another study further characterized the distribution of calretinin⁺ and mGluR1 α ⁺ in the rat cochlear nucleus (Diño and Mugnaini, 2008). Furthermore, mGluR1 α was found to be restricted to the dendritic brush while mGluR2 was found in the somato-dendritic compartment. And at the dendritic brush, both mGluR1 α and mGluR2 were found to be located in non-synaptic areas of the fine dendritic branchlets (Jaarsma *et al.* 1998).

Through the following years, calretinin, mGluR1 α and mGluR2 were used as molecular markers for UBCs in a variety of studies and species (Nakamura *et al.*, 2004; Sekerková *et al.*, 2005; Ando *et al.*, 2005; Vig *et al.*, 2005; Harashima *et al.*, 2006; Meek *et al.*, 2008; Bazwinsky *et al.*, 2008; Kalinichenko and Pushchin, 2008; Alvarez *et al.*, 2008; Russo *et al.*, 2008; Chung *et al.*, 2009a; Chung *et al.*, 2009b; Rousseau *et al.*, 2012; Toledano *et al.*, 2012; Kim *et al.*, 2012). However, in 2009, a study in mouse cerebellum identified a new subset of UBCs expressing PLC β 4 that seemed to be different from calretinin⁺ UBCs and mGluR1 α ⁺ UBCs. Chung and colleagues (Chung *et al.*, 2009a) proposed rather three distinct UBC subtypes, in which the mGluR1 α ⁺ UBCs also co-expressed PLC β 4, while calretinin⁺ UBCs did not, but there was a subset of cells negative for both calretinin and mGluR1 α , but positive for PLC β 4. A more recent comprehensive immunohistochemical study in vestibulocerebellar UBCs of mice and rats, clarified this matter, finding that all PLC β 4⁺ UBCs were in fact also positive for mGluR1 α , while calretinin⁺ UBCs were negative for PLC β 4 and that combined, the two mGluR1 α ⁺ and the calretinin⁺ UBCs subtypes comprise the entire UBC population (Sekerková *et al.*, 2014).

In terms of physiological distinction, one recent study (Kim *et al.*, 2012) thoroughly characterized intrinsic properties of each UBC subtype, by using targeted patching in a transgenic mouse expressing GFP selectively in mGluR1 α ⁺ UBCs. This study compared several characteristics of GFP positive cells and GFP negative cells (including the calretinin⁺ UBCs). They found slight differences in soma size, membrane resistance, and regularity of intrinsic firing. The later was suggested to be due to differences in density of background K⁺ currents, voltage-gated calcium channels and

hyperpolarization-activated currents (I_h). Although synaptic transmission to each subtype was not investigated in this study, altogether, their findings support the prediction that the two different UBC subtypes likely have different functions.

Synaptic transmission from mossy fiber terminals to UBCs

UBCs in cerebellum and the dorsal cochlear nucleus have similar morphology, suggesting similar physiology. However, there are very few studies of synaptic transmission from mossy fibers to UBCs; moreover all of these were done in cerebellar UBCs and did not distinguish subtypes. Thus DCN UBCs have never been characterized, and the function of UBCs in either region is unclear.

The first characterization of synaptic transmission at the mossy to UBC synapse was done by Rossi and colleagues (Rossi *et al.*, 1995). They made the remarkable finding that UBCs display a biphasic excitatory post-synaptic current (EPSC), with a fast inward transient mediated by AMPARs followed by a very slow component (Fig 6). This slow

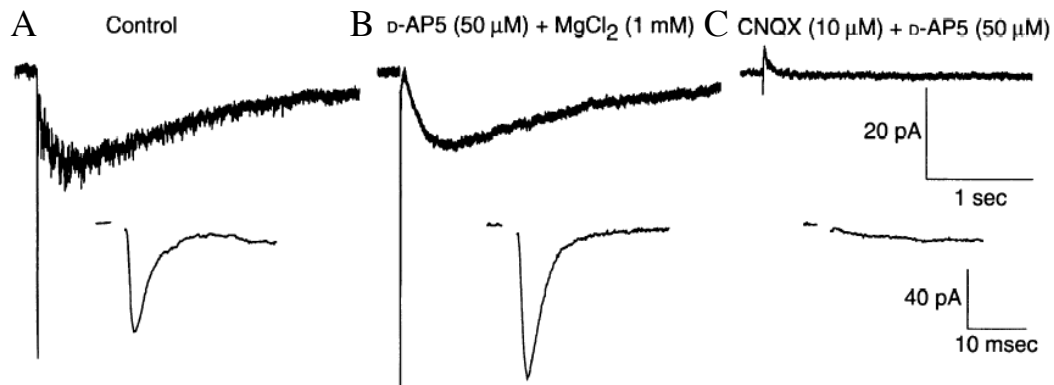


Figure 7: (taken from Rossi *et al.*, 1995) Slow EPSC in some UBCs of cerebellum is predominantly mediated by AMPA/KAR receptors. (A) Biphasic EPSC of a patch-clamped UBC at low and high (inset) time resolution in Mg²⁺-free saline. Both fast and slow components of the EPSC were blocked by AMPA/KAR receptor antagonist CNQX (C), whereas application of NMDA receptor antagonist D-AP5 and Mg²⁺ (B) only reduced the current variance during slow EPSC.

component rose slowly, and had a very prolonged decay, taking hundreds of milliseconds to return to baseline. And, although there was some NMDAR contribution in some cells, the slow phase had surprisingly large contribution of AMPARs (Fig 7). They demonstrated that with the application of cyclothiazide, a drug that blocks AMPAR desensitization, the gap in the EPSC between fast and slow components was eliminated, and decay time increased (Fig 8).

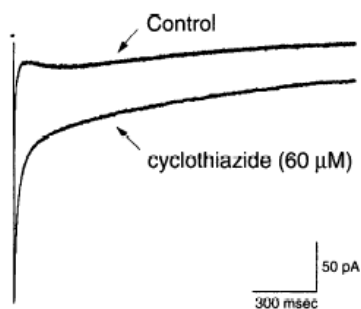


Figure 8: (taken from Kinney *et al.*, 1997) Effect of cyclothiazide on amplitude and time-course of the slow EPSC component.

A previous study at the time had characterized AMPAR responses and their relation to the extracellular glutamate concentration (Raman and Trussell, 1992). The study demonstrated that the steady-state dose-response curve of AMPAR to glutamate is biphasic. That is, there is an increase in the steady-state current at a range of glutamate concentration at around 70-100 μM , while at higher concentrations (up to 2 mM), there is a rapid decrease or desensitization in AMPAR currents, declining to at least half of the steady-state maximum (Fig 9A).

The follow up study on UBCs from the same group (Kinney *et al.*, 1997), further investigated the slow AMPAR mediated current in UBCs, demonstrating that it remarkably fits with the glutamate dose-response curve. Based on these results and the unusual ultrastructure of the mossy fiber-UBC synapse, they proposed the “entrapment hypothesis”. The dendritic brush and the mossy fiber terminal interlock, forming an intricate synaptic cleft, which is proposed to create a physical barrier to diffusion of neurotransmitter (Fig 4). They hypothesized that, upon glutamate release leading to the

initial fast EPSC transient, glutamate gets entrapped in the synaptic cleft, rapidly raising the glutamate concentration to which AMPARs are being exposed, subsequently rapidly desensitizing those receptors leading to the sag in the EPSC (Fig 9B-D) – hence this

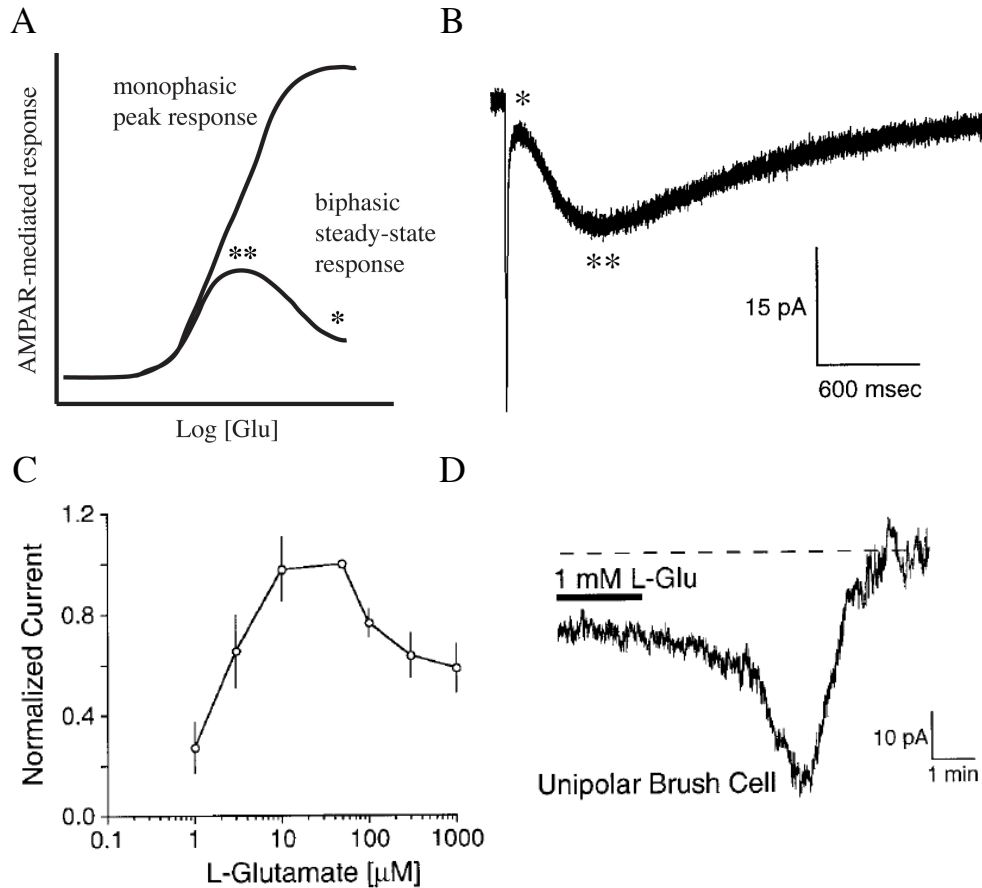


Figure 9: (A) (Adapted from Raman and Trussell, 1992) Dose-response curve of the AMPAR-mediated response in relation to glutamate concentration. The single and double asterisk in A correspond to the same points of the example UBC biphasic EPSC shown in (B). At high glutamate concentrations there is a current undershoot (*), before reaching a quasi steady-state peak (**). (C) and (D) (taken from Kinney *et al*, 1997) In C, the authors built a dose-response curve specifically for the AMPAR-mediated response of UBCs in response to glutamate application (example in D), and it fits with the predicted biphasic response as per Raman and Trussell, 1992).

current undershoot is sensitive to cyclothiazide (Fig 8). As glutamate slowly diffuses out of the cleft and the concentration decreases, a quasi-steady state is maintained. The current continues to further decay back to baseline with gradual diffusion of neurotransmitter out of the cleft.

Normally the lifetime of glutamate in the cleft is brief (1-2 ms) (Clements *et al*, 1992), thus most AMPARs do not reach a steady-state, and the response is fast and monophasic. By taking into consideration the geometry of the synapse between mossy terminals and UBCs, the glutamate “entrapment hypothesis” explains the prolonged biphasic EPSC.

Additional results from these studies showed the all-or-none nature of both EPSC components, further supporting the anatomical evidence that UBCs receives one mossy fiber terminal input (Mugnaini and Flores, 1994). These studies also found that the prolonged EPSC led to extended firing of action potentials. Based on these results, the initial prediction of UBCs function was the amplification of multisensory signals from mossy fibers to their target, granule cells.

Since these initial studies, there has been only one other characterizing their post-synaptic currents (van Dorp and de Zeeuw, 2014), and two other studies investigated mossy input impact on UBC firing or post-synaptic potentials (Diana *et al.*, 2007; Locatelli *et al.*, 2012). One of these (von Dorp and de Zeeuw, 2014) reported a very similar UBC response to presynaptic stimulation as described above – with a biphasic EPSC and slow decaying component. They further characterized the synaptic response and investigated the temporal transformation of multisensory input from mossy fiber to UBC, with this slow ‘resurgent’ EPSC that can be activated at variable delays, sometimes of hundreds of milliseconds, depending on the frequency of presynaptic stimulation. The study shows that the onset of the slow component peak is frequency dependent – it becomes more pronounced at higher frequencies, and only reaches quasi-steady state peak after high-frequency stimulation has ceased.

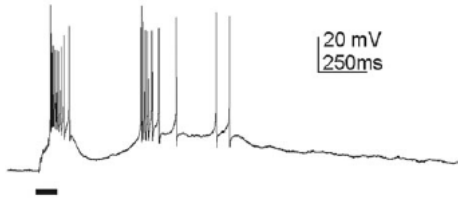


Figure 10: (taken from Locatelli *et al.*, 2012): Example of a UBC response to mossy fiber stimulation with an early and a late onset burst firing.

In vitro recordings from UBCs in rat vestibulocerebellum investigated the firing patterns in response to mossy fiber stimuli, finding that response pattern depended on the UBC's resting potential— tonic firing occurred at more depolarized potentials (~ -60 mV), while

bursts of action potentials arose from more hyperpolarized potentials (< -70 mV) (Diana *et al.*, 2007). This study focused on the effect of calcium signaling, particularly of voltage-gated calcium conductances, as T-type calcium channels control burst firing, in UBC intrinsic excitability; the authors did not, however, identify specific UBC subtypes. More recently, Locatelli and colleagues (Locatelli *et al.*, 2012) observed that upon mossy fiber stimulation, cerebellar UBCs displayed an early onset burst firing of action potentials, followed by a late-onset burst, after tens of hundreds of milliseconds (Fig 10). They were able to block the early-onset burst with AMPAR/NMDAR antagonists

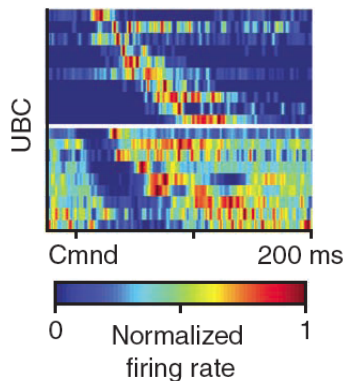


Figure 11: (Adapted from Kennedy *et al.*, 2014) UBCs showing late (top) and pause (bottom) response to motor command input

NBQX/APV, but the late-onset burst remained. With further experiments they show evidence that hyperpolarization-activated currents (I_h) and transient receptor potential (TRP)-currents are involved in mediating this late-onset excitation. They also noted that some UBCs displayed only the late-onset response, without the early onset burst.

Another finding worth mentioning, are the results from *in vivo* whole-cell recordings from UBCs in the electrosensory lateral lobe of the cerebellum of the mormyrid

electric fish (Kennedy *et al.*, 2014) – as mentioned above, another cerebellum-like network with UBCs. In this study, they evoked motor commands in the fish to evoke mossy fiber stimulation to UBCs (Fig 11). In UBCs that were firing spontaneously, a command stimulus lead to a pause in firing followed by rebound excitation. However, in some UBCs that were not firing spontaneously or had little spontaneous activity, they noticed a ‘late’ response, with increase in firing frequency.

Intrinsic firing of unipolar brush cells

Cerebellar UBCs have been shown to fire regularly *in vitro* (Russo *et al.*, 2007), and *in vivo* (Simpson *et al.*, 2005; Barmack and Yahknitsa, 2008; Ruigrok *et al.*, 2011, Kennedy *et al.*, 2014).

All mammalian *in vivo* recordings of UBCs were done extracellularly, with juxtacellular labeling, in vestibulocerebellum (uvula-nodulus) of anesthetized animals. In anesthetized mice, UBCs displayed spontaneous firing with occasional quieter cells with burst responses. These recordings were done during vestibular stimulation, with sinusoidal roll tilt. Over 70% of the UBCs that responded to stimulation, increased discharge with ipsilateral roll tilt (Barmack and Yahknitsa, 2008). UBCs in vestibular cerebellum of anesthetized rats and rabbits also show regular spontaneous firing, with few action potential failures and sharp inter-spike interval distributions (Ruigrok *et al.*, 2011). In addition to mammals, whole-cell *in vivo* recordings of UBCs in the lateral line lobe of the cerebellum of the mormyrid electric fish showed that UBCs also display regular spontaneous activity, although a fraction of the cells were quieter, with occasional bursts of action potentials (Kennedy *et al.*, 2014).

Spontaneous firing of UBCs *in vitro* was investigated in slices of mouse cerebellum and they displayed intrinsic firing in whole-cell and cell-attached patch-clamping mode, as the latter mode is less invasive and maintains the integrity of the intracellular space preventing dialysis of conductances involved in maintenance of spontaneous firing. Russo *et al* (2007) demonstrated that a persistent Na⁺ current and a TRP-like cationic current underlie their intrinsic firing. If there are other factors contributing to or underlying UBC spontaneous firing, these have not been further investigated beyond this study.

Considering such regular spontaneous firing of UBCs, it would be expected to see some level of spontaneous activity in granule cells being targeted by UBCs. During *in vitro* recordings, granule cells rarely show spontaneous activity in cerebellum or DCN (DiGregorio *et al.*, 2002; Sargent *et al.*, 2005; DiGregorio *et al.*, 2007; Schwartz *et al.*, 2012; Balakrishnan and Trussell, 2008; Balakrishnan *et al.*, 2009). Whole-cell recordings of granule cells *in vivo* in anesthetized animals show that there seems to be a variation in the rate of spontaneous activity, depending on the cerebellar lobe where those cells are located (Arenz *et al.*, 2008). In lobes I and IIa in rat cerebellum, spontaneous activity was absent in granule cells (Chadderton *et al.*, 2004; Rancz *et al.*, 2007), while in lobes IV and V in cat cerebellum, although present, spontaneous activity had a very low rate (Jorntel and Ekerot, 2006). However, in mouse flocculus (vestibulocerebellum), granule cells have high rates of tonic activity (Arenz *et al.*, 2008). It is not known whether or not this higher rate of spontaneous activity of granule cells *in vivo* in vestibulocerebellum is due to a higher presence of UBCs. Moreover, their impact on granule cell activity *in vivo* or *in vitro* has also not been directly tested.

Overview of thesis

The work presented in this thesis focused upon understanding the importance of glutamate receptor-mediated currents for UBC function and how they influence the processing of multisensory signals. These studies primarily utilized single cell patch-clamp electrophysiological recording techniques in brainstem and cerebellum slice preparations. Glutamate receptor subtypes were probed using pharmacological tools – agonists and antagonists, and with immunohistochemistry. The work presents the first recordings of UBCs in the DCN. I discovered two subtypes of DCN UBC characterized by their responses to glutamatergic synaptic transmission (Chapter 1), and showed using immunohistochemistry a correlation of UBC subtypes defined by molecular markers with the physiological profiles that I observed. Moreover, I found a similar pattern in vestibulocerebellum, suggesting UBCs are probably not very different in the two regions. Finally, I discovered a role of glutamate receptors in maintaining intrinsic firing of UBCs in response to cell-specific background levels of glutamate (Chapter 2).

CHAPTER 1. ON and OFF unipolar brush cells transform multisensory inputs to the auditory system

Carolina Borges-Merjane^{1,2}, Laurence O. Trussell²

¹Neuroscience Graduate Program, Vollum Institute, Oregon Health & Science University, Portland, OR, 97239, U.S.A. and ²Vollum Institute and Oregon Hearing Research Center, Oregon Health & Science University, Portland, OR, 97239, U.S.A

(Borges-Merjane and Trussell, 2015)

Abstract

Unipolar brush cells (UBCs) of the dorsal cochlear nucleus (DCN) and vestibular cerebellar cortex receive glutamatergic mossy fiber input on an elaborate brush-like dendrite. Two subtypes of UBC have been established based on immunohistochemical markers and physiological profiles, but the relation of these subtypes to the response to mossy fiber input is not clear. We examined the synaptic physiology of auditory UBCs in mouse brain slices, identifying two response profiles and correlated each with a specific UBC subtype. One subtype had a striking biphasic excitatory response mediated by AMPAR and mGluR1 α . The second was mGluR1 α negative and was dominated by a strongly inhibitory outward K⁺ current. These two subtypes up-or downregulated spontaneous firing, respectively. By analogy to the retina, we propose that UBCs comprise ON and OFF cells with respect to their response to glutamatergic input, and may therefore provide distinct parallel processing of multisensory input to their targets.

Introduction

Unipolar brush cells (UBCs) are excitatory interneurons present in cerebellum-like structures. In mammals, they are found in cerebellum and the dorsal cochlear nucleus (DCN) (Floris *et al.*, 1994; Mugnaini *et al.*, 1997; Bell *et al.*, 2008; Roberts and Portfors, 2008). The DCN is the earliest stage of the auditory pathway in which multisensory input is integrated with auditory input (Fig 1.1A,B). This multisensory input modifies auditory responses in the DCN and thus may be important for processing of acoustic signals (Shore *et al.*, 1991; Young *et al.*, 1995; Shore and Moore, 1998; Shore, 2005; Koehler *et al.*, 2010; Kanold *et al.*, 2011). Auditory UBCs receive direct one-to-one multisensory input via mossy fibers and relay that input to granule cells for integration with auditory nerve input by the principal output neurons (Fig 1.1B) (Diño *et al.*, 2000; Nunzi *et al.*, 2001, Oertel and Young, 2004; Mugnaini *et al.*, 2011). Intermediary cell types in excitatory feedforward pathways necessarily delay transmission but offer opportunity for significant transformation of input signals.

Early studies of synaptic properties of cerebellar UBCs revealed a slow-decaying biphasic excitatory postsynaptic current (EPSC) that triggered a long train of postsynaptic action potentials (APs) (Rossi *et al.*, 1995, Kinney *et al.*, 1997). Thus, UBCs seemed to amplify and prolong multisensory signals from mossy fibers to their target granule cells. However, later immunohistochemical studies revealed two distinct UBC populations: calretinin⁺ UBCs and mGluR1 α ⁺ UBCs (Nunzi *et al.*, 2002; Diño and Mugnaini, 2008; Sekerková *et al.*, 2014). A recent study characterized intrinsic (nonsynaptic) electrophysiological properties of these subtypes in cerebellum (Kim *et al.*, 2012). Those findings and others (Knoflack and Kemp, 1998; Diana *et al.*, 2007; Russo *et al.*, 2007;

Russo *et al.*, 2008; Rousseau *et al.*, 2012) are consistent with a model in which two UBC subpopulations exist, each with different functions. These observations therefore raise the question of whether mossy fiber input is differentially transformed by the two UBC subtypes.

In this study (Borges-Merjane and Trussell, 2015), we investigated glutamate sensitivity and synaptic transmission from mossy fibers to UBCs in the DCN. We found that the two UBC subtypes, like retinal bipolar cells, may function as ON and OFF cells with respect to their response to glutamatergic input, due to dual actions of glutamate and differential expression levels of glutamate receptor types in the two subtypes. mGluR1 α positive UBCs had an excitatory (ON) response to glutamate, due to high expression of AMPARs and mGluR1 α , and small GIRK currents elicited by mGluR2 activation. mGluR1 α negative UBCs had an inhibitory (OFF) response to glutamate resulting from small AMPAR-mediated currents and large outward K⁺ currents activated by mGluR2. These UBC subtypes provide distinct parallel processing of multisensory input to their target granule cells.

Methods

Animals

All animals used in this study were C57BL/6J wild-type mice or were from the C57BL/6J-TgN(*grm2-IL2RA/GFP*)1kyo line. The latter express GFP tagged to human interleukin-2 receptor α subunit driven by the mGluR2 promoter (Watanabe *et al.*, 1998). The mGluR2 receptor is present at both UBC subtypes and therefore this transgenic line labels both subtypes (Nunzi *et al.*, 2002) with GFP targeted to the plasma membrane. mGluR2 is a reliable marker for identification of UBCs in DCN and cerebellum of various species, including humans (Jaarsma *et al.*, 1998; Ohishi *et al.*, 1998; Petralia *et al.*, 2000; Spatz, 2001; Meek *et al.*, 2008). All experiments were performed in brain sections from males and females, postnatal days 21 to 32 (P21-32). Animals were bred in a colony maintained in the animal facility managed by the Department of Comparative Medicine and all procedures were approved by the Oregon Health and Science University's Institutional Animal Care and Use Committee. Synapse formation between the presynaptic mossy fiber terminal and the postsynaptic dendritic brush structure of the UBCs is mature in animals older than P21 (Morin *et al.*, 2001). Transgenic mice were genotyped by PCR, with DNA extracted from tail clippings.

Immunohistochemistry

Immunohistochemistry of transgenic mice (Figures 1.1, 1.S1 and 1.S4) and of slices with biocytin filled cells (Figures 1.S3, 7 and 1.S5) were performed as per the following protocols. Mice were transcardially perfused with warm ($\sim 38^{\circ}\text{C}$) 100 mM PBS solution, pH 7.4, followed by ice-cold 4% paraformaldehyde in PBS (PFA). The brains

were dissected from the skull and incubated overnight in 4% PFA for complete tissue fixation and rinsed in PBS prior to sectioning. Brainstem and cerebellum coronal sections were acquired at 40 μ m on a vibratome (VT1000S, Leica) at room temperature in PBS. After sectioning, the tissue was washed in PBS solution 3 times at 10 minutes each. Sections were then incubated for 2 hours in permeabilization solution (2% fish gelatin, 0.2% Triton X-100, 2% BSA, in PBS). After being washed in PBS again, they were incubated for 30 minutes in blocking solution (2% fish gelatin in PBS). Next, they were incubated for 48 hours at 4°C in primary antibodies in blocking solution. Subsequently sections were washed in PBS and incubated in blocking solution for 30 minutes again, before secondary antibody incubation overnight at 4°C. Finally, sections were washed in PBS, post-fixed in 4% PFA for 1 hour and washed again PBS. The tissue was then coverslipped using Fluoromount G medium (Southern Biotechnology Associates). Fluorescence images were acquired using a confocal microscope (Olympus FV1000) by sequential scanning of fluorescent signals using an oil-immersion objective (10x, 20x, 40x and 60x magnification, numerical aperture 1.42) with Olympus Fluoview-1000 software. Confocal images were analyzed with NIH ImageJ software. A median filter was applied to reduce noise.

Primary antibodies used were chicken polyclonal anti-GFP (1:2000; GFP-1020, AVES LABS), rabbit polyclonal anti-mGluR2/3 (1:1000; 06-676, Millipore), rabbit polyclonal anti-GFP Alexa Fluor 488 Conjugate (1:200; A21311, Life Technologies), rabbit polyclonal anti-calretinin (1:5000; 7697, Swant) and mouse monoclonal anti-mGluR1 α (1:800; 556389, BD Pharmingen). In addition, to target biocytin filled cells, we used streptavidin Alexa Fluor 488 conjugate (1:2500; S-11223, Molecular Probes/Life

Technologies). Secondary antibodies used were donkey polyclonal anti-rabbit Cy3 Conjugate (1:500; 711-165-152, Jackson Immuno Research), donkey polyclonal anti-chicken Alexa Fluor 488 Conjugate (1:500; 703-545-155, Jackson Immuno Research), goat polyclonal anti-mouse Cy3 Conjugate (1:500; 115-165-146, Jackson Immuno Research); goat anti-rabbit Alexa Fluor 647 Conjugate (1:500; A-21245, Molecular Probes/Life Technologies) and donkey polyclonal anti-rabbit Alexa Fluor 594 (1:500; 711-585-152, Jackson Immuno Research).

Brain slice experiments

Mice were anesthetized with isoflurane, decapitated, and the brainstem was dissected from the skull under ice-cold high-sucrose artificial cerebral spinal fluid (ACSF) solution containing the following (in mM): 87 NaCl, 75 sucrose, 25 NaHCO₃, 25 glucose, 2.5 KCl, 1.25 NaH₂PO₄, 0.4 Na-ascorbate, 2 Na-pyruvate, 0.5 CaCl₂, 7 MgCl₂ and 5 μm R-CPP, bubbled with 5% CO₂/95% O₂ (Bischofberger *et al.*, 2006). Coronal brainstem slices with DCN were cut at 250-300 μm with a vibratome (VT1200S, Leica) in ice-cold high-sucrose ACSF solution. Slices were transferred to a recovery holding chamber and allowed to recover at 35°C for 30-40 minutes, in ACSF containing the following (in mM): 130 NaCl, 2.1 KCl, 1.2 KH₂PO₄, 3 Na-HEPES, 10 glucose, 20 NaHCO₃, 0.4 Na-ascorbate, 2 Na-pyruvate, 2 CaCl₂, 1 MgSO₄, and 5 μm R-CPP, bubbled with 5% CO₂/95% O₂ (300–305 mOsm). After this recovery period, the recovery holding chamber was kept at room temperature (~23°C) until recording. Recording ACSF was the same as the recovery ACSF but lacked R-CPP. Slices were transferred to the recording chamber and superfused with recording ACSF and maintained at ~35°C. With the

exception of experiments measuring intrinsic firing rate with cell-attached and whole-cell recordings in Figure 1.2, all glutamate-activated currents evoked by electrical stimulation or by puff application of agonist were recorded in the presence of 5-10 μM SR95531 and 2 μM strychnine. Recordings from slices were performed within 6 hours of preparation. Parasagittal cerebellum slices of lobes IX and X used for comparative experiments were acquired with the same procedure and solutions as described above.

Electrophysiological recordings

Slices were visualized with a Zeiss Axioskop 2 FS Plus microscope with Dodt gradient contrast optics (Dodt *et al.*, 2002), using 10x and 60x (water immersion) Olympus objectives. Fluorescent signals were visualized with an X-Cite 120Q excitation light source through Semrock BrightLine Bandpass filters 469/35 and 525/39, with a 497 dichroic mirror. UBCs were initially identified by soma size or GFP fluorescence. Additionally, intracellular recording solution always contained 20-30 μM Alexa Fluor 488 hydrazide sodium salt (Molecular Probes Life Technologies). Thus, in whole-cell mode after dialysis of the Alexa dye, we could easily confirm the identity of an UBC by the presence of a distinct dendritic brush. UBCs were also readily distinguished from granule cells by electrophysiological properties: intrinsic firing at $\sim 5\text{Hz}$, voltage sag due to hyperpolarization activated current (I_h), and rebound firing following a hyperpolarizing step. Patch electrodes were pulled with borosilicate glass capillaries (OD 1.2 mm and ID 0.68 mm, World Precision Instruments) with a horizontal puller (P-97, Sutter Instruments) or with an upright puller (PC10, Narishige). For whole-cell recordings, pipettes were filled with a solution containing (mM): 113 K-gluconate, 9 HEPES, 4.5

MgCl₂, 0.1 EGTA, 14 Tris-phosphocreatine, 4 Na₂-ATP, 0.3 tris-GTP (adjusted to 290 mOsm with sucrose), pH 7.2-7.25. For neurons shown in Figure 1.7 and supplemental Figures 1.3 and 1.5, the same pipette solution was used with the addition of 0.3% biocytin (Molecular Probes). All membrane potential values and current clamp recordings were corrected for a -10 mV junction potential. All recordings were acquired using a Multiclamp 700B amplifier and pClamp 9 software (Molecular Devices). In voltage and current clamp, signals were sampled at 20-50 KHz, low-pass filtered at 10 KHz and digitized (10 kHz) using a Digidata (1322A, Molecular Devices) analog-digital converter board. Current signals in voltage-clamp were acquired with 5x gain and Bessel filtered at 8-10 KHz, with further filtering applied offline. Patch pipettes in whole-cell recordings ranged from 6-8 MΩ tip resistance; series resistance was compensated with correction 20-40% and prediction 60-70%, bandwidth 2-2.5 kHz. Membrane potential was held constant at -70mV, unless otherwise noted. In current-clamp recordings no current was injected, unless otherwise noted. Electrical stimulation was performed with silver wires in theta double-barreled glass electrodes (OD 1.5mm, Sutter Instrument) filled with recording ACSF. Single and train stimuli were evoked using a stimulus generator (Master 8, A.M.P.I.) delivering 200-250 μs duration pulses, and a stimulus isolation unit (Iso Flex, A.M.P.I.), set to 30-70 V. Puff application of agonists and antagonists were delivered through a Picospritzer II (Parker Instrumentation), at 5 psi, with borosilicate glass capillaries. Glutamate puffs were always used for subtype identification. For experiments in which the puff solutions were being exchanged mid-recording, the pipettes were always brought back to the original location before delivering the new solution. Applications were of brief duration and the pipette was kept

>20 μm away from the dendritic brush and soma to avoid mechanical disturbance of the cell following the puff. All glutamate applications were at 1 mM (puff pipette concentration) and 7-10 ms in duration. If puff durations of other drugs were >20 ms, the pipette was moved farther away than 20 μm . Puff application of control solution without drugs ruled out puff artifacts.

Pharmacology

Agonists and antagonists were delivered by puff or bath application as indicated, and corresponding concentrations are specified under the results section for each appropriate assay. Receptor antagonists: LY367385 (mGluR1 α ; Tocris), LY341495 (group II mGluR; Tocris), NBQX disodium salt (AMPA/KAR; Abcam), GYKI53655 (AMPA; IVAX Corporation), (R)-CPP (NMDAR; Abcam). Receptor agonists: (S)-3,5-DHPG (group I mGluR; Tocris), LY354740 (group II mGluR; Tocris), sodium L-glutamate (all glutamate receptors; Sigma-Aldrich).

Data analysis and Statistics

All traces acquired were analyzed with Clampfit 9 (Molecular Devices) and Axograph X. All graphs were built with IgorPro (WaveMetrics). All data are displayed as mean \pm SEM and all statistical analysis for Student's t-tests were run on StatPlusPro in Excel or on GraphPad Software.

The time constant for ON UBC biphasic EPSCs was measured after a single stimulus or after a train of stimuli. For the fast phase of decay after a single stimulus, a time constant was measured using a single exponential fit extrapolated to baseline. Due to

the wide variation of the shape of the second phase of the EPSC, a decay time constant for this phase was calculated as the normalized integral of charge beginning at the peak of the event to its decay. The values reported are therefore an underestimate of the time constant, since a slow rising phase of the second component (e.g. Fig 1.2A) was not taken into account in this analysis. The decay time constant for the IPSC of OFF UBCs elicited after a train was calculated in the same manner, and the charge value reported was measured immediately after the last stimulus artifact, it is therefore also an underestimate (e.g. Fig 1.2B). The histogram in Figure 1.5 was built using the histogram bin-width optimization method from Shimazaki and Shinomoto, 2007.

Results

Identification of DCN UBCs

Recordings were made from DCN slices taken from either wild-type or from transgenic mice with selective expression of GFP driven by the promoter of the receptor mGluR2 (Watanabe *et al.*, 1998; Jaarsma *et al.*, 1998). GFP in this mouse line co-localizes with mGluR2 and clearly labeled UBCs in the deep layer of the DCN (Fig 1.1C). They are easily identifiable by their unique morphology with a single short dendritic stalk and fine dendritic mesh (Mugnaini and Floris, 1994) (Fig 1.1D and Fig 1.S1). With practice, candidate UBCs could also be reliably identified in wild type tissue. In addition, for every recording, internal solution contained Alexa Fluor 488, allowing visualization of the distinct UBC morphology during whole-cell recording. In some experiments the internal also contained biocytin for post-hoc identification described below.

UBC populations defined by response to synaptic input

Early studies of UBCs in cerebellum reported biphasic EPSCs mediated primarily by AMPA receptors (Rossi *et al.*, 1995, Kinney *et al.*, 1997), and proposed that a complex synaptic organization led to entrapment of glutamate and slowing of the EPSC. The combined effects of lingering transmitter and the kinetic features of AMPARs may generate this biphasic inward current, ultimately prolonging the firing of UBCs (Kinney *et al.*, 1997). In order to further investigate mechanisms of synaptic transmission properties of the mossy fiber-UBC synapse in the DCN, we made whole-cell voltage and

current-clamp recordings, while delivering electrical stimuli to mossy fiber inputs (Fig 1.2). This approach readily revealed distinct UBC populations.

One UBC subtype displayed an inward biphasic EPSC, similar to responses described in cerebellar UBCs (Rossi *et al.*, 1995). This response was composed of a rapid inward current (mean peak amplitude -62.6 ± 13.8 pA; decay tau 3.6 ± 0.8 ms) followed by a second phase decaying with a much longer time constant (tau 260.7 ± 46.8 ms; mean charge of fast and slow EPSC components combined -3.5 ± 1.1 pC; n=9). A single shock was sufficient to elicit fast and slow EPSCs, but after a stimulus train of 10x or 20x at 100 Hz, the second component grew in size and duration (tau 898.8 ± 99.0 ms; mean charge -11.7 ± 2.0 pC; n=9) (Fig 1.2A, left panel), as described in cerebellum (Rossi *et al.*, 1995; Kinney *et al.*, 1997). As in cerebellum (Russo *et al.*, 2007), DCN UBCs fire spontaneous APs. The slow EPSC component sharply increased the ongoing firing rate (Fig 1.2A right panel).

Other UBCs displayed a very different response profile upon presynaptic fiber stimulation. After a stimulus train, these cells showed an initial small and brief inward component, immediately followed by a pronounced outward current with a prolonged decay (tau 645.4 ± 183.1 ms; mean charge $+4.1 \pm 1.6$ pC; mean peak amplitude $+5.1 \pm 1.3$ pA; n=8) (Fig 1.2B). This slow outward component, obtained in the presence of GABA_A and glycine receptor antagonists, was a genuine inhibitory postsynaptic current (IPSC) as it led to a prolonged pause in spontaneous firing of the UBC (1.1 ± 0.2 s; n=4), similar in time-course to the duration of the current (Fig 1.2B, right panel).

The contrasting responses to presumptive glutamatergic input in UBC subtypes is reminiscent of the opposing retinal bipolar cell responses to glutamate. The first subtype,

with an inward, excitatory response, will therefore be referred to as ON UBC and the second subtype, with an outward current that inhibits spontaneous firing, will be referred to as OFF UBCs (Rousseau et al., 2012).

In order to confirm the postsynaptic nature of the different UBC responses, we used brief (7-10 ms) puff application of glutamate (1 mM) (Fig 1.2C, 1.2D). The current profiles observed with glutamate puff were strikingly similar to the synaptic responses in current and voltage clamp. Additionally, in OFF UBCs, the pause in intrinsic firing was followed by a rebound increase in firing that could be interpreted as delayed excitation in this subtype. Investigation of whether this rebound increase in firing is directly mediated by glutamate currents is described in Figure 1.8.

To highlight the similarity of synaptic and puff responses, we plotted the amplitudes of the two responses obtained for a data set in which synaptic and puff stimuli were applied to the same neurons (Fig 1.2E-H). In each case, the polarity of the puff responses predicted accurately the polarity of the slow synaptic response. In subsequent experiments analyzing receptor subtypes, puff application of glutamate was always applied prior to any treatment, to identify the ON/OFF phenotype of UBCs.

Characterization of mossy fiber input to ON and OFF UBCs

Previous studies in cerebellum only reported the ON synaptic response. Thus to reveal specific features of both ON and OFF UBC responses we varied the parameters of mossy fiber stimulation while recording from each cell type.

First, the frequency of synaptic stimulation was varied from 10 Hz to 100 Hz (Fig 1.3A-D). For ON UBCs (Fig 1.3A), although there was a slight apparent increase in mean

amplitude (Fig 1.3C) and charge of the slow EPSC (Fig 1.3D), the means at 10 Hz versus 100 Hz were not significantly different (black symbols in Fig 1.3C,D; amplitude $p=0.52$ and charge $p=0.24$; $n=7$). For OFF UBCs (Fig. 1.3B), although there was a significant difference in the amplitude of the slow IPSC between 10 and 100 Hz ($n=6$; $p=0.0085$) there was no significant difference in their charge ($p=0.07$), and the overall change in amplitude or charge with frequency was shallow (Fig 1.3C,D blue symbols).

Next, at a fixed frequency of 100 Hz, we applied 1, 3, 5, 10, 20 or 50 stimuli (Fig 1.3E-G). For both ON and OFF UBCs, the number of stimuli had a significant impact on synaptic charge. In particular, for OFF UBCs, responses were undetectable with 1 or 3 stimuli (Fig 1.3F-G). However mean charge increased 5.1 fold going from 3 stimuli (charge 3.9 ± 1.8 pC; $n=5$) to 10 stimuli (charge 20.0 ± 8.2 pC; $n=5$), and an additional 2.1 fold increase in the charge from 10 to 50 stimuli (charge 53.3 ± 18.1 pC; $n=5$) (Fig 3G). Similarly, for ON UBCs there was a 2.2 fold increase in the charge from 3 stimuli (charge -10.0 ± 4.3 pC; $n=7$) to 10 stimuli (charge -22.2 ± 12.4 pC; $n=7$) and an additional 3.4 fold increase in charge from 10 to 50 stimuli (charge -52.1 ± 19.4 pC; $n=7$).

Interpretation of these results depends upon whether they arise from the activity of single or convergent inputs. Previous studies showed that UBCs receive only one mossy fiber input (Diño *et al.*, 2000; Nunzi *et al.*, 2001), but this has not been confirmed physiologically, and it is possible that some of the response arises from spillover from neighboring cells. To explore this further we used minimal stimulation, finding that ON cells show clear all-or-none responses for both the fast and slow EPSCs (Fig 1.S2A). We focused on analyzing the charge of the slow ON cell and OFF responses after a train of stimuli (10 shocks, 100 Hz) in order to increase the slow PSC response. For both

subtypes, stimulus voltages were observed in which either there was or was not a slow current. While both cell types reached a maximum with increase in stimulus strength, OFF cells showed a somewhat more gradual increase in the response, while ON cells reach maximum response quickly, with a clearer all-or-none slow responses (Fig 1.S2B and D). We conclude that ON slow currents are largely derived from a single input. If both subtypes indeed carry only a single mossy input, OFF cells may respond to increasing glutamate spillover; alternatively, increasing voltage may simply raise the number of successful trials during the train and lead to a graded amplitude, since response amplitudes are sensitive to stimulus number (Fig 1.3F).

We also measured synaptic responses to ‘naturalistic’ Poisson stimulation trains. Five-second stimulus trains were constructed having 10-Hz and 50-Hz mean frequencies and Poisson distribution of inter stimulus intervals. For ON cells, fast EPSCs were apparent at 10 Hz, and depressed at 50 Hz (Fig 1.3H); this depression was not studied further here. Strikingly, slow EPSCs (Fig 1.3H) or IPSCs (Fig 1.3I) summated to generate relatively smooth plateau currents, regardless of the 5-fold difference in frequency and the random intervals between individual shocks. To explore this further, we analyzed synaptic charge transfer over the 5-second period of stimulation (Q1 line in Fig. 1.3I) and for an additional 4 seconds thereafter (9 seconds total, Q2 line) and contrasted the total charge in these two periods. These data showed that the synaptic currents exceeded the last stimulus by seconds, particularly at 50 Hz stimulation. The histogram in Figure 1.3J illustrates the ratio of currents at the two time points showing that significant charge is always delivered beyond the stimulus period regardless of stimulus rate or cell subtype. Mean charge was at Q2 was not different at the two

frequencies for ON cells (Fig. 1.3K; charge -75.8 ± 28.8 pC; $n=7$ and -144.1 ± 55.3 pC, $n=6$, respectively), but was greater at 50 Hz for OFF cells (charge 30.1 ± 9.5 pC for 10 Hz, $n=6$; and 137.8 ± 34.2 pC, for 50 Hz, $n=5$, $p=0.0092$).

We conclude that mossy fiber activity is translated to prolonged, steady postsynaptic ON and OFF currents that increase with stimulus number, are relatively insensitive to the pattern of stimuli but markedly outlast the period of stimulation. UBCs therefore appear well suited to encode the appearance of mossy fiber spiking with steady increases or decreases in postsynaptic spiking, dependent upon UBC cell type.

ON UBCs are mGluR1 α positive

To classify ON and OFF UBCs using previous histochemical criteria (Diño *et al.*, 1999; Nunzi *et al.*, 2002; Sekerková *et al.*, 2014), we correlated the ON/OFF subtype with the presence or absence of an mGluR1 α -activated current (Schwartz *et al.*, 2012). After identifying the response of each cell by glutamate application, the puff pipette was switched to 200 μ M (S)-3,5-DHPG, a selective group I mGluR agonist (Fig 1.4A). A 10-35 ms puff (depending on brush location and pipette placement) elicited a slow inward current in 13/13 ON UBCs (mean peak amplitude -8.2 ± 1.2 pA; half-width 3.5 ± 0.42 s; 10-90% rise time 1.34 ± 0.25 s). This current elicited AP firing in cells held just below threshold with bias current, and increased firing frequency in cells firing spontaneously (Fig 1.4B). The current elicited by (S)-3,5-DHPG was completely blocked by the selective mGluR1 α antagonist LY367385 (Fig 1.4B). In contrast, in 7 of 7 OFF cells, (S)-3,5-DHPG did not elicit a current or change in AP firing frequency (Fig 1.4C), even with puff durations up to 100-ms long. The peak current elicited in ON cells was

significantly greater than baseline (> 2 SD of noise), while in OFF UBCs the puff generated no deviation from baseline. This result confirms that ON UBCs are likely identical to the previously defined mGluR1 α^+ UBC subtype and, since OFF UBCs had no mGluR1 α mediated current, they are likely calretinin $^+$ UBCs. In the cerebellum, mGluR1 α^+ and mGluR1 α^- UBCs composed 70% and 30% of the UBC population, respectively (Diño and Mugnaini, 2008; Kim *et al.*, 2012). In the DCN, based on their response to glutamate puff or synaptic stimulation, we found a division of 61% mGluR1 α^+ (n=128 cells) and 39% mGluR1 α^- (n=82 cells).

Despite the presence of mGluR1 α -mediated currents in ON cells, the mGluR1 α antagonist LY367385 had no effect on the charge of current elicited by a single stimulus, while NBQX fully blocked the response (99.3% blocked; $p < 0.0001$, n=5) (Fig 1.4D,G). However after a train of 20 stimuli, LY367385 blocked 32.5% of the charge ($p = 0.0016$, n=5), while NBQX blocked the remainder of the response (97.0% blocked, $p < 0.0001$) (Fig 1.4E,G). Thus, although AMPARs mediate the majority of the current in the slow EPSC component, mGluR1 α s are synaptically activated, presumably by spillover of transmitter after 20 high-frequency stimuli.

LY367385 also blocked 64.7% of the charge ($p < 0.0001$, n=7) following glutamate puffs. This is roughly twice the proportion of charge blocked by LY367385 after a train of synaptic stimuli ($p = 0.0029$). This difference between response to synaptic and exogenous glutamate suggests that many mGluR1 α are located far from the sites of synaptic contact. As expected, NBQX blocked the remainder of the puff-elicited response (97.8% blocked, $p < 0.0001$, n=7).

Both fast and slow phases of the inward synaptic current of ON cells were entirely blocked by the AMPA/kainate receptor antagonist NBQX, in combination with LY367385 (Fig. 1.4D-G). Moreover, the AMPAR selective antagonist GYKI-53655 (20 μ M) blocked all glutamate responses in the presence of LY367385 (98.2% blocked, $p < 0.0001$, $n=3$). Thus, we find that both mGluR1 α and AMPAR contribute to the excitatory synaptic response of ON UBCs to mossy fiber input, but to different extents depending on the frequency of presynaptic activity.

Since mGluR1 α is a selective activator of ON UBCs, we investigated the effect of ON UBCs on DCN granule cells. We used long DHPG puffs to activate a higher number of UBCs in the deep layer of the DCN and recorded ESPCs from granule cells, which are mGluR1 negative and therefore cannot be directly activated by DHPG (Fig 1.S3A,B). With a DHPG puff, we expected to see an increase in the number of spontaneous EPSCs in those granule cells connected to an ON UBC. Since this is a feed-forward excitatory connection, the DHPG effect would thereby be blocked by the glutamate receptors AMPAR/NMDAR antagonists NBQX and (R)-CPP, respectively. This prediction was verified in 3 of 26 patched granule cells, as shown in Fig 1.S3C, suggesting that ON UBCs relay prolonged excitation to granule cells with a ~ 0.12 connection probability. This value could be an underestimate, since UBC axons are often severed during brain slicing. Nevertheless, the data suggest that ON UBCs project to and strongly activate a select group of granule cells, consistent with results in cerebellum (Schwartz et al., 2012).

ON and OFF UBCs of cerebellum

All previous studies of UBC physiology have been done in cerebellum. However, the initial studies of mossy fiber-UBC synaptic transmission (Rossi *et al.*, 1995; Kinney *et al.*, 1997; Billups *et al.*, 2002) were done prior to subtype characterization, and only the ON UBC was described. Since then, one other study of cerebellar UBCs investigated synaptic kinetics, again only describing ON UBCs (van Dorp and de Zeeuw, 2014). We therefore sought to determine whether the ON and OFF responses are a feature of all UBCs, and not specific to UBCs in the DCN, by examining the glutamate sensitivity of UBCs in the cerebellum. In rodents, UBCs are concentrated in the vestibular cerebellum (Diño *et al.*, 1999; Takács *et al.*, 1999), and therefore recordings were made from UBCs in lobe X. As in DCN, the response to glutamate was correlated to the (S)-3,5-DHPG response for subtype identification. Cerebellar UBCs also showed distinct ON and OFF responses (Fig 1.5Ai and 1.5Bi) with the same current profiles and corresponding effects on intrinsic firing, as in DCN. Only ON UBCs had inward currents elicited in response to puff application of (S)-3,5-DHPG (mean amplitude $-15.3 \text{ pA} \pm 2.9 \text{ pA}$; half-width $1.7 \pm 0.27 \text{ s}$; 10-90% rise time $1.2 \pm 0.18 \text{ s}$; $n=8$ ON UBCs). OFF UBCs did not respond to puffs of (S)-3,5-DHPG (currents $< 2 \text{ SD}$ of the baseline noise; $n=6$; Fig 5Aii and 5Bii). Thus, in both the DCN and cerebellum, UBCs comprise two populations, defined by their ON or OFF response to glutamate.

The histogram in Figure 5C shows the distribution of peak current responses to glutamate puffs for a population of DCN and cerebellar UBCs ($n=182$). The histogram has a clear bimodal distribution; cells identified morphologically as UBCs by dye-fill almost never failed to give a response to glutamate, and for the majority, the slow responses were either inward or outward. Averaging just the negative or positive

responses gave mean amplitudes of -22.2 ± 1.41 pA (n=108) and $+15.2 \pm 1.55$ pA (n=74), affirming that UBCs fall in two classes based on their glutamate response.

mGluR2 mediated outward K⁺ current in ON and OFF UBCs

Cerebellar UBCs express mGluR2 in both calretinin⁺ and mGluR1 α ⁺ subtypes (Nunzi *et al.*, 2002, Russo *et al.*, 2008). Moreover, mGluR2 activate G protein-coupled inwardly rectifying K⁺ (GIRK) currents in UBCs (Knoflach and Kemp, 1998; Russo *et al.*, 2008). We hypothesized that mGluR2 in OFF UBCs bind synaptically released glutamate, leading to activation of GIRK channels and an IPSC. Indeed, when the group II mGluR antagonist LY341495 was applied to the bath, the IPSC was eliminated, revealing a small slow decaying NBQX-sensitive inward current (tau 403.6 ± 137.8 ms, mean charge -1.2 ± 0.4 pC; mean charge in NBQX -0.2 ± 0.07 pC; n=6), a response apparently normally occluded by the larger outward current (Fig 1.6A, C and E). The effect of the mGluR2 IPSP, which blocks intrinsic firing (Fig. 1.2B), was completely prevented by the mGluR2 antagonist LY341495 (Fig 1.6B). These results confirm that an inhibitory mGluR2 is synaptically activated in the OFF UBC subtype.

As with the mGluR1 α synaptic responses in ON cells, an obvious mGluR2 outward current in OFF cells was observed only following train stimulation in control solutions. However, subtraction of currents in the presence of LY341495 from control currents revealed that mGluR2 could be activated even following a single stimulus (Fig. 1.6C). The presence of this current, although small and variable from cell-to-cell (Fig 1.6E; mean 0.199 ± 125 pC, range -0.121 to $+0.683$ pC), indicates that mGluR2 must be positioned close to synaptic sites in order to sense transmitter after a single presynaptic

AP, even though spike trains generate a more physiologically significant mGluR2 response capable of inhibition (subtracted value for trains: 7.0 ± 1.9 pC; Fig 1.6E). In the presence of LY341495 a small inward AMPAR current remained (-1.8 ± 0.38 pC; Fig 1.6C and E), just sufficient to obscure an outward mGluR2 response after single stimuli. This AMPAR response is overwhelmed by the outward current during a stimulus train.

To test whether the IPSC was generated by GIRK channels, voltage ramps were delivered before and during application of the selective group II mGluR agonist LY354740. Subtraction of the two ramp responses revealed the current-voltage relation for the LY354740-sensitive current. This current-voltage relation displayed prominent inward rectification and a reversal potential of -81.4 ± 1.8 mV ($n=8$), close to a calculated E_K of -90 mV (Fig 1.6D). Thus, it is likely that the outward synaptic current in OFF cells is generated by GIRK channels.

It seemed surprising that mGluR2 are expressed in both UBC subtypes (based on mGluR2-GFP expression), yet are only synaptically activated in OFF UBCs. In order to determine whether or not ON UBCs have an mGluR2 gated current, the subtype of UBC was first identified by puff application of glutamate, the puff pipette was then exchanged for one containing LY354740, and the new drug applied for 100 ms in current-clamp and in voltage clamp. In both UBC subtypes, the selective agonist elicited an outward current and a pause in intrinsic firing (Fig 1.6G-H). However, the response in ON UBCs had a mean amplitude of only 6.14 ± 1.71 pA ($n=6$; half-width 1.47 ± 0.95 s; 10-90% rise time 457 ± 193 ms; 10-90% decay time 4.03 ± 2.56 s), leading to a mean pause in firing of 6.9 ± 2.2 s ($n=4$), while OFF UBCs had a mean current amplitude of 14.56 ± 2.75 pA ($n=7$, half-width 6.91 ± 1.7 s; 10-90% rise time 2.07 ± 0.61 s; 10-90% decay time 15.03 ± 2.20 s),

leading to a mean pause in firing of 15.6 ± 2.4 s ($n=5$). Thus mGluR2-activated outward currents are present in both subtypes but produce larger, longer lasting responses in OFF UBCs.

As previously described in cerebellum, the mGluR2 is present at both mGluR1 α ⁺ and calretinin⁺ UBC subtypes (Jaarsma *et al.*, 1998, Nunzi *et al.*, 2002). We confirmed this result by performing immunohistochemical labeling for GFP, mGluR1 α and calretinin, in the mGluR2-GFP mouse line, finding that both mGluR1 α ⁺ and calretinin⁺ UBCs colocalize with GFP (Fig 1.S4). The variation of dendritic brush shape, size, and distance from the soma was similar in both subtypes, as shown in Fig 1.S4 B and D. Examples of UBCs in Fig. 1.S4Bi-iii and Di-iii show that UBCs appear similar, but are molecularly distinct, in line with findings in cerebellar UBCs (Nunzi *et al.*, 2002). It remains to be determined whether the axonal projections of these subtypes may differ.

Correlation of ON and OFF UBC physiology with known UBC subtypes

We next directly correlated the ON and OFF phenotype with immunohistochemically defined calretinin⁺ and mGluR1 α ⁺ UBC populations (Nunzi *et al.*, 2002; Diño and Mugnaini, 2008; Sekerková *et al.*, 2014). Each patched UBC was identified as ON or OFF with a glutamate puff. The patch pipette solution contained biocytin, enabling identification of the cell after fixation and processing of tissue (Fig 1.7A and B, left panels). Each brain section was labeled with streptavidin-conjugated Alexa Fluo 488 to resolve biocytin, and a primary antibody to mGluR1 α with a Cy3 secondary antibody, as well as a primary antibody to calretinin with Alexa 647 secondary antibody. ON UBCs colocalized with mGluR1 α but not with calretinin, while OFF UBCs

colocalized with calretinin but not with mGluR1 α (Fig. 1.7). In some cases, OFF UBCs did not colocalize either marker (Fig 1.S5B, top 2 cells). In these cases, the recording time lasted for over 10 minutes, and we suspect that calretinin was dialyzed by the patch pipette solution; indeed endogenous calcium buffers are known to quickly (< 5 minutes) dialyze out of cells during whole-cell recordings (Müller *et al.*, 2005). When cells were recorded for only ~ 3 minutes, we were apparently able to retain calretinin, finding that OFF cells do express calretinin (Fig 1.7B and 1.S5B), and ON cells do not (Fig 1.7A and 1.S5A).

Excitability of ON and OFF UBCs

Both UBC subtypes generated spontaneous APs but at slightly different frequencies (OFF UBCs: 5.9 ± 0.6 Hz, n=16; ON UBCs: 4.1 ± 0.5 Hz, n=15; difference $p < 0.05$) (Fig 1.8A,B). Moreover, the input resistance of UBCs was quite high, averaging 987 ± 47 M Ω s for ON UBCs (n=18) and 895 ± 38 M Ω s for OFF UBCs (n=16; $p = 0.25$, not significantly different). Together, these intrinsic properties rendered UBCs exquisitely sensitive to small synaptic and glutamate-evoked currents. Indeed, changes in bias current of just a few pAs exhibited clear effects on firing rate (Fig 1.8B).

After the OFF response, AP firing resumed but transiently at a higher rate than baseline, particularly after glutamate puffs or larger IPSPs (Fig 1.2B,D). This delayed excitation might reflect either a secondary excitatory action of glutamate or an intrinsic response to a transient hyperpolarization. Consistent with the latter, cerebellar UBCs express ion channels appropriate for rebound firing, such as T-type Ca²⁺ channels (Diana *et al.*, 2007; Birnstiel *et al.*, 2009) and hyperpolarization-activated currents (I_h) (Russo *et*

al., 2007; Kim *et al.*, 2012; Locatelli *et al.*, 2013). To test the idea of intrinsically generated rebound firing, a step-wise hyperpolarizing current ramp was used to mimic the pause in firing in OFF UBCs, and was applied to both ON and OFF UBCs. Both UBC subtypes (n=3 ON UBCs, n=4 OFF UBCs) exhibited similar rebound firing, which was greater and longer lasting for more negative current ramps (Fig. 1.8Ci & 1.8Cii). OFF UBCs displayed rebound firing following a glutamate-activated IPSC even in the presence of the AMPAR and NMDAR antagonists NBQX and R-CPP, respectively (data not shown), arguing against residual excitation by ionotropic receptors. Furthermore, delayed firing could commence even at a time point when glutamate currents (measured in voltage-clamp) were still net outward, suggesting that the current is an intrinsic rebound response (e.g., compare the voltage- and current-clamp traces in Figures 1.2D and 1.5Bi). Thus, both UBC subtypes have the capacity for rebound firing but this feature is only utilized by OFF UBCs due to its glutamate-activated outward currents.

Discussion

This study reveals two classes of UBC that differ strikingly in their response to mossy-fiber input. The first displayed an inward, biphasic EPSC, similar to the EPSC characterized in cerebellar UBCs (Rossi *et al.*, 1995, Kinney *et al.*, 1997). This ON subtype was mGluR1 α ⁺ and showed an immediate prolonged increase in firing frequency due to a slow EPSC mediated by both AMPARs and mGluR1 α . The OFF subtype had a small inward AMPAR component that was overwhelmed by a larger, slow outward current that paused intrinsic firing, and in some cases led to delayed, rebound firing. This is the first observation to our knowledge, outside of the retina and the well characterized ON and OFF responses of retinal bipolar cells, of a vertebrate cell class with subtypes displaying such opposing responses to glutamatergic input (Fig 1.S6).

Dual action of glutamate and geometry of the synapse

The primary functional difference between the UBC subtypes was the relative magnitudes of AMPAR, mGluR1 α and mGluR2-GIRK-mediated responses to glutamate (Fig 1.S6). The difference in these currents could reflect receptor density or distribution within the area of the subsynaptic membrane. According to Jaarsma *et al.* (1998), although these receptors are expressed at the dendritic brush, neither mGluR1 α nor mGluR2 are associated with the postsynaptic densities but rather are found at nonsynaptic appendages. However the distribution of mGluR2 in this study were not linked to different subtypes. Such a peripheral distribution of receptors is consistent with our observation that mGluR1 α and mGluR2 receptors are activated mainly by train stimuli. The UBC's dendritic brush has fine appendages interlocking with the presynaptic

terminal, and may therefore be exposed to glutamate spillover from synaptic sites. Considering that cerebellar mossy fibers fire at very high frequencies (Rancz *et al.*, 2007, Ritzau-Jost *et al.*, 2014), glutamate released during synaptic activity may spillover to mGluRs on these appendages. Interestingly, we were able to detect tiny mGluR2-mediated currents after a single shock, while mGluR1 α required a train of stimuli. This suggests that distribution and location of these receptors may differ, with mGluR2s closer to the site of synaptic contact in OFF UBCs, than mGluR1 α in ON UBCs.

mGluR2 are known to inhibit pre- or postsynaptically, and their presynaptic action in inhibiting transmission in various neurons is particularly well established. However, while their postsynaptic presence has also been shown in various neurons, including UBCs (Knoflach and Kemp, 1998; Russo *et al.*, 2008), synaptic activation of postsynaptic mGluR2 is uncommon (Hull and Regehr, 2012; Holtzman *et al.* 2011; Watanabe and Nakanishi, 2003). However, except for the case of the ON retinal bipolar cell, we are unaware of a vertebrate synapse in which glutamate almost entirely mediates inhibition.

For either subtype, the results we described here suggest that the brush morphology is well suited to the gradual activation of perisynaptic metabotropic receptors and the entrapment of glutamate for prolonged activation of AMPAR (Rossi *et al.*, 1995, Kinney *et al.*, 1997, van Dorp and de Zeeuw, 2014). Electron microscopic studies show this synapse as having extended synaptic clefts but also extended postsynaptic densities and release sites (e.g., Diño & Mugnaini, 2000). Although the amplitudes of the evoked currents generated by this 'giant synapse' are quite small (similar to that of a single-quantal current at the calyx of Held; Ishikawa *et al.*, 2002),

their very long time-courses, combined with the high input resistance of UBCs, seems ideal for generating stable excitatory or inhibitory responses to brief or periodic activation of mossy fibers.

Distinction of UBC subtypes

The initial characterization of UBC subtypes was based on immunohistochemical identification of molecular markers (Nunzi *et al.*, 2002). A recent study further characterized and distinguished the subtypes based on intrinsic properties (Kim *et al.*, 2012). However, there are very few studies of synaptic physiology of UBCs. Although uncorrelated to subtypes, studies of inhibitory transmission also showed differentially targeted subpopulations of UBCs (Dugué *et al.*, 2005). Studies characterizing glutamatergic synaptic inputs to UBCs only reported the postsynaptic current profile of ON UBCs, and our results characterizing mossy fiber input to this subtype showed similar findings to what has been found in cerebellum (Rossi *et al.*, 1995; Kinney *et al.*, 1997, van Dorp and de Zeeuw, 2014). Another recent study reported two different onsets of AP burst responses in cerebellar UBCs, an early onset mediated by ionotropic GluRs and a late onset mediated by H⁺ and TRP currents, both evoked by mossy fiber stimulation (Locatelli *et al.*, 2012). Although that study ruled out the involvement of group I or II mGluRs in the late onset response, it was unclear how they identified the subtypes. By contrast, we distinguished the two UBC subtypes based on mossy fiber glutamatergic input, correlating each receptor's mediated current with their corresponding impact in AP firing. Besides uncovering the OFF UBC response profile,

we found that mGluR1 α and AMPAR conspire together in generating slow excitation specifically in the ON UBC.

Impact of ON and OFF responses to downstream targets

Granule cells integrate different modalities (Arenz *et al.*, 2008; Huang *et al.*, 2013; Sawtell, 2010) relayed by mossy fibers, possibly with different spiking patterns depending on the origin of fibers. Given their spontaneous activity, the long duration of their response to mossy input, and the ON-vs-OFF character of their responses, UBCs could potentially transform signals that converge upon a single granule cell. Moreover, the interaction of UBCs with inhibitory Golgi cells, which may receive input from mossy fibers, UBCs and/or parallel fibers, could also participate in this transformation in complex ways, depending on the circuitry of the local networks.

Like cerebellar UBCs (Russo *et al.*, 2007), DCN UBCs fire spontaneously *in vitro*. While some activity may reflect small leakage currents in the recordings, cerebellar UBCs have been shown to fire spontaneously *in vivo* (Simpson *et al.*, 2005; Barmack and Yahknitsa, 2008; Ruigrok *et al.*, 2011). Such spontaneous activity is critical for the increase or decrease in baseline firing evoked by the glutamate activated currents, characteristic of the ON and OFF responses of each subtype. However, although *in vitro* studies of granule cells have not reported many spontaneous EPSCs, such events have been observed *in vivo* in vestibular cerebellum (Arenz *et al.*, 2008; Arenz *et al.*, 2009). Thus, further *in vitro* studies investigating the impact of ON and OFF responses of UBCs to their downstream targets must take such activity into consideration.

The DCN and the cerebellar cortex are often compared to another cerebellum-like structure, the electrosensory lateral line lobe (ELL) of mormyrid electric fish (Bell *et al.*, 2008; Roberts and Portfors, 2008), a structure believed to generate negative images of predicted sensory input in order to highlight novel sensory input. Cancellation of self-generated commands is mediated by spike-timing dependent plasticity at the granule cells axon (parallel fiber) to medium ganglion cells, the principal neurons in ELL (Bell and Russell, 1978; Bell *et al.*, 1997). This plasticity also happens at the correlate parallel fiber synapses in the DCN, onto cartwheel cells (Tzounopoulos *et al.*, 2004), and in cerebellum, onto Purkinje cells (Safo and Regehr, 2008; Wang *et al.*, 2000).

UBCs in the ELL have recently been shown to play a significant role in the suppression of predicted sensory input (Kennedy *et al.*, 2014). In ELL, UBCs exhibit intrinsic properties similar to mammalian UBCs and may have distinct responses to mossy fiber input. Based on a model paradigm, Kennedy *et al.* (2014) showed that cancellation of natural patterns of self-generated sensory input was slower and less effective in the absence of UBC input to granule cells. By analogy to the ELL, mammalian UBCs might therefore play an important role in plasticity of sensory processing. The DCN, in particular, functions in sound localization, as DCN principal cells are sensitive to the elevation-dependent shifts in spectral notches generated by distortion of sounds by the pinna (Oertel and Young, 2004). The function of multisensory input to DCN remains somewhat speculative. Primary sources consist of proprioceptive signals originating from the trigeminal sensory structures and dorsal column nuclei (Shore *et al.*, 2000; Zhou and Shore, 2004; Haenggeli *et al.*, 2005; Itoh *et al.*, 1987; Li

and Mizuno, 1997), with contributions from other regions, such as vestibular nucleus (Burian and Gstoettner, 1988; Bukowska, 2002).

In cerebellum, UBCs are distributed among cerebellar lobes in a species dependent manner. In carnivores and primates they are located in areas involved in modulation of sensorimotor transformation. However, as a general principal, UBCs are primarily concentrated in vestibular cerebellum of most mammalian species, particularly in rodents (Diño *et al.*, 1999). In the context of vestibular function, Arenz *et al.* (2008), showed *in vivo* that granule cells in mouse flocculus can receive input from different sources. Moreover, with isolated horizontal canal stimulation at the time of recordings, granule cells have increased or decreased EPSC frequency, depending on the direction preference of that cell. For example, cells may have more EPSCs during ipsilateral movement and cessation of EPSCs with contralateral movement from a centered position, or vice-versa depending on the cell. Since UBCs relay feedforward input from mossy fibers, and their ON and OFF responses have opposing polarities, they may play a role in aiding this bidirectional response of granule cells to encode direction of motion. Establishing the sources of mossy input to ON versus OFF UBCs, in both DCN and cerebellum will aid in predicting the impact of multisensory input to sound localization and cerebellar function.

Acknowledgements

This study was funded by National Institutes of Health (N.I.H) Grants NS028901 and DC004450 (PI: L.O.T); NIH-National Institute on Deafness and Other Communication Disorders Fellowship F31 DC012454 and N.L. Tartar Trust Fellowship (PI: C.B.M); P30DC005983 (PI: Gillespie, Peter) and P30 NS061800 (PI: Aicher, Sue). We would like to thank Dr. Craig Jahr and members of the Trussell Lab for helpful discussions. The authors declare no competing financial interests.

Figure 1.1

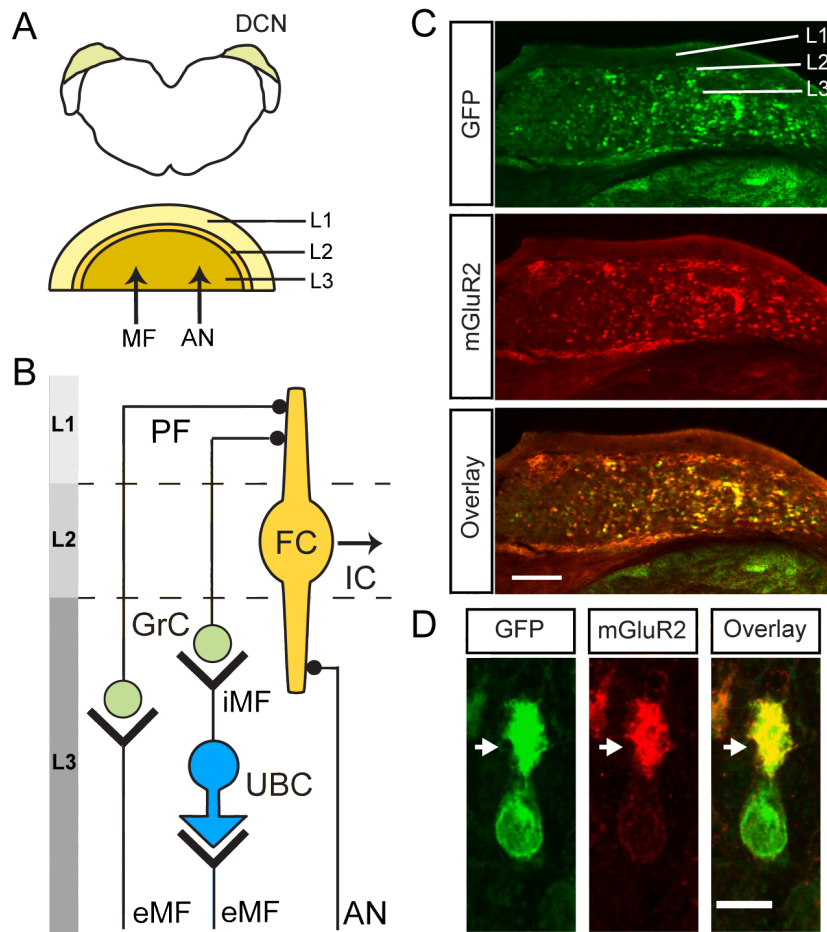


Figure 1.1. UBC localization in the DCN. (A) Location of the DCN (yellow) in the brainstem (top), and the three components of DCN (bottom) comprising the molecular superficial layer (L1), principal cell body cell layer (L2) and deep layer (L3), the latter receiving multisensory input via mossy fibers (MF) and auditory input from the auditory nerve (AN). (B) The cerebellum-like organization of the DCN: AN fibers project to L3 and contact the basal dendrites of fusiform cells (FC), the output neurons of the DCN, located in L2 and projecting to the inferior colliculus (IC). Extrinsic glutamatergic mossy fibers (eMF) relaying multisensory input, terminate in L3, in large presynaptic terminals.

eMF contact granule cells (GrC) and unipolar brush cells (UBC). UBCs contact GrCs via large glutamatergic intrinsic mossy fibers (iMF). GrC axons project to the molecular layer as parallel fibers (PF) and contact the apical dendrites of FC, as well as other L1 interneurons. Black circles indicate excitatory contacts. (C) Confocal immunofluorescence images of a coronal section of DCN in a mouse expressing GFP under control of the mGluR2 promoter. Top panel shows GFP labeling with Alexa 488 secondary antibody, middle panel shows mGluR2 labeling with Cy3 secondary antibody, and bottom panel shows overlay of the two channels. UBCs are labeled in the L3. Scale bar: 150 μm . (D) High magnification of the image in panel C, shows GFP and mGluR2 co-localization of a labeled UBC. Scale bar: 10 μm . White arrow indicates the dendritic brush.

Figure 1.2

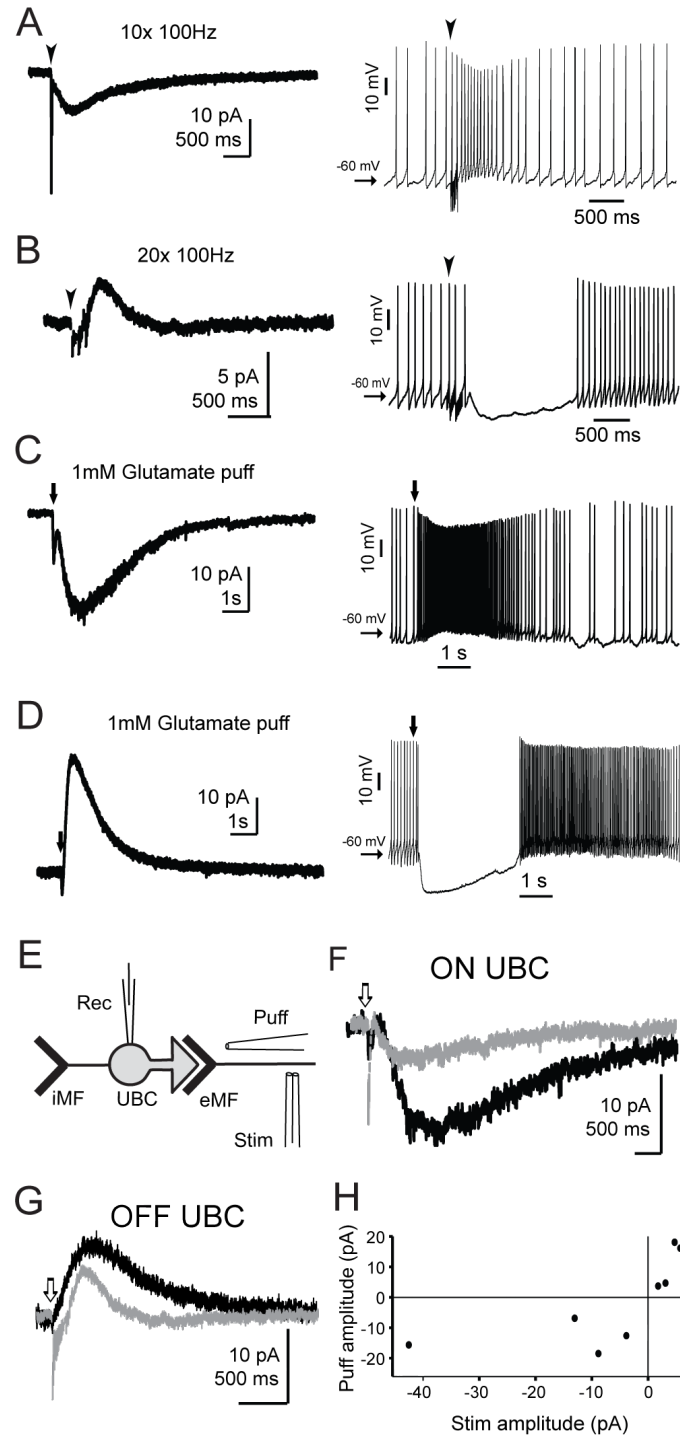


Figure 1.2. ON and OFF responses of UBCs. (A) and (B) Postsynaptic responses to electric stimulation of presynaptic mossy fibers. (C) and (D) Responses to 1 mM glutamate puff application (7 ms, 5 psi). In each panel, left traces are in voltage-clamp and right are in current clamp (no bias current) from the same cells. (A) and (C) Example recordings show an inward biphasic EPSC for two ON cells (fast peak, followed by a sag in the current and a second slow decaying component), which led to prolonged increase in firing. (B) and (D) Example recordings from two OFF cells showing a small, brief inward current followed by a large slow decaying outward component; the latter pauses intrinsic firing. Black arrowheads indicate onset of stimulation in A and B and downward black arrows indicate onset of puff application in C and D. (E) Puff responses correlate with synaptically evoked signals. Diagram of the recording configuration: within the same cell both glutamate puff and subsequent electrical stimulus of presynaptic fibers were performed to confirm the current profiles in ON and OFF UBCs. (F) and (G) Puff responses in black, electrical stimulation in gray. Overlay of traces from an ON UBC in (F) and from an OFF UBC in (G). The white arrows indicate the onset of puff and electrical stimulus (H) Scatter plot comparing the amplitudes of postsynaptic currents in response to synaptic stimulation and amplitude of currents elicited in response to glutamate puff in both ON and OFF cells acquired in the experiments as the ones shown in panels F and G. $N=8$, $r^2=0.48$, $P=0.057$.

Figure 1.3

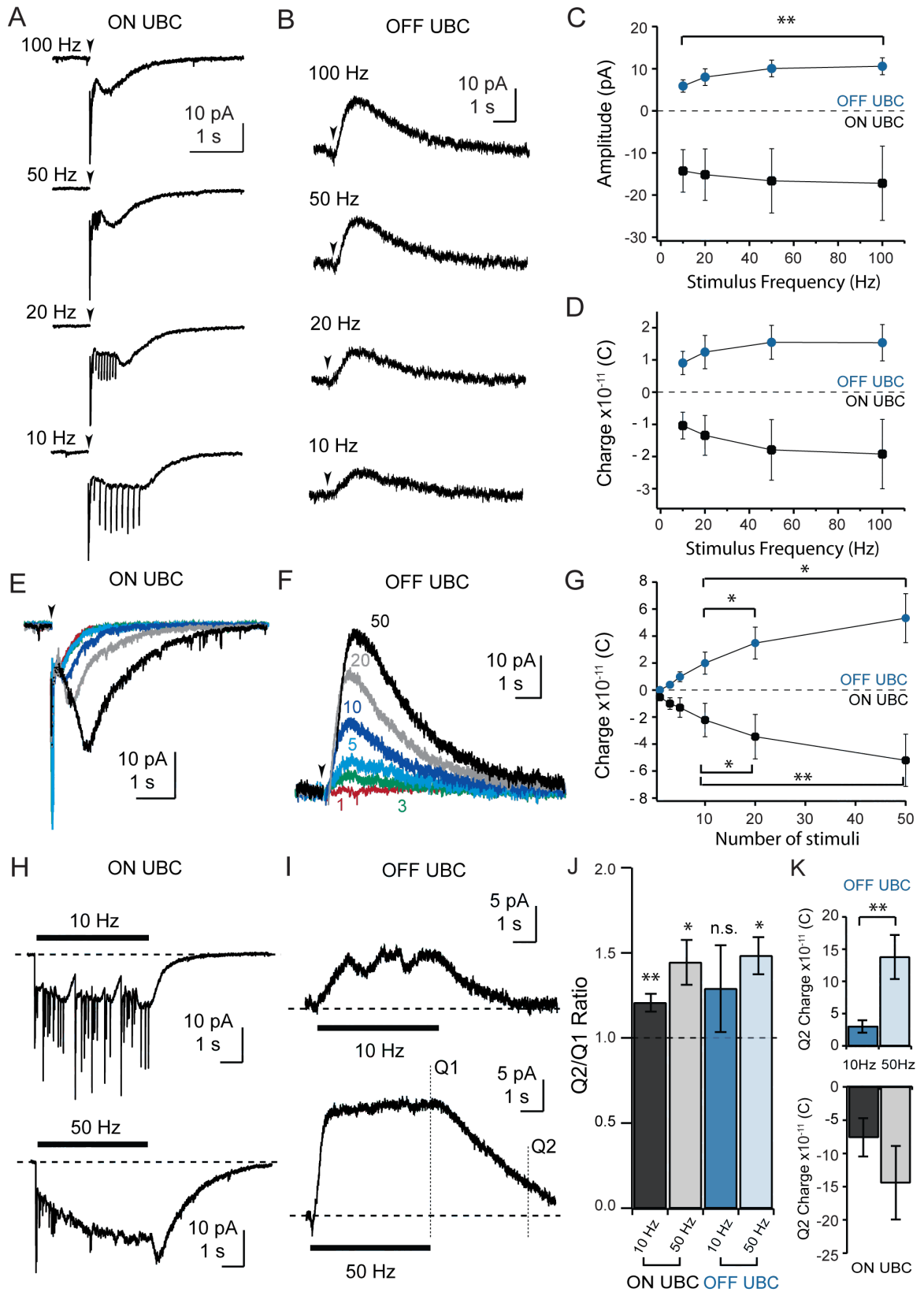


Figure 1.3. Characteristics of responses of ON and OFF UBCs to mossy fiber input. (A) and (B), examples of postsynaptic responses to synaptic stimulation of ON (n=7) and OFF (n=6) UBCs, respectively. A train with 10 stimuli was applied at 100 Hz, 50 Hz, 20 Hz and 10 Hz. Black arrowhead indicates the onset of the stimulus. (C) and (D) Graphic representation of the change in amplitude and charge of both ON (black) and OFF (blue) UBCs with the change of frequency. (E) and (F) Example of postsynaptic responses to changing synaptic stimulation number for ON (n=7) and OFF (n=5) UBCs respectively. A train at 100 Hz was applied with 1 (red), 3 (yellow), 5 (green), 10 (blue), 20 (gray) and 50 (black) stimuli. (G) Graphic representation of the change in charge of the postsynaptic response with the increase in number of stimuli, as shown in E and F for ON (black) and OFF (blue) UBCs. Black arrowheads indicated the onset of the stimulus. (H) and (I) Example of postsynaptic responses to Poisson stimulation trains at 10 Hz and 50 Hz for ON and OFF UBCs. The stimulus duration is indicated by the black bar and lasted 5 s. (J) Comparison of the ratio of the first charge measurement (Q1) taken at the time-point of the last stimulus and the second charge measurement (Q2) taken 4 seconds after the last stimulus. Data for ON (black) and OFF (blue) cells at 10 Hz (darker colors) and 50 Hz (lighter colors) poisson stimulation. (K) Mean charge elicited at Q2 with Poisson stimulation for OFF (blue) and ON (black) UBCs respectively. For 10 Hz OFF UBC n=6, ON UBC n=7 and for 50 Hz OFF UBC n=5 and ON UBC n=6. Error bars indicate \pm SEM and significance level symbols are ns (non-significant, $p > 0.05$), (*) ($p \leq 0.05$), (**) ($p \leq 0.01$).

Figure 1.4

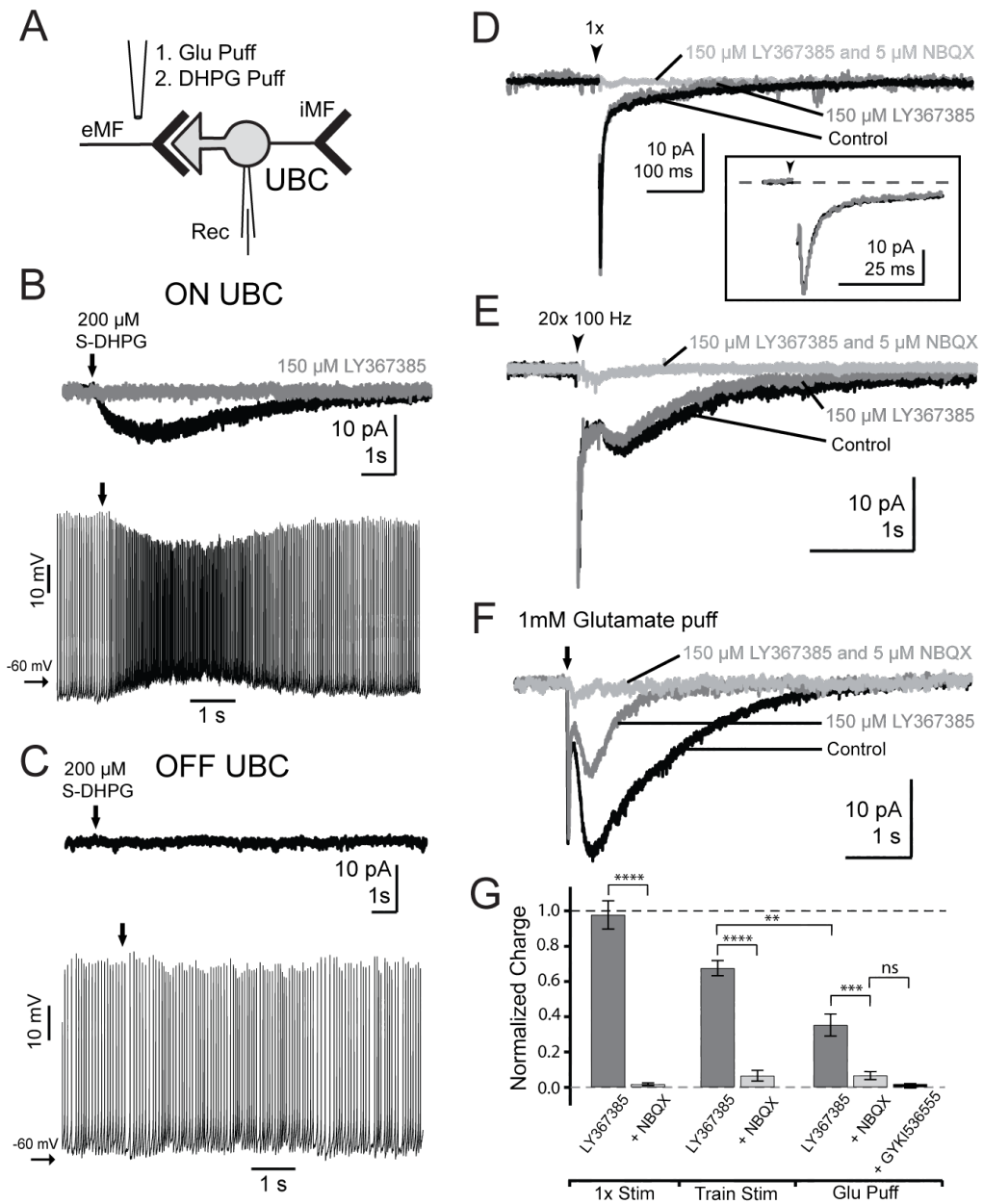


Figure 1.4. ON UBCs are mGluR1 α^+ . (A) Diagram of the recording configuration: whole-cell recording from an UBC: (1) Puff application of glutamate was done to identify the UBC subtype; (2) Subsequently, a puff pipette was exchanged for a pipette containing 200 μ M (S)-DHPG. (B) ON UBC recordings. Top panel: voltage-clamp

recordings and an inward current elicited in response to (S)-DHPG puff (black trace). This current is completely blocked by 150 μ M LY367385 (gray trace). Bottom panel: the pronounced increase in intrinsic firing in response to the (S)-DHPG current. (C) OFF UBC recordings. Top panel: complete absence of currents elicited by (S)-DHPG puff, suggesting this subtype is mGluR1 α negative. Bottom panel: no change in intrinsic firing in response to the puff application of the agonist. Black arrows in B and C indicate puff onset. Puff duration was of 10 to 35 ms depending on the location of the pipette. (D) ON UBC response to a single synaptic stimulus (arrowhead) in control (black), in the presence of the mGluR1 α antagonist LY367385 (dark gray) and in the presence of LY367385 plus 5 μ M NBQX (light gray). LY367385 had no effect on the fast EPSC peak amplitude (inset) and it did not affect the decay time. (E) ON UBC response to 20 stimuli at 100 Hz (arrowhead shows onset of the stimulus) in control (black), in LY367385 (dark gray) and in LY367385 plus 5 μ M NBQX (light gray). LY367385 had a mild affect in amplitude and the decay time of the slow EPSC. (F) ON UBC response to 7-ms puff application of 1 mM glutamate (black arrow shows onset of the puff) in control (black), in LY367385 (dark gray) and in LY367385 plus 5 μ M NBQX (light gray). LY367385 had a clear affect in amplitude and the decay time of the slow EPSC. (G) Histogram of the charge difference between control, LY367385, NBQX and GYKI53655 blocked currents, in ON UBC currents elicited by electrical stimulation, single pulse as in D or train as in E, and by glutamate puff, as in F. Responses were normalized to control of each cell control recording. Error bars show \pm SEM and significance level symbols are: ns, non-significant or ($p > 0.05$), (*) ($p \leq 0.05$), (**) ($p \leq 0.01$), (***) ($p \leq 0.001$), (****) ($p \leq 0.0001$).

Figure 1.5

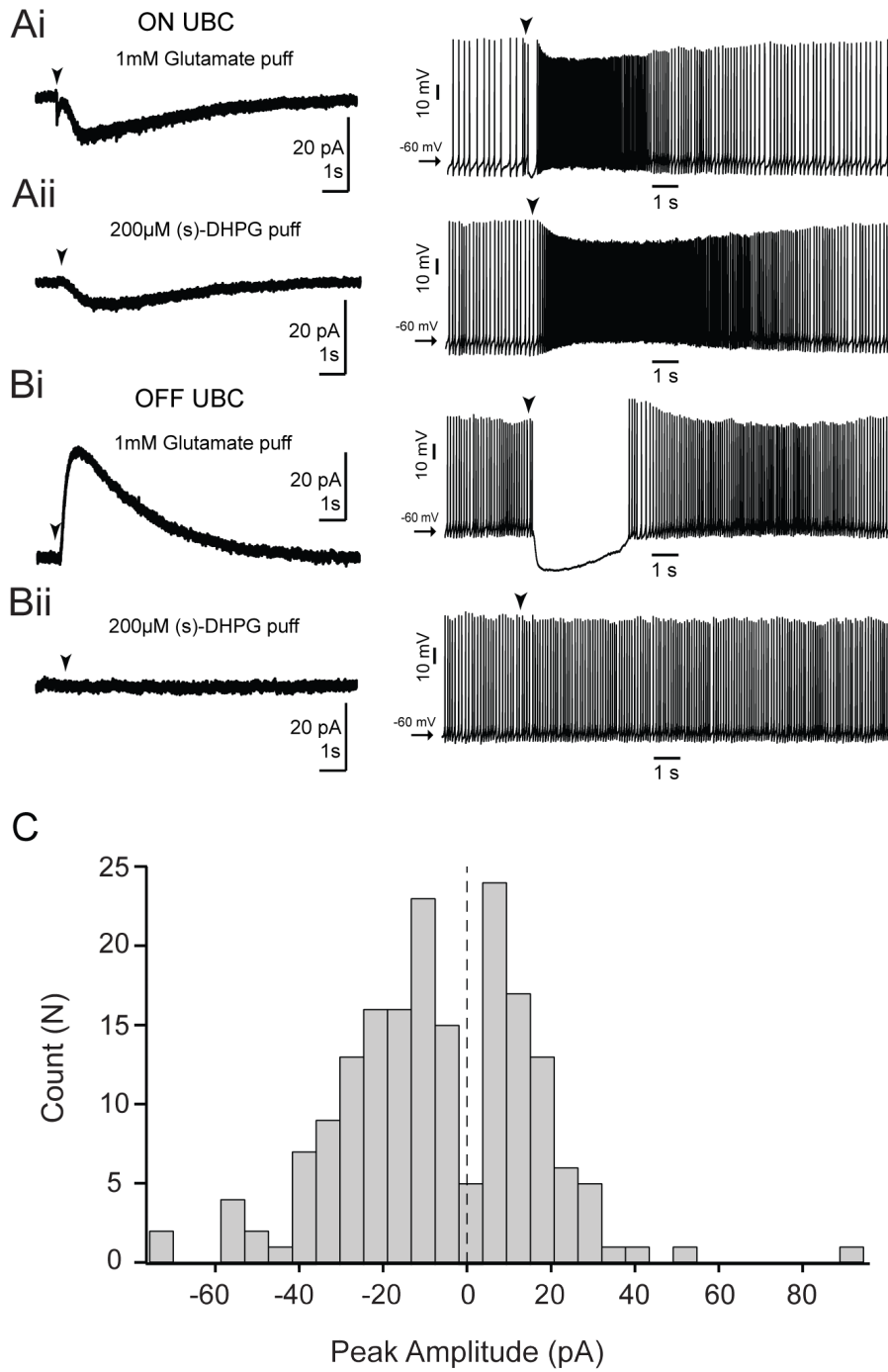


Figure 1.5. Cerebellar UBCs also show either ON or OFF subtypes. Left panels show voltage-clamp recordings and right panels show current-clamp recordings. Arrowheads

show onset of puff application. (A) Responses of a cerebellar ON UBC. (Ai) Biphasic inward response to 1 mM glutamate puff application (7 ms at 5 psi) and the corresponding increase in intrinsic firing frequency. (Aii) Example of a cell with inward current elicited in response to (S)-DHPG puff application and the corresponding increase in firing frequency. (B) Responses of a cerebellar OFF UBC. (Bi) Example of a cell with pronounced outward current in response to 1 mM glutamate puff application and the corresponding pause in firing. (Bii) Absence of any current elicited by (S)-DHPG and no change in intrinsic firing frequency after the puff. (C) Histogram showing the distribution of peak amplitudes of puff responses for 182 UBCs from both cerebellum and DCN.

Figure 1.6

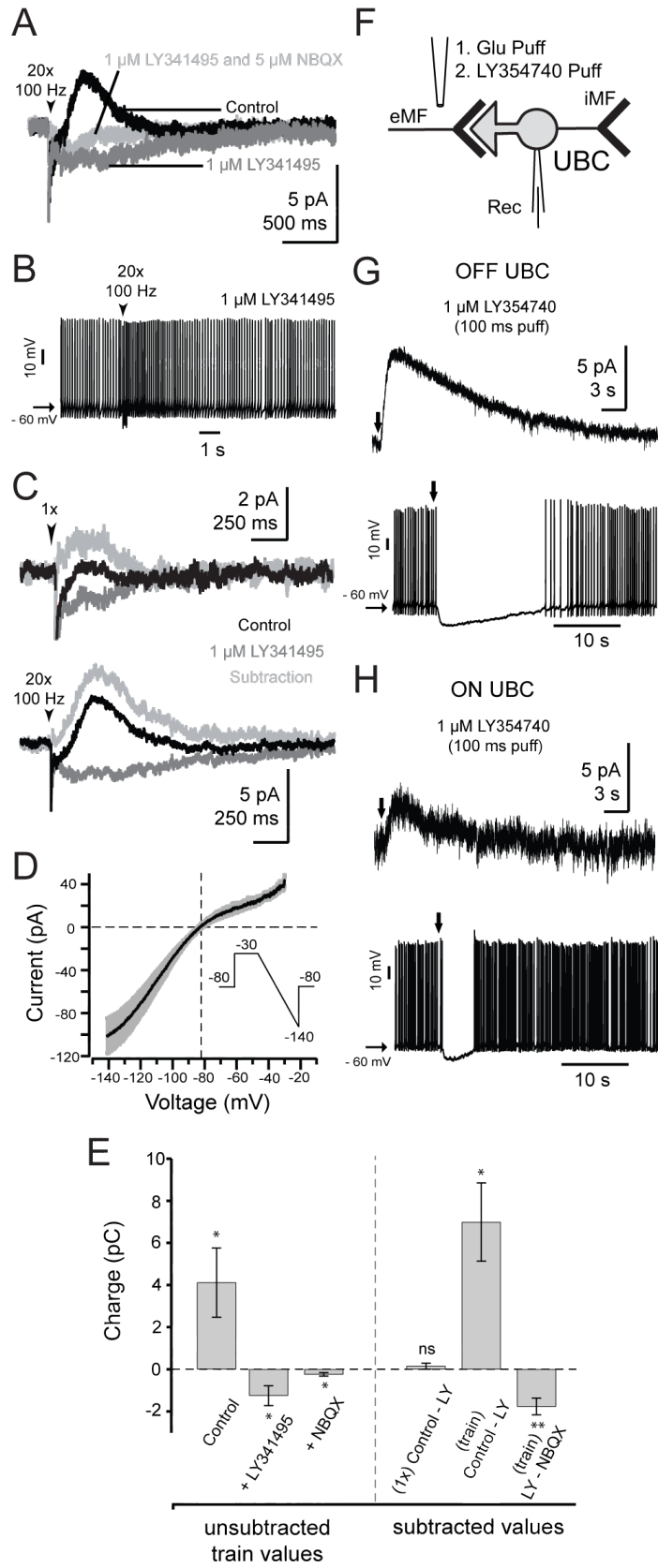


Figure 1.6. Synaptic activation of mGluR2 receptors in OFF UBCs. (A) voltage-clamp recording of an OFF UBC in response to 20x 100 Hz stimuli (arrowhead indicates onset of the stimulus) in control (black), in the presence of LY341495 (dark gray) and in LY341495 plus NBQX (light gray). LY341495 completely blocked the IPSC and revealed an occluded inward current that was blocked by NBQX. (B) Response of the same cell to electrical stimuli with absence of the pause in firing in the presence of LY341495. (C) Top panel: OFF UBC response to a single synaptic stimulus and bottom panel: OFF UBC response to a train of stimuli (arrowhead indicates onset of the stimulus). Both panels show the current in control (black) and in the presence of group II mGluR antagonist LY341495 (dark gray). The subtraction of the response in the antagonist from control is shown in light gray, making evident the current blocked by the antagonist. (D) I/V curve obtained with a current ramp from -30 mV to -140 mV, showing inward rectification and a reversal potential of -81.4 ± 1.8 mV, close to the calculated reversal potential of K^+ under our recording conditions. Gray shading shows \pm S.E.M. (n=8) (E) Histogram of the charge difference between control, plus LY341495 and NBQX blocked currents in OFF UBC. Unsubtracted values show the overall charge measurements after a train of stimuli, measured after the last stimulus artifact. Subtracted values show the charge values of the subtraction of LY341495 from control after a single stimulus or after a train, respectively, without the stimulus artifact. The last bar shows the absolute NBQX blocked current charge, as the subtraction of the NBQX response from the response in LY341495. Error bars show \pm SEM and significance symbols are: ns, non-significant or ($p > 0.05$), (*) ($p \leq 0.05$), (**) ($p \leq 0.01$). (F) Diagram of recording configuration for G and H. Glutamate was applied first for subtype identification and

switched to LY354740. (G) and (H) Responses of OFF and ON UBCs to the puff application of the group II mGluR agonist LY354740 in both voltage clamp (top panels) and current clamp (bottom panels). Both UBC subtypes showed an outward current in response to a 100-ms puff and a pause in intrinsic firing. However ON UBCs showed smaller amplitude currents and significantly shorter pause in firing under the same conditions.

Figure 1.7

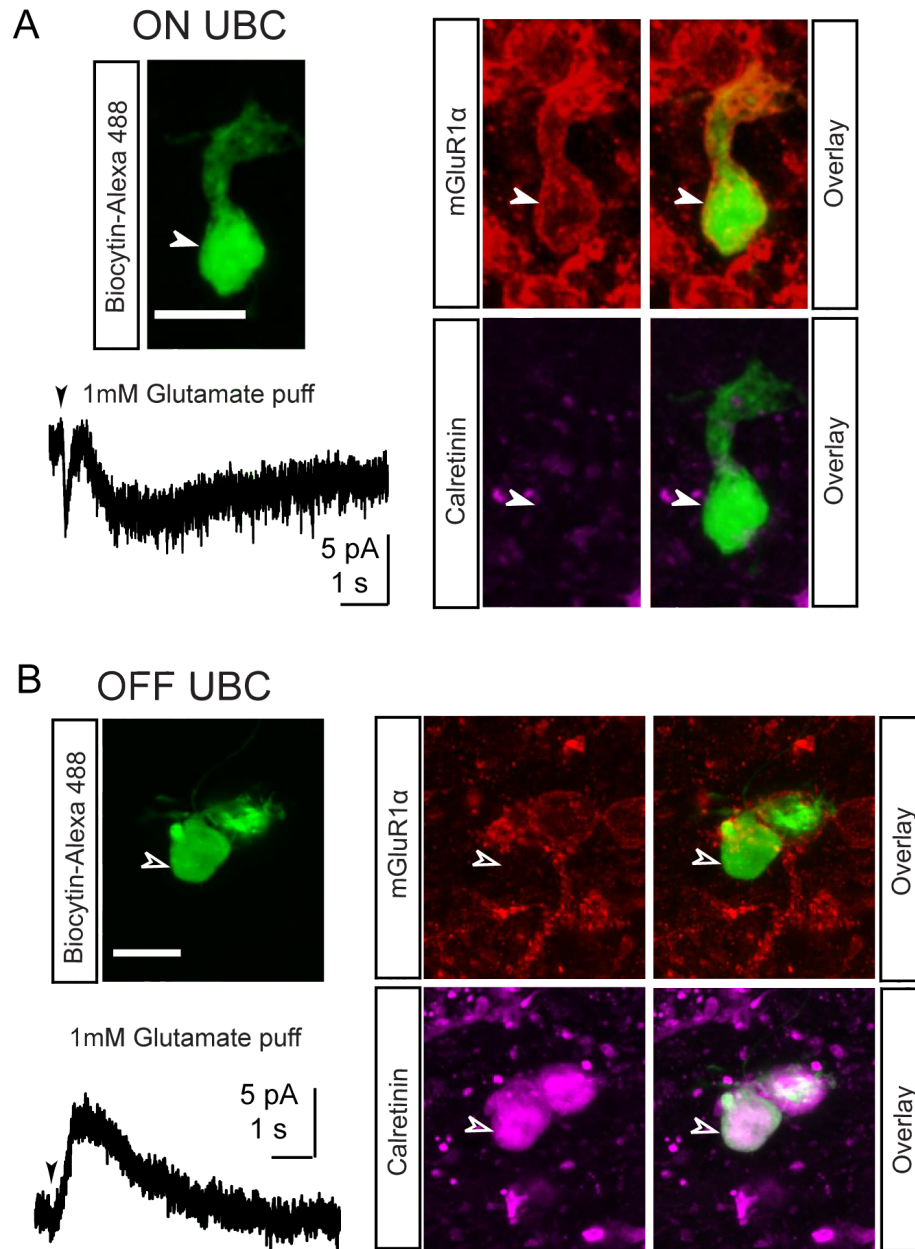


Figure 1.7. Correlation of physiology and UBC subtype with immunohistochemistry. For each (A) and (B) Top left panels shows confocal image of an ON or OFF UBC, respectively, identified by puff application of glutamate shown in the bottom left panel,

patched with biocytin added to the pipette solution. Biocytin was detected with streptavidin-Alexa 488 conjugate. Right panels show confocal immunofluorescence images of the same UBC identified with glutamate puff after triple labeling with streptavidin-Alexa 488 (green), mGluR1 α with Cy3 secondary antibody (red) and calretinin with Alexa 647 secondary antibody (magenta). Scale bar: 10 μ m. Solid white arrowhead indicates ON UBC and open white arrowhead indicates OFF UBC. Black arrowhead indicates onset of the application of glutamate for both ON and OFF UBCs.

Figure 1.8

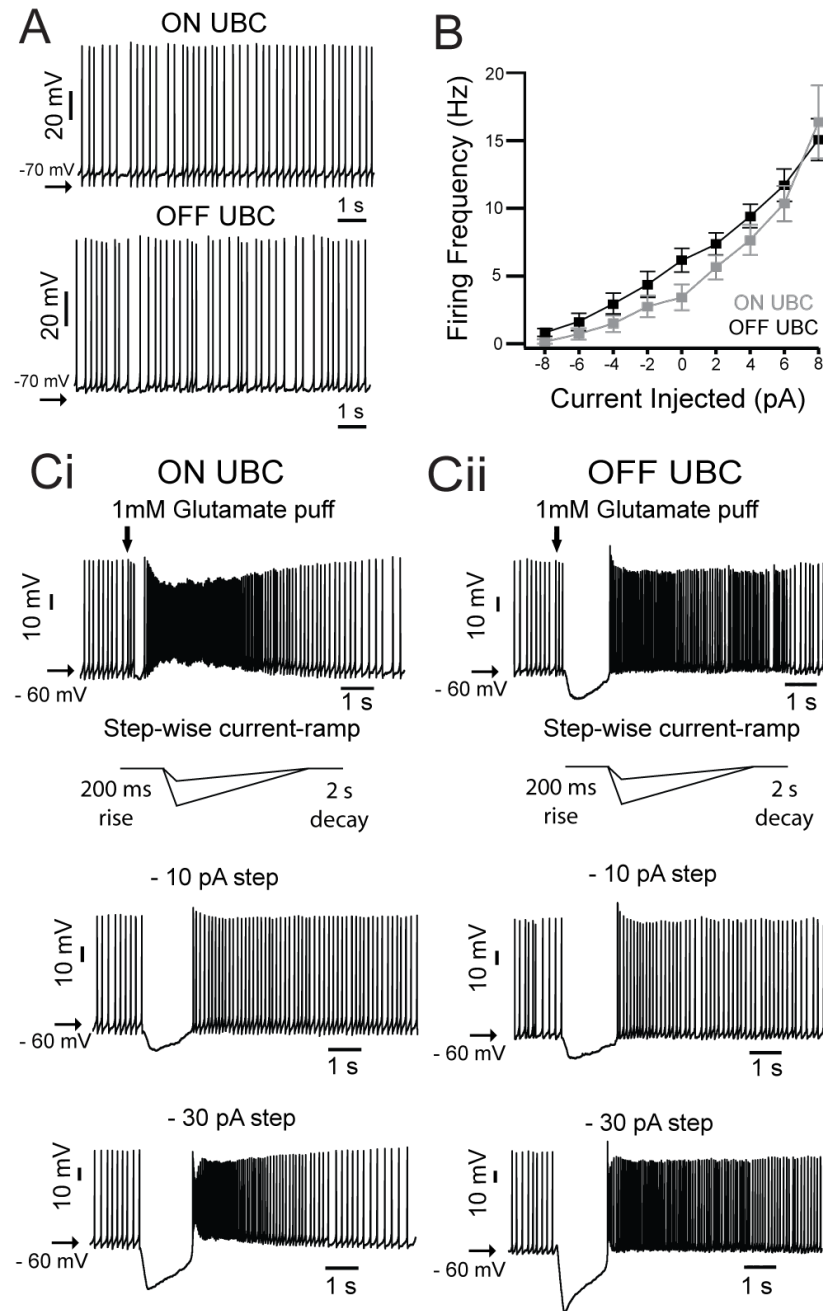


Figure 1.8. Intrinsic firing of ON and OFF UBCs. (A) Example traces of ON and OFF UBCs firing intrinsically with no bias current injected. (B) Change in firing frequency of each UBC subtype in response to 2-pA increment changes in bias current. Samples were

taken from 20-second long sweeps. ON UBC in gray, OFF UBC in black. (C) Top panels: corresponding responses to puff application of glutamate (arrowhead) for subtype identification as ON (Ci) or OFF (Cii) UBCs. A step-wise current-ramp was applied to each subtype with the same protocol of 200-ms rise time, 2000-ms decay time and steps down to -10 pA and -30 pA. The two bottom panels of Ci and Cii show the response to the current-ramp for each subtype. Both UBCs had identical pause in firing and rebound excitation in response to the hyperpolarizing steps.

Figure 1.S1

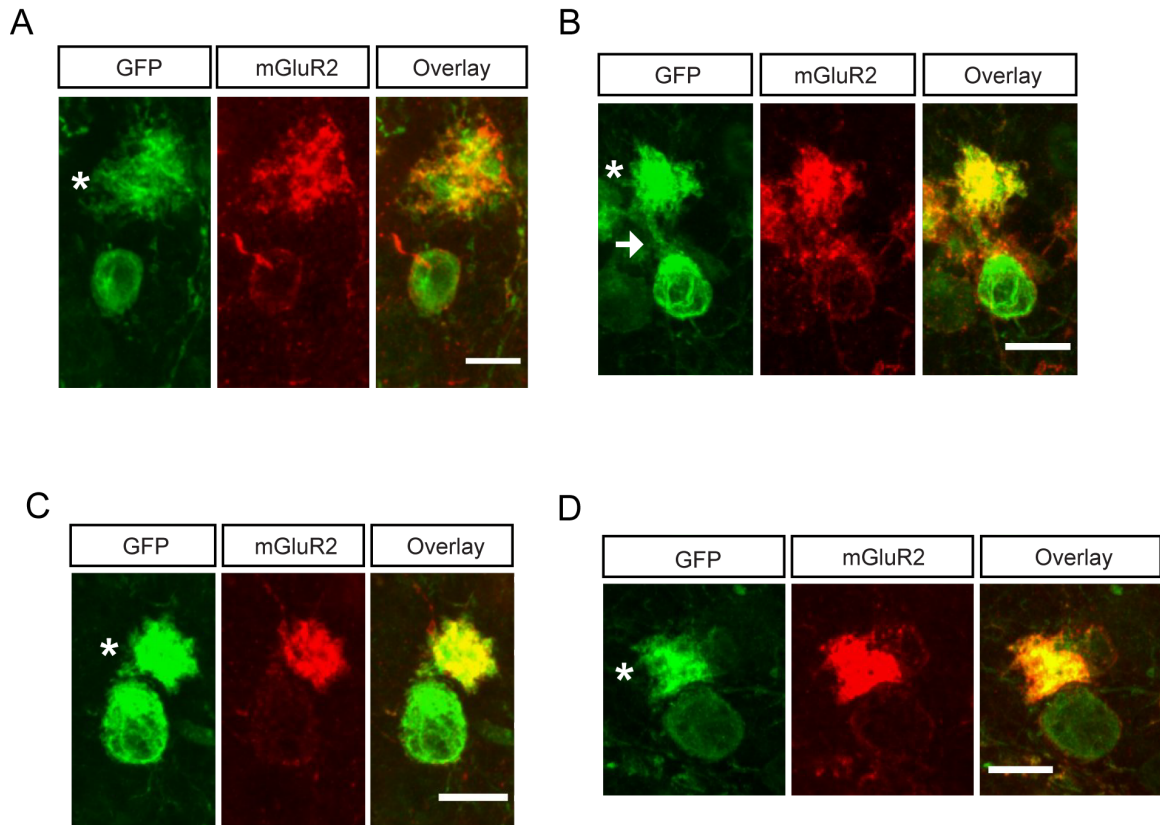


Figure 1.S1. Morphology of UBCs. Additional results related to Figure 1.1. Four cells from the transgenic mouse line that were used for targeted patching of UBCs. As in Fig. 1.1D, these examples show colocalization of GFP (green) with mGluR2 (red), with the third panel of each cell showing an overlay of the two channels. Scale bar: 10 μm . As in cerebellum, DCN UBCs exhibit variation in the size of the dendritic brush (shown by an asterisk in each GFP panel), as well as in the length of the dendritic shaft (better seen in B, shown by the white arrow). The dendritic shaft also apparently varied in thickness. As further shown in figure 1.S5 (supplemental to figure 1.7), this variation is seemed uncorrelated to UBC subtype.

Figure 1.S2

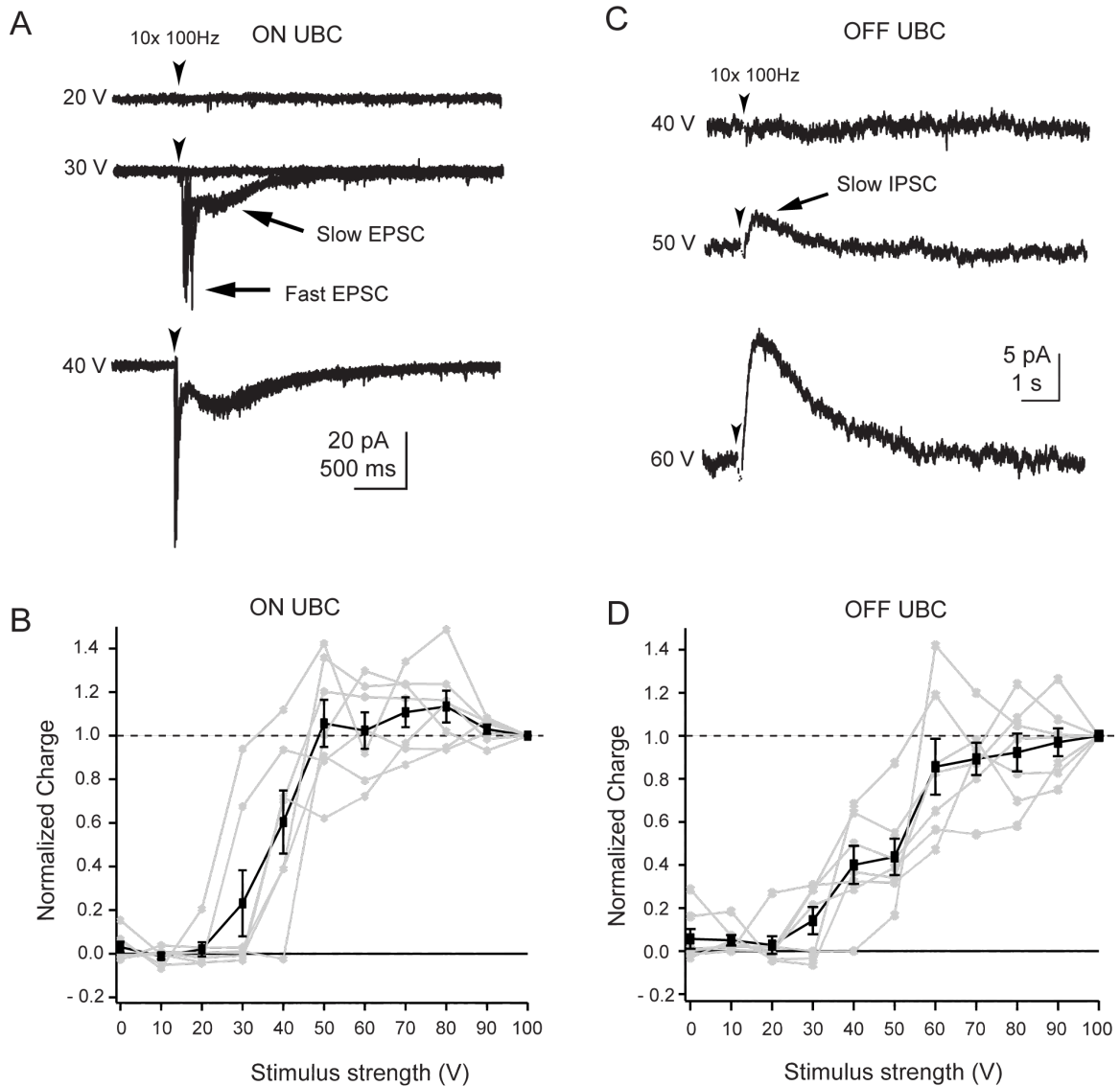


Figure S2. Minimal stimulation of pre-synaptic mossy fiber input to ON and OFF UBCs.

Additional results related to Figure 3. (A) and (C) Example of post-synaptic response to 10 stimuli at 100 Hz with variation of the stimulus strength from 0 to 100 V, at 10 V steps, for both ON and OFF UBCs respectively. In A, the overlaid traces at 30V exemplifies the all-or-none nature of the ON UBC response to the train of stimuli with

successes and failures. The black arrowheads indicate the onset of the stimulus. (B) and (D) The normalized charge measurements to the maximum response at 10 V, of the responses of ON and OFF UBCs to the respective stimulus strength. In cases where there were failures, only successes were used to acquire these measurements. Both ON and OFF UBCs $n = 7$. Average in black, single cells in gray. Error bars \pm S.E.M.

Figure 1.S3

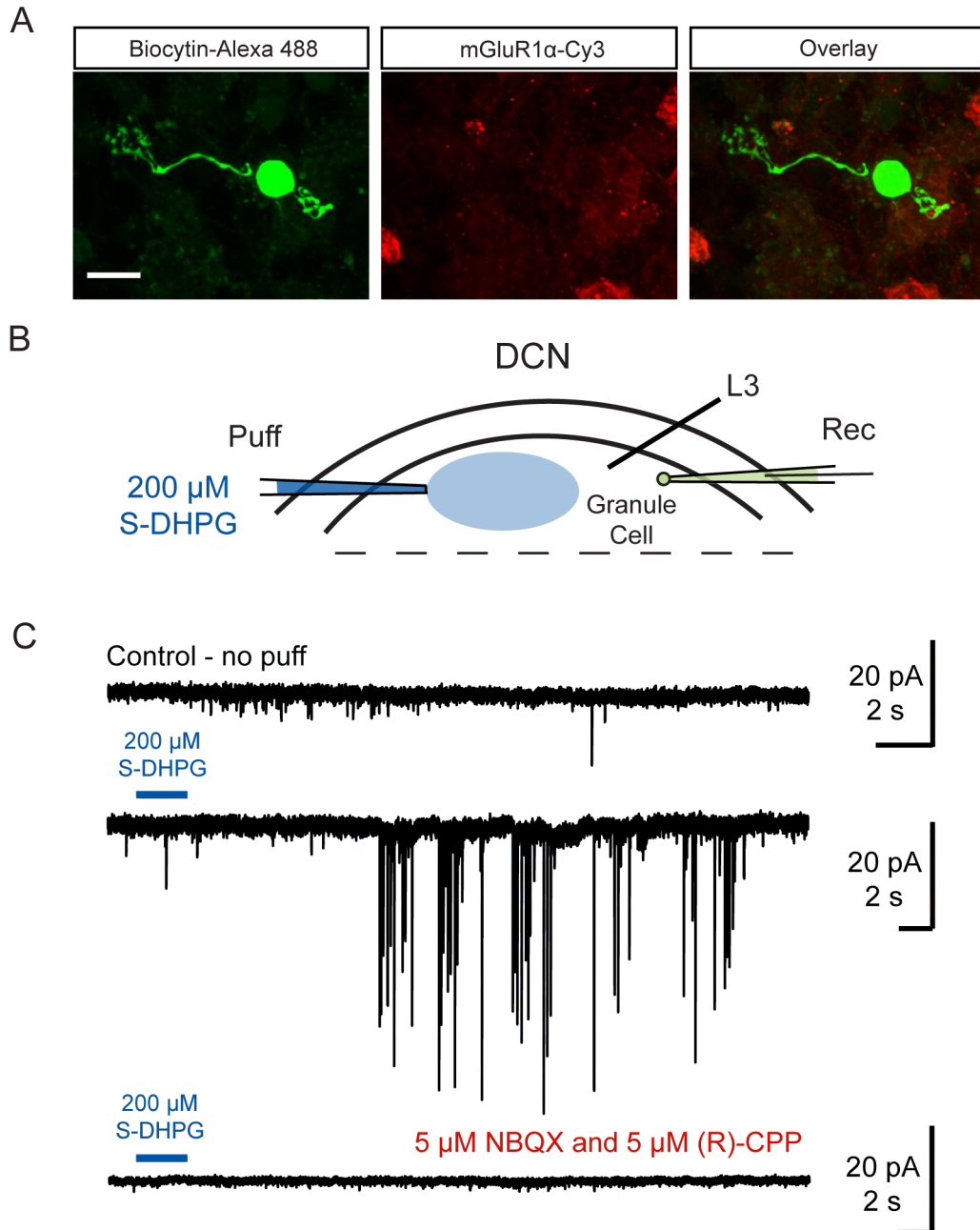


Figure 1.S3. ON UBCs relay feedforward excitation to granule cells in DCN. Additional results related to Figure 4. (A) Left panel shows a biocytin filled granule cell labeled with Alexa-488 streptavidin and middle panel shows mGluR1 α labelling with Cy3 secondary

antibody. The right panel shows overlay of the two channels and no colocalization of mGluR α in the granule cell. Scale bar, 10 μ m. (B) Diagram of the experimental setup. Recordings were made of granule cells in the deep layer of the DCN and DHPG was puffed to activate ON UBCs. (C) Top trace shows example control baseline recording of a granule cell exhibiting period spontaneous EPSCs. Middle trace shows a sharp increase in EPSCs after a 3-second long puff of DHPG in the deep layer (indicated by the blue bar). Bottom trace shows blockade of the DHPG-evoked EPSCs in the presence of AMPAR and NMDAR blockers, NBQX and CPP, respectively.

Figure 1.S4

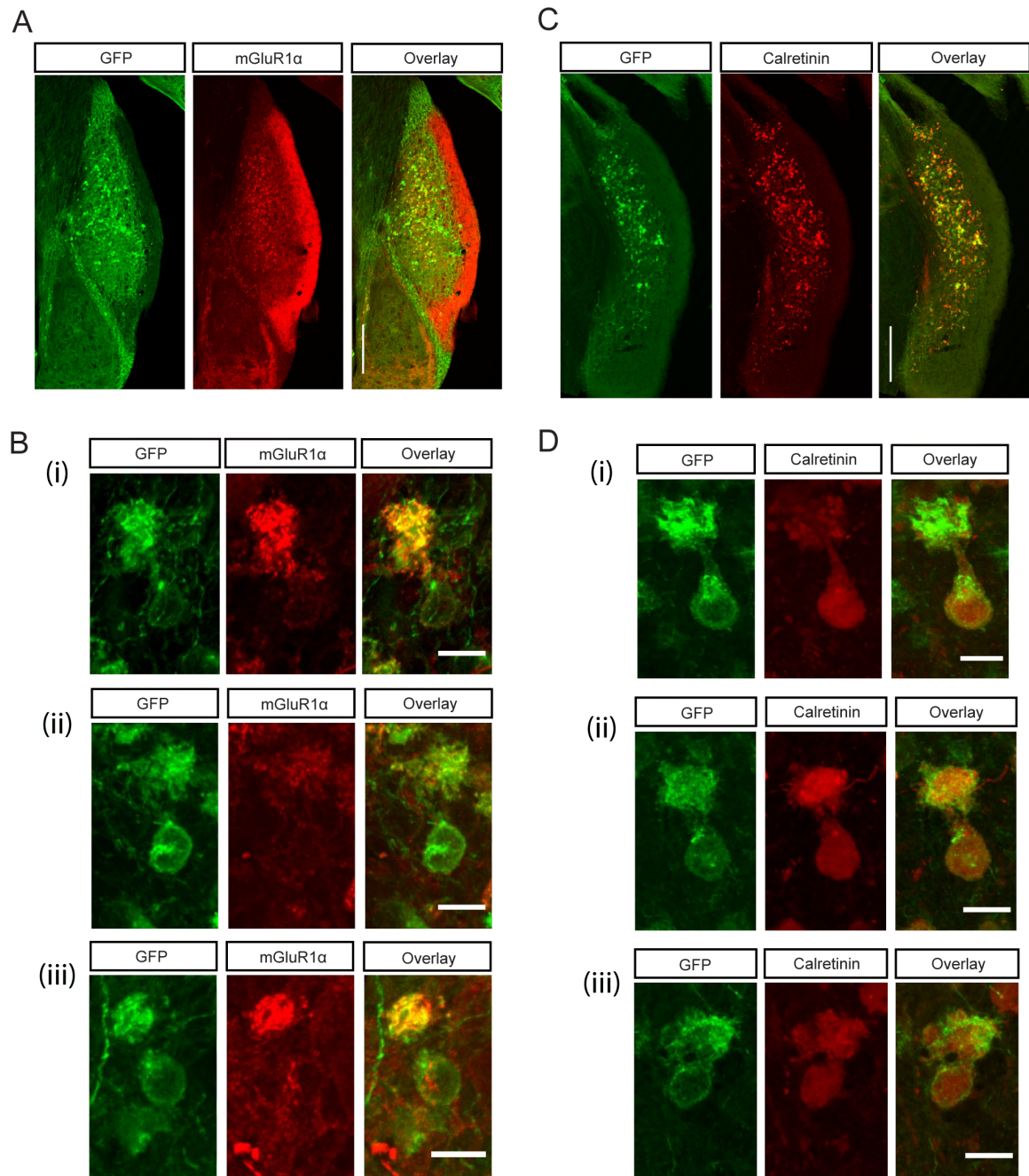


Figure 1.S4. mGluR1 α positive and calretinin positive UBCs colocalize with mGluR2. Additional results related to Figure 1.6. Confocal immunofluorescence images of coronal sections of DCN in a mouse expressing GFP under control of the mGluR2 promoter. (A)

Left panel shows GFP labeling with Alexa 488 secondary antibody, middle panel shows mGluR1 α labeling with Cy3 secondary antibody, and right panel shows overlay of the two channels. Scale bar: 200 μ m. (B) High magnification of the image in A, showing GFP and mGluR1 α colocalization of 3 different UBCs. Scale bar: 10 μ m. (C) Left panel shows GFP labeling with Alexa 488 secondary antibody, middle panel shows calretinin labeling with Alexa 647 secondary antibody, and right panel shows overlay of the two channels. Scale bar: 200 μ m. (D) High magnification of the image in C, showing GFP and calretinin colocalization of 3 different UBCs. Scale bar: 10 μ m. As shown in the high magnification images, mGluR1 α positive and calretinin positive subtypes are not distinguishable by obvious somatodendritic morphological features.

Figure 1.S5

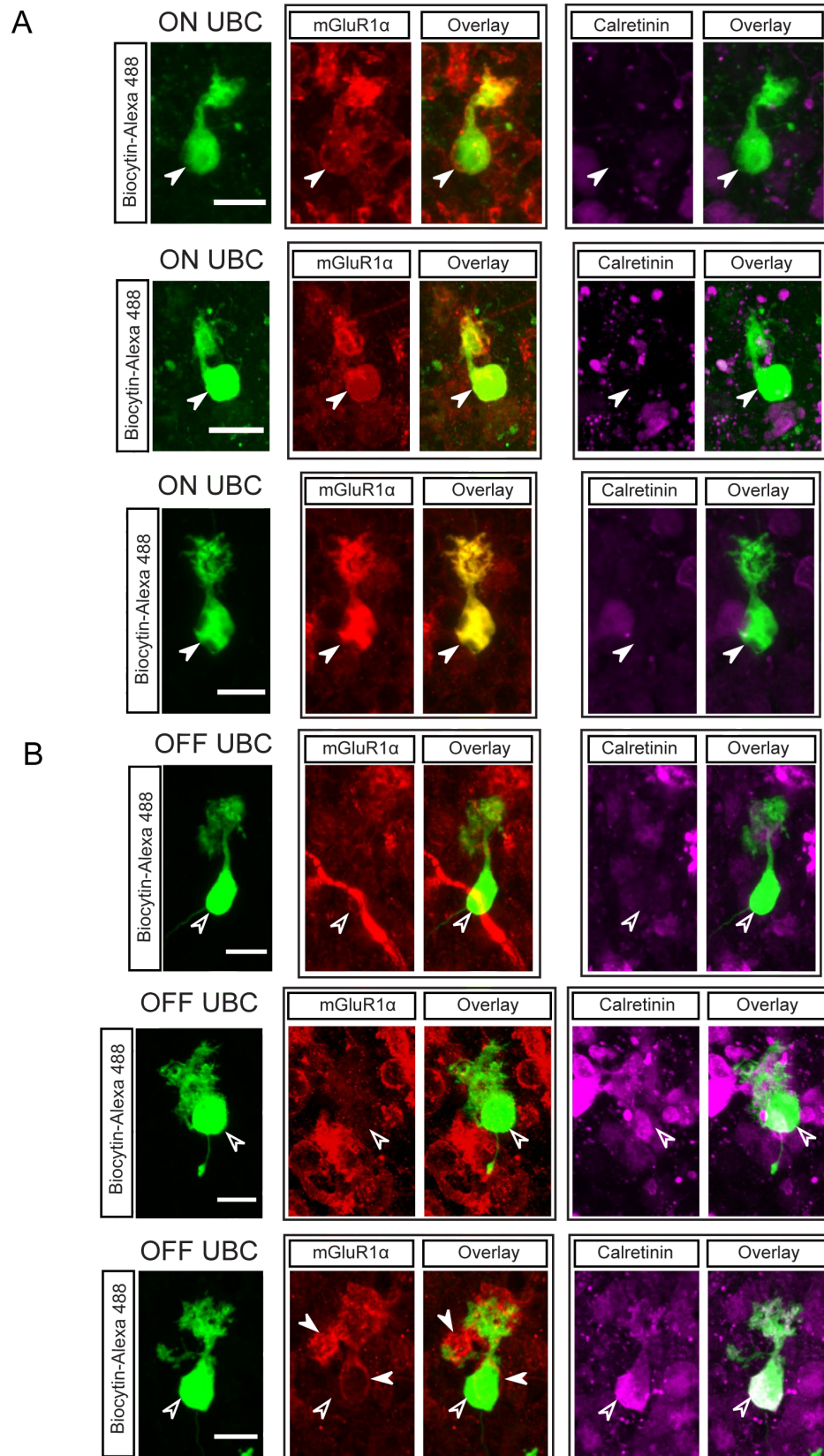


Figure 1.S5. Correlation of physiology and immunohistochemistry for UBC subtypes. Additional results related to Figure 7. Additional examples of UBCs identified as ON or OFF by puff application of glutamate and loaded with biocytin. Following triple labeling, ON UBCs (A) co-label with mGluR1 α and not calretinin. While OFF UBCs (B) do not co-label with mGluR1 α . As described in the text, in some cases with long recordings calretinin was dialyzed after whole-cell mode (see top 2 OFF UBCs in B), but with shorter recordings (< 3 minutes), calretinin remained in the cell and colocalized with OFF cells (Figure 7 and bottom cell in B). In the bottom cell in B, an mGluR1 α + cell was positioned on top of the recorded cell but was clearly distinguished in optical sections. Scale bar: 10 μ m. Solid white arrowhead indicates ON UBC and open white arrowhead indicates OFF UBC.

Figure 1.S6

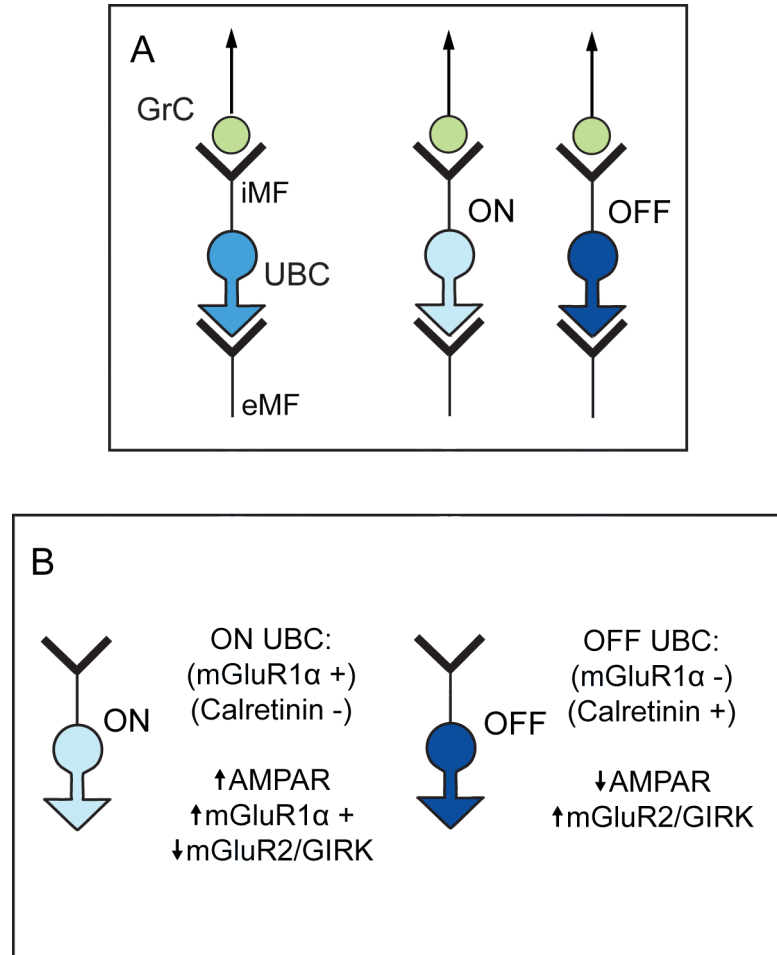


Figure 1.S6. Summary diagram. Additional results related to Figure 1.8. (A) UBCs have two distinct responses to glutamatergic input from mossy fibers - an excitatory (ON) and an inhibitory (OFF) response. (B) ON and OFF responses of UBCs are correlated to subtypes previously established based on the molecular markers mGluR1 α and calretinin.

CHAPTER 2. Maintenance of intrinsic firing in cerebellar unipolar brush cells by ambient glutamate

Carolina Borges-Merjane^{1,2}, Laurence O. Trussell²

¹Neuroscience Graduate Program, Vollum Institute, Oregon Health & Science University, Portland, OR, 97239, U.S.A. and ²Vollum Institute and Oregon Hearing Research Center, Oregon Health & Science University, Portland, OR, 97239, U.S.A

Abstract

Unipolar brush cells (UBCs) are spontaneously firing, glutamatergic interneurons present in cerebellum-like structures and relay multisensory input from mossy fibers to granule cells. UBCs are either excited (ON cells) or inhibited (OFF cells) by mossy input. We report the presence of a cell-specific standing glutamate current in both UBC subtypes that regulates spontaneous firing. We examined the contribution of different glutamate receptors to this standing current and found that receptor blockade changed the spontaneous firing rate, by either hyperpolarizing or depolarizing the cells, according to the receptor and UBC subtype. Blockade of excitatory mGluR1 or AMPA receptors decreased firing in ON cells, and blockade of inhibitory mGluR2 receptors increased firing in OFF cells. Since ON and OFF responses in UBCs, which up- or down-regulate of firing, are directly related to spontaneous firing, this glutamate standing current could be involved in modulating synaptic responses in UBCs. Furthermore we found that the ambient glutamate mediating this standing current to be of vesicular origin. Restricted clearance of glutamate from the mossy fiber-UBC synaptic cleft may thus drive background electrical activity of the UBC as well as shape its response to mossy fiber signaling.

Introduction

Spontaneously firing neurons are ubiquitous throughout the central nervous system (Llinás, 1988; Llinás, 2014). Early studies identified a variety of mechanisms underlying intrinsic spiking: Pacemaking, a well-characterized phenomenon, depends on the hyperpolarization-activated current (I_h), first identified in cardiac cells. For instance, I_h drives spontaneous, rhythmic firing in neurons of the thalamus (Jahnsen and Llinás, 1984; McCormick and Pape, 1990), as well as dopaminergic neurons of the midbrain (Williams *et al.*, 1984; Neuhoff *et al.*, 2002). Other intrinsic firing mechanisms include calcium currents (McCormick and Pape, 1990; Bal & McCormick, 1993; Raman and Bean, 1999; Puopolo *et al.*, 2005) and persistent TTX-sensitive sodium currents (Bevan and Wilson, 1999; Raman and Bean, 1999; Raman *et al.*, 2000; Taddese and Bean, 2002; Do and Bean, 2003).

In particular, several types of neurons in the cerebellum have been shown to display spontaneous firing (Raman and Bean, 1999; Häusser and Clark, 1997; Carter and Regehr, 2002, Forti *et al.*, 2006, Russo *et al.*, 2007). Among these, the glutamatergic interneuron unipolar brush cell (UBC), fires spontaneously *in vitro* (Chapter 1 Figure 5 and 8; Russo *et al.*, 2007; Kim *et al.*, 2012) and *in vivo* (Simpson *et al.*, 2005; Barmack and Yahknitsa, 2008; Ruigrok *et al.*, 2011). Russo *et al.* (2007) demonstrated that a persistent TTX-sensitive sodium current and a ruthenium red-sensitive TRP-like cationic current underlie their intrinsic firing of UBCs. Diana *et al.* (2007) also showed that voltage-gated calcium conductances could contribute to the nature of UBC output – tonic firing or bursts of action potentials. Additional factors contributing to or underlying this intrinsic firing, have not been reported. In this study, we uncover a novel mechanism

wherein background levels of glutamate control the spontaneous firing of UBCs, by means of tonic activation of excitatory or inhibitory glutamate receptors.

We examined the contribution of different glutamate receptors to this standing current in ON and OFF UBC subtypes (described in Chapter 1), and found that receptor blockade changed the baseline current and - more importantly - modulated the spontaneous firing rate. This rate control resulted from either hyperpolarization or depolarization of the cells, according to the receptor and UBC subtype: Blockade of excitatory mGluR1 or AMPA receptors decreased the firing rate in ON cells, and blockade of inhibitory mGluR2 receptors increased the firing rate in OFF cells. Since ON and OFF responses up- or down-regulate spontaneous firing (Chapter 1), ambient glutamate driving background electrical activity may also modulate UBCs response to mossy fiber signaling.

Methods

Animals

Animals used in this study were primarily C57BL/6J wild-type mice and on occasion were from the C57BL/6J-TgN(*grm2-IL2RA/GFP*)1kyo line. In this mouse line, GFP is tagged to human interleukin-2 receptor α subunit with expression driven by the mGluR2 promoter (Watanabe et al., 1998). Both ON and OFF UBCs express mGluR2, thus both subsets are labeled in this line (Nunzi *et al.*, 2002) with GFP targeted to the plasma membrane. They were bred in a colony maintained in the animal facility managed by the Department of Comparative Medicine and all procedures were approved by the Oregon Health and Science University's Institutional Animal Care and Use Committee. All experiments were performed in brain sections from males and females, postnatal days 21 to 32 (P21-32). Synapse formation between the presynaptic mossy fiber terminal and the postsynaptic dendritic brush structure of the UBCs is mature in animals older than P21 (Morin *et al.*, 2001; Hamori and Somogyi, 1983). Transgenic mice were phenotyped by light at P0-P3.

Immunohistochemistry

Mice were transcardially perfused with warm ($\sim 38^{\circ}\text{C}$) 100 mM PBS solution, pH 7.4, followed by ice-cold 4% paraformaldehyde in PBS (PFA). Brains were dissected from the skull and incubated overnight in 4% PFA for complete tissue fixation and rinsed in PBS prior to sectioning. Cerebellum parasagittal sections were acquired at 50 μm on a vibratome (VT1000S, Leica) at room temperature in PBS. After sectioning, the tissue was washed in PBS solution and then incubated for 2 hours in permeabilization solution

(2% fish gelatin, 0.2% Triton X-100, 2% BSA, in PBS). After being washed in PBS again, sections were incubated for 30 minutes in blocking solution (2% fish gelatin in PBS) and subsequently incubated for 48 hours at 4°C with primary antibodies in blocking solution. Sections were again washed in PBS and incubated in blocking solution prior to secondary antibody incubation overnight at 4°C. Finally, sections were washed in PBS, post-fixed in 4% PFA for 1 hour and washed again PBS. Sections were mounted on glass slides and coverslipped using Fluoromount G medium (Southern Biotechnology Associates). For biocytin filled cells, after electrophysiology recordings, cerebellum sections were fixed in 4% PFA overnight and subsequently kept in PBS for no longer than one week before processing as described above. A confocal microscope (Olympus FV1000) was used to acquire fluorescent images, with an oil-immersion objective (10x, 20x, 40x and 60x magnification, numerical aperture 1.42) with Olympus Fluoview-1000 software. Image analysis was conducted using NIH ImageJ software.

Primary antibodies used were chicken polyclonal anti-GFP (1:2000; GFP-1020, AVES LABS) and rabbit polyclonal anti-mGluR2/3 (1:1000; 06-676, Millipore). Secondary antibodies used were donkey polyclonal anti-rabbit Cy3 Conjugate (1:500; 711-165-152, Jackson Immuno Research), donkey polyclonal anti-chicken Alexa Fluor 488 Conjugate (1:500; 703-545-155, Jackson Immuno Research).

Brain slice preparation

Animals were anesthetized with isoflurane, decapitated, and the cerebellum was dissected from the skull under ice-cold high-sucrose artificial cerebral spinal fluid (ACSF) solution containing the following (in mM): 87 NaCl, 75 sucrose, 25 NaHCO₃, 25 glucose, 2.5

KCl, 1.25 NaH₂PO₄, 0.4 Na-ascorbate, 2 Na-pyruvate, 0.5 CaCl₂, 7 MgCl₂ and 5 μM R-CPP, bubbled with 5% CO₂/95% O₂ (Bischofberger *et al.*, 2006). Sagittal cerebellum sections were cut at 300 μm with a vibratome (VT1200S, Leica) in ice-cold high-sucrose ACSF. Slices recovered at 35°C for 30-40 minutes, in ACSF containing the following (in mM): 130 NaCl, 2.1 KCl, 1.2 KH₂PO₄, 3 Na-HEPES, 10 glucose, 20 NaHCO₃, 0.4 Na-ascorbate, 2 Na-pyruvate, 2 CaCl₂, 1 MgSO₄, and 5 μM R-CPP, bubbled with 5% CO₂/95% O₂ (300–305 mOsm). Slices were kept at room temperature (~23°C) until recording. Recordings were performed from cerebellar lobe X, within 6 hours of preparation.

Electrophysiological recordings

During recordings, slices were superfused with recording ACSF (same as recovery ACSF, but lacked R-CPP) using a peristaltic pump (Ismatec) at 2-3 ml/min, and maintained at ~34°C with an inline heater (SH-27B, Warner Instruments). All experiments were done in the presence of 5-10 μM SR95531 and 2 μM strychnine, with the exception of cell-attached recordings in Figure 2.2. The recording set up was composed of a Zeiss Axioskop 2 FS Plus microscope with Dodt gradient contrast optics (Dodt *et al.*, 2002), with 10x and 60x (water immersion) Olympus objectives. An X-Cite 120Q excitation light source through Semrock BrightLine Bandpass filters 469/35 and 525/39, with a 497 dichroic mirror, was used for fluorescent signals visualization. UBCs were initially identified by soma size or GFP fluorescence but intracellular recording solution always contained 20-30 μM Alexa Fluor 488 hydrazide sodium salt (Molecular Probes Life Technologies). Thus, in whole-cell mode UBCs were easily identifiable by

morphology after dye dialysis. UBCs were also readily distinguished from granule cells by electrophysiological properties: intrinsic firing, voltage sag due to hyperpolarization activated current (I_h), and rebound firing following a hyperpolarizing step. Patch electrodes were pulled with borosilicate glass capillaries (OD 1.2 mm and ID 0.68 mm, World Precision Instruments) with an upright puller (PC10, Narishige). For whole-cell recordings, intracellular recording solution contained (mM): 113 K-gluconate, 9 HEPES, 4.5 $MgCl_2$, 0.1 EGTA, 14 Tris-phosphocreatine, 4 Na_2 -ATP, 0.3 tris-GTP (adjusted to 290 mOsm with sucrose), pH 7.2-7.25. All recordings were corrected for a -10 mV junction potential. For cell-attached recordings, pipettes were filled with a solution containing (in mM): 142 NaCl, 2.1 KCl, 1.7 $CaCl_2$, 1.0 $MgSO_4$, 1.2 KH_2PO_4 , 10 Na-HEPES, 11 glucose; adjusted to about 300mOsm, pH 7.35 with NaOH. There were no blockers in the bath during cell-attached recordings. For data acquisition we used a Multiclamp 700B amplifier and pClamp 9 software (Molecular Devices). Signals were sampled at 20-50 KHz, low-pass filtered at 10 KHz and digitized (10 kHz) using a Digidata (1322A, Molecular Devices) analog-digital converter board. Current signals in voltage-clamp were acquired with 5x gain and Bessel filtered at 8-10 KHz, with further filtering applied offline. Patch pipettes tip resistance was 6-8 $M\Omega$; series resistance was compensated with correction 20-40% and prediction 50-70%, bandwidth 2 kHz. Membrane potential was held constant at -70mV, unless otherwise noted. In current-clamp recordings no current was injected, unless otherwise noted. Electrical stimulation was performed with silver wires in theta double-barreled glass electrodes (OD 1.5mm, Sutter Instrument) filled with recording ACSF. Stimuli were evoked using a stimulus generator (Master 8, A.M.P.I.) delivering 200-250 μs duration pulses, and a stimulus isolation unit (Iso Flex, A.M.P.I.),

set to 60-70 V. Puff application of agonists and antagonists were delivered through a Picospritzer II (Parker Instrumentation), at 5 psi, with borosilicate glass capillaries. Glutamate applications were at 1 mM (puff pipette concentration) and 7-10 ms in duration, and were always used prior to recordings for subtype identification. Puff application of control solution without drugs ruled out puff artifacts. The puff pipette was kept >20 μm away from the dendritic brush and soma to avoid mechanical disturbance of the cell following the puff. If puff durations of other drugs were >20 ms, the pipette was moved farther away than 20 μm .

Pharmacology

Agonists and antagonists were delivered by puff or bath application as indicated, and corresponding concentrations are specified under the results section for each appropriate assay. Receptor antagonists: LY367385 (mGluR1 α ; Tocris), LY341495 (group II mGluR; Tocris), NBQX disodium salt (AMPA/KAR; Abcam), (R)-CPP (NMDAR; Abcam). Receptor agonists: (S)-3,5-DHPG (group I mGluR; Tocris), sodium L-glutamate (all glutamate receptors; Sigma-Aldrich). Additionally: cyclothiazide (AMPA desensitization inhibitory; Abcam) and bafilomycin A1 (vacuolar H⁺ ATPase inhibitor; Invivogen).

Data analysis and Statistics

All recordings were analyzed with Clampfit 9 (Molecular Devices) and Axograph X. Graphs were built with IgorPro (WaveMetrics). All data are displayed as mean \pm

S.E.M. and all statistical analysis for one or two sample Student's t-tests were run on StatPlusPro in Excel or on GraphPad Software.

Results

Identification of ON and OFF UBCs in cerebellum

Recordings were made from cerebellum slices, particularly lobe X (Fig 2.1A, 2.1C), primarily taken from wild-type mice, or from transgenic mice with selective expression of GFP driven by the promoter of the receptor mGluR2 (Watanabe *et al.*, 1998; Jaarsma *et al.*, 1998). In this mouse line, GFP co-localizes with mGluR2 and labeled UBCs in the granule cell layer (Fig 2.1C-D), for targeted patching. UBCs could be easily identified in every recording by their distinctive single short dendrite and fine dendritic mesh, visualized either by GFP expression or after cell fills with Alexa Fluor 488 in the internal solution (Mugnaini and Floris, 1994) (Fig 2.1D). We have shown that DCN and cerebellar UBCs have two strikingly different responses to mossy-fiber input, one excitatory (ON UBC) and one inhibitory (OFF UBC) (Chapter 1). These responses correlate with the previously described mGluR1 α^+ and calretinin $^+$ subtypes, and both co-localize with mGluR2 (Chapter 1; Nunzi *et al.*, 2002; Sekerková *et al.*, 2014).

Ambient glutamate desensitize AMPAR-mediated baseline current

During the experimental procedures in Chapter 1, we noticed that 22.2% of ON UBCs (24/108 cells) displayed an outward sag in the current from baseline in response to brief puff applications of glutamate (Fig 2.2A). This apparent outward current was similar in time scale to the current sag between fast and slow inward phases of the ON

UBC EPSCs or glutamate puff response (Chapter 1; Rossi *et al.*, 1995; Kinney *et al.*, 1997; van Dorp and De Zeeuw, 2014), and in current clamp led to a pause in intrinsic firing, while the subsequent slow inward current was associated with prolonged excitation (Fig 2.2A).

Despite the outward current, cells showing this response were in fact ON cells, rather than OFF cells. Just as with the experiment performed in Figure 1.4 of chapter 1, in Figure 2.2A-B, a brief puff of glutamate was applied for subtype identification, and the puff pipette was subsequently replaced with a pipette containing 200 μ M of the metabotropic glutamate receptor group I agonist S-DHPG. In cells with the brief outward current sag, DHPG elicited inward currents with peak (mean peak amplitude -5.96 ± 2.4 pA; n=4) currents significantly greater than baseline (>2 standard deviation of noise) and induced an increase in spontaneous firing frequency (Fig 2.2B).

We have shown that ON UBC synaptic currents are mediated primarily by AMPAR as previously described (chapter 1, Figure 1.4) (Rossi *et al.*, 1995; Kinney *et al.*, 1997; van Dorp and De Zeeuw, 2014). Kinney *et al.* (1997) proposed that the undershoot of the biphasic EPSC in UBCs was due to AMPAR desensitization induced when glutamate was trapped in the synaptic cleft after release. In their model, the subsequent rise in current occurs as glutamate levels fall and receptors sensitivity increases, consistent with non-monotonic dose-response relations (Raman and Trussell, 1992). To investigate the nature of this outward current sag in ON UBCs in response to a brief puff of glutamate, we bath applied 100 μ M cyclothiazide (CTZ), a compound that inhibits AMPAR desensitization. We immediately noticed several striking effects of CTZ. Firstly, the *outward* peak was abolished, and both the inward peak amplitude (control: $-20.90 \pm$

6.3 pA; CTZ: -54.58 ± 9.6 pA; $n=5$, $p=0.0099$) and the charge (control: -69.00 ± 31.1 pC; CTZ: -142.14 ± 40.4 pC; $n=5$, $p=0.0091$) of the inward current were significantly greater than control (Fig 2.3A-D). In Figure 2.3 B, with 2 glutamate puffs 3-seconds apart in control solutions, the second puff occurring at the slow peak of the first response caused an outward current rather than fast inward current, while in CTZ, all the currents were inward. These data suggest that receptor activation, desensitization, and a non-monotonic dose response curve shape the response to the glutamate puff.

However, why is there an outward current during a single puff in these ON cells? An additional effect of CTZ was a significant inward shift in baseline current (control mean baseline: -15.79 ± 3.9 pA, CTZ mean baseline: -39.7 ± 10.3 pA; $n=5$; $p=0.04$; Fig 2.3A-B, 2.3E). This result suggests that, under control conditions, a fraction of AMPARs are already desensitized, presumably by a baseline level of extracellular glutamate. Consistent with this interpretation, bath application of the AMPAR antagonist NBQX ($5\mu\text{M}$) caused the baseline current to shift outward suggesting again, that a fraction of AMPARs were active in control conditions (Fig 2.3F-G). Furthermore, in current-clamp, NBQX decreased the frequency of spontaneous action potentials (Fig 2.3H).

As mentioned above, we noticed the outward current sag after a puff of glutamate in 22.2% of ON UBCs. However, after a train of electrical stimuli (10 stimuli at 50 Hz), we observed an outward sag above baseline current following the initial fast EPSC transient only in a single ON cell (Fig 2.3I, inset Ii). In the presence of NBQX the outward peak was blocked, and 4.9pA of the baseline current was blocked (Fig 2.3I, inset Iii). As shown in Chapter 1 NBQX, blocked the majority of the EPSC elicited in response to synaptic stimuli. The remainder of the current in Fig 2.3I is likely due to mGluR1 α -

mediated currents (chapter 1, Fig 1.4). This suggest that in normal conditions, it would be unlikely that the desensitization sag of ON UBCs would become outward, above baseline. We were able to notice it more commonly with glutamate applications since receptors probably experience high glutamate levels for a longer period during a puff as compared to a synaptic response. Nevertheless, this outward current in puff or synaptic responses indicates the presence of a standing glutamate-mediated current.

In order to further distinguish this ON UBC outward current from OFF UBCs, we compared charge and half-width measurements of both in response to a brief puff of glutamate (Fig 2.4). Although ON UBC outward current charge values ($+2.01 \pm 0.29$ pC; $n=24$; positive charge values under 'out', Fig 2.4B) were significantly less than inward current charge (-84.55 ± 10.3 pC; $n=24$; negative charge values under 'in', Fig 2.4E, $p<0.0001$), ON UBCs outward current charge values were still significantly greater than baseline ($p<0.0001$; $n=24$). As expected, in OFF UBCs the outward current charge ($+24.84 \pm 3.31$ pC; $n=24$; positive charge values under 'out', Fig 2.4B) was significantly greater than inward current charge (-2.19 ± 0.87 pC; $n=24$; negative charge values under 'in', Fig 2.4B, $p<0.0001$). More importantly, the outward charge in OFF UBCs was significantly greater than the outward charge of ON UBCs ($p<0.0001$) by over 12-fold. Furthermore, to emphasize that the kinetics of ON UBC outward current sag is different than OFF UBC outward currents, we measured the half-width of the peak of each (ON UBC mean half-width 165.8 ± 30.1 ms, $n=24$; OFF UBC mean half-width 994.9 ± 160.3 ms, $n=24$) and found them to be significantly different ($p<0.0001$) (Fig 2.4C). OFF UBCs have larger and more prolonged outward current.

We also investigated the sensitivity of OFF cells to CTZ. We described in Chapter 1 that OFF UBCs have inward currents mediated by AMPARs, although these are almost entirely occluded by the dominant mGluR2 mediated GIRK currents. When the characteristic OFF UBC IPSC is blocked by the mGluR2 antagonist LY341495 (Fig 2.4D), we observed two things. Firstly the outward current is blocked as expected, revealing a small inward current as described in the previous chapter. But we also noticed a shift in the control baseline, which became more inward. This suggests that mGluR2s might also be mediating a baseline standing outward current in OFF UBCs; this current will be further investigated in the next section. After blocking mGluR2 with LY341495, we bath applied CTZ and noticed that the small inward current response increased significantly from control (Fig 2.4D-E; mean peak in LY341495 -8.72 ± 3.1 pA and mean peak in LY341495 and CTZ -51.82 ± 12.75 pA, $p=0.011$, $n=5$) as well as a corresponding increase in inward charge (Fig 2.4F; mean charge in LY341495 -7.10 ± 2.8 pC and mean charge in LY341495 and CTZ -94.61 ± 27.0 pC, $p=0.027$, $n=5$), suggesting that a large fraction of AMPARs in OFF cells are also desensitized by background levels of glutamate. In agreement with this finding, we noted a significant increase (mean change in baseline -20.0 ± 7.6 pA; $p=0.047$, $n=6$) in baseline in the presence of CTZ almost as large in amplitude as what we found in ON UBCs (Fig 2.4G), suggesting that OFF UBCs also have a fraction of AMPARs that, although not well activated by the synapse, are constitutively active and desensitized due to the presence of extracellular glutamate.

The experimental procedure of sectioning a mouse brain for electrophysiology recordings can lead to glutamate excitotoxicity. In this pathological process, extracellular

glutamate becomes ubiquitous throughout the tissue. In order to verify that the presence of this glutamate-mediated standing current is not an artifact, we made recordings from granule cells and measured the baseline current in control, and in the presence of CTZ. Granule cells are a reliable control, since they share mossy fiber inputs with UBCs and have well characterized AMPAR currents that can exhibit desensitization (Xu-Friedman and Regehr, 2003; DiGregorio *et al.*, 2007). Thus, we predicted that if the glutamate standing current in UBCs is cell-specific, CTZ would not have an effect in the baseline current of granule cells. We confirmed this prediction, as change in baseline current in CTZ for granule cells was not significant (mean change in baseline -1.76 ± 0.9 pA; $p=0.1206$, $n=6$). The mean change in baseline in granule cells with CTZ was in fact over 13-fold smaller than the effect in ON UBCs and 11-fold smaller than the change in OFF UBCs.

mGluRs also mediate glutamate standing currents in UBCs

We noted in the previous section that bath application of the mGluR2 antagonist LY341495 (Fig 2.4D) resulted on an increase in the baseline current of OFF UBCs, suggesting that mGluRs are also being activated by ambient glutamate and contributing to a glutamate standing current in UBCs. We further investigated the role of mGluRs in mediating this current through mGluR1 α and mGluR2 in ON and OFF UBCs, respectively.

Bath application of the mGluR1 α antagonist LY367385 significantly decreased the baseline in ON UBCs (mean change from control 6.9 ± 0.9 pA; $n=16$, $p<0.0001$; Fig 2.5A and E) and significantly decrease the frequency of spontaneous firing (control

frequency 4.04 ± 1.78 Hz, LY367385 frequency 1.57 ± 0.96 Hz; $n=6$, $p=0.034$) (Fig 2.5B and F), in two occasions completely silencing firing in each cell.

Conversely, bath application of the mGluR2 antagonist LY341495 significantly increased the baseline in OFF UBCs (mean change from control -9.1 ± 1.7 pA; $n=15$, $p<0.0001$; Fig 2.5B and E) and although not statistically significant, in the presence of the antagonist the frequency of spontaneous firing almost doubled (control frequency 7.27 ± 1.90 Hz, LY341495 frequency 11.13 ± 2.27 Hz; $n=3$, $p=0.087$) (Fig 2.5D and G), in one case (not shown), leading the cell into depolarization block. These results suggest that mGluRs also have an important role in maintaining a basal level of glutamate-mediated standing current that can highly influence UBCs threshold for intrinsic firing by either depolarizing or hyperpolarizing each cell accordingly.

Intrinsic firing of UBCs

Cerebellar UBCs exhibit regular firing *in vitro* (Russo *et al*, 2007) and *in vivo* (Simpson *et al*, 2005; Barmack and Yahknitsa, 2008; Ruigrok *et al*, 2011, Kennedy *et al*, 2014). We recently showed in Chapter 1 that DCN UBCs also displayed spontaneous firing *in vitro* while in whole-cell mode. We wanted to verify that intrinsic firing and ON/OFF responses in cerebellar UBCs was present independently of whole-cell recordings. Cell-attached recordings are a less invasive patch-clamp mode that maintains the integrity of the intracellular space, preventing loss of conductances involved in spontaneous firing. However, some problems can arise when cell-attached recordings are used to measure the firing rate of neurons with high input-resistance, such as UBCs (Perkins, 2006; Alcamí *et al.*, 2012). Thus, to minimize these problems, experiments

were made with loose, low-resistance seals (40-75 M Ω), with a Na⁺ based pipette solution and at room temperature. On occasion, when cells formed a gigaseal, the recordings were made in less than 5 minutes after seal formation (Alcami *et al.*, 2012). Spontaneous firing was measured first, prior to glutamate puff application to verify the ON and OFF responses were intact. And after each recording, a tight seal was formed and broken-in for whole-cell dialysis with Alexa 488 in the pipette solution to confirm UBC identify by cell morphology. The glutamate puff application was performed with the pipette a few 10s of microns away from the cell body, in order avoid puff pipette placement near or on top the dendritic bush to prevent cell damage. Thus, the puff duration and location was varied accordingly to get a reliable response.

We found that both ON and OFF UBCs had spontaneous firing in cell-attached mode. OFF UBCs had very regular firing; similar to what was observed in whole-cell mode (Fig 2.6A top panel, mean frequency 9.25 ± 1.01 Hz; n=8). ON UBCs also displayed spontaneous firing (Fig 2.6C top panel, mean frequency 3.76 ± 0.68 Hz; n=6). However ON cells firing displayed less regular and more variable than OFF cells (Fig 2.6A and 2.6C, top traces; 2.6E-F; OFF cells mean ISI 126.2 ± 16.3 ms, C.V. = 0.3 ± 0.08 , n=8; ON cells mean ISI 386.7 ± 101.3 ms; C.V. = 1.0 ± 0.16 , n =6). Some cells were quieter with occasional periods of tonic or bursting activity, while others had more consistent tonic firing, although less regular and slower than OFF UBCs. ON and OFF cells firing frequency was statistically different (p=0.0013). For both cell types, the response to glutamate puff was very reliable and either significantly increased intrinsic firing frequency (Fig 2.6C bottom panel and 2.6D; mean frequency over 2 seconds immediately after the puff 27.43 ± 9.07 Hz; p=0.26; n=6) or caused a prolonged pause in

firing (Fig 2.6B; mean frequency over 2 seconds immediately after the puff 1.05 ± 0.34 Hz; $p < 0.0001$; $n=8$) in both ON and OFF UBCs, respectively. Although the corresponding up or down regulation of firing was always present, the duration of this response was dependent on the duration of the puff and pipette placement. Our results are consistent with the majority of the results shown in the field regarding UBCs spontaneous firing (Russo *et al*, 2007; Simpson *et al*, 2005; Barmack and Yahknitsa, 2008; Ruigrok *et al*, 2011; Kennedy *et al*, 2014), in particular with Kim *et al* (2012). In that study, the authors showed that although mGluR1 α^+ UBCs do show spontaneous firing in whole cell and cell attached mode (Chapter 1; and Fig 2.4), they fire less regularly than mGluR1 α^- UBCs.

Vesicular glutamate contributes to glutamate-mediated standing current

In order to explore the origin of the glutamate that mediates the standing current in UBCs, we considered the distinct synaptic morphology of their mossy fiber terminals. The intricate synaptic geometry forms a physical barrier to diffusion, and may lead to prolonged post-synaptic currents in both subtypes due to accumulation of glutamate in the cleft and spillover to extra-synaptic mGluRs (Chapter 1; Kinney *et al.*, 1997; Jaarsma *et al.*, 1998). We hypothesized that the synapse is unable to fully clear the glutamate from ongoing vesicular release. To test this vesicle hypothesis, we used bafilomycin A1 (BafA1), a compound that inhibits vacuolar H⁺ ATPase (V-ATPase), thus decreasing the synaptic vesicle glutamate concentration. We predicted that if vesicular glutamate contributes to the standing current, we would see a significant decrease in baseline currents mediated by glutamate receptors.

During the experiments, we let slices recover normally after sectioning, used the first slice of each mouse for control recordings and each subsequent slice used was incubated in 2 μ M BafA1 for at least 1 hour. We used one animal to perform control recordings from molecular layer interneurons (stellate cells). Stellate cells have a very reliable response to electrical stimulation and many spontaneous EPSCs, and thus were useful controls to verify whether or not BafA1 was decreasing vesicular release. In control ACSF, stellate cells had normal evoked EPSCs and spontaneous EPSCs (Fig 5A). After 1 hour of incubation in BafA1, stimulus evoked EPSCs were abolished and no spontaneous EPSCs were present. Additionally, to ensure that the post-synaptic receptors could in fact still respond to glutamate, we applied a brief puff of 1 mM glutamate and was able to record a reliable response (Fig 5B).

We focused on the standing current generated by AMPAR in ON UBCs, as described in Figure 2, knowing that they offered a reliable response, and because we could take advantage of their property of desensitization. If in fact extracellular glutamate was maintaining a recurrent baseline activation of AMPARs, the constant exposure to glutamate would maintain a fraction of these receptors in a desensitized state. Therefore block of desensitization would result in an increased inward standing current (Fig 5C, left panel and Fig D). Moreover, this enhanced current would be absent when vesicular release is inhibited.

We identified ON UBCs with brief puff application of glutamate, removed the puff pipette and applied CTZ, and observed a significant increase in the baseline current (mean increase from baseline 24.3 ± 5.1 pA; $p = 0.0006$, $n=12$, Fig 5C-D). Subsequent application of the AMPAR antagonist NQBX, blocked this current, sending it below the

control baseline (mean decrease from baseline -5.9 ± 1.8 pA; $p=0.0081$, $n=12$, Fig 5C-D), suggesting that a fraction of AMPARs were open and mediating current in control measurements.

Upon repeating this procedure in ON UBCs in slices incubated in 2 μ M BafA1 for at least 1 hour there was a significant decrease (almost 6-fold) in the effect of CTZ (mean increase from baseline 4.16 ± 1.64 ; $p = 0.028$; CTZ treatment in control significantly greater than in BafA1, $p=0.001$; $n=12$, Fig 5C-D. The effect of NBQX in BafA1 was no longer significant (mean decrease from baseline -0.63 ± 0.73 pA; $p=0.41$; $n=12$, Fig 5C-D) and significantly decreased from NBQX treatment in control ($p=0.014$).

These results suggest that a significant portion of the glutamate standing current in UBCs was abolished when vesicular glutamate concentration was decreased, and that it is thus of vesicular origin, although there was still a small fraction of current increase with CTZ treatment in BafA1 sections ($p=0.028$). While BafA1 had a highly significant effect on the standing current, we cannot rule out that it may not have eliminated all vesicular glutamate content nor that a very small portion of the glutamate may be from non-vesicular origin, which would be unaffected by this treatment.

Discussion

This study reveals that a cell type-specific glutamate-mediated standing current maintains a fraction of glutamate receptors constitutively active, driving background electrical activity and playing a role in regulating spontaneous firing in UBCs. Blockade of excitatory mGluR1 receptors in ON UBCs hyperpolarized the cells with a decrease in baseline current and decreased intrinsic firing frequency. Conversely, blockade of mGluR2 receptors depolarized OFF UBCs with an increase in baseline, increasing the cell's firing rate. A remarkable effect of this standing current, in both UBC subtypes, is the maintenance of a fraction of AMPARs activated at baseline, constitutively in a desensitized state due to the constant exposure to glutamate.

Synaptic structure may play a role in generating glutamate standing currents

The observation that the V-ATPase inhibitor BafA1 decreased the glutamate standing current in UBCs significantly, leads us to propose that the ambient glutamate in this standing current is of vesicular origin. Additionally, based on the known kinetics of UBC synaptic physiology (Chapter 1, Rossi *et al.*, 1995; Kinney *et al.*, 1997; von Dorp and De Zeeuw, 2014) and what is known about synaptic morphology (Mugnaini *et al.*, 1994; Floris *et al.*, 1994; Rossi *et al.*, 1995; Mugnaini *et al.*, 1997), we hypothesize that restricted clearance of glutamate from the mossy fiber-UBC synaptic cleft and limited access by transporters lead to accumulation and maintenance of a basal level of ambient glutamate.

Mossy fiber terminals form glomerular synapses with dendrites of granule cells, UBCs and Golgi cells. Glomerular structure has been shown to influence post-synaptic responses of granule cells in a number of ways: slow diffusion of glutamate from the synaptic cleft contributes to spillover currents (DiGregorio *et al.* 2002; Sargent *et al.*, 2005), slow-rising AMPAR EPSCs (Nielsen *et al.*, 2004) and desensitization of AMPARs (Xu-Friedman and Regehr, 2003; DiGregorio, 2007). However, the time-course of granule cell EPSCs remains faster than that of UBCs, with high frequency transmission (DiGregorio *et al.*, 2002; DiGregorio *et al.*, 2007; Sargent *et al.*, 2005; Rancz *et al.*, 2007) and we observed the glutamate standing current in UBCs, but not in granule cells. Interestingly, within the glomerular synapse, it is typical for the UBC dendritic brush and granule cell dendrites to inter-twine and form synaptic contacts with the same mossy fiber terminal (Mugnaini *et al.*, 1997). One possibility is that the ultrastructure of synapses formed between mossy fiber terminals and granule cells or UBCs might underlie the observed physiological differences.

Although glial cells are positioned in the vicinity, they have very limited access to the glomerulus and are not present in between synaptic contacts, but rather encompassing the synapse. This suggests that clearance of glutamate from the cleft by glia is limited. Each granule cell dendritic digit can form between 2 and 3 small synaptic contacts with the mossy fiber terminal. These contacts are located in close proximity to each other (less than 0.5 μm away), with an average postsynaptic density diameter of 0.22 μm (Rossi *et al.*, 1995; Mugnaini *et al.*, 1997; Xu-Friedman and Regehr, 2003). In a striking contrast, several UBC dendritic branchelets infiltrate the glomerulus and forms synaptic contacts with the terminals. Electron microscopic studies reveal this synapse as having extended

synaptic clefts but also extended postsynaptic densities and release sites. The highly irregular synaptic morphology gives rise to asymmetric synaptic junctions with multiple short ($\geq 0.6 \mu\text{m}$) discontinuous sections or long continuous postsynaptic junctions (up to $2 \mu\text{m}$; 9-fold greater than on granule cells). Additionally, the area of apposition between pre and postsynaptic components might be much greater than currently estimated and therefore much larger than the granule cell-mossy terminal contacts (Mugnaini *et al.*, 1997; Rossi *et al.*, 1995; Diño and Mugnaini, 2000; Xu-Friedman and Regehr, 2003). Figure 5 in the Introduction chapter of this dissertation, adapted from Rossi *et al.* (1995), highlights this remarkable difference in contacts formed by granule cells and UBCs with the same mossy fiber terminal.

Surface area of postsynaptic density is not necessarily indicative of glutamate receptor types or density in synaptic contacts or extrasynaptic areas. However, these disparities in morphological characteristics might underlie the difference in time-course of synaptic transmission and as well as the level of exposure to the slow diffusing glutamate, which mediates a standing current in UBCs but not in granule cells.

Previous studies, have shown presence of AMPARs at the synapse and expression of mGluR1 α and mGluR2 in the dendritic brush of UBCs, however they are not found in postsynaptic densities, but rather in perisynaptic areas (Jaarsma *et al.*, 1998). Thus the receptors might be exposed to spillover glutamate at different levels. Further high-resolution ultrastructure studies investigating receptor type, density and location in postsynaptic densities and non-synaptic areas, within the dendritic brush might reveal how these parameters influence UBC physiology, as well as how diffusion of glutamate from the restricted cleft in a glomerulus can impact granule cells and UBCs differently.

How much glutamate could produce such standing current?

Glutamate receptors have different glutamate dependence of activation. mGluRs can be activated by relatively low concentrations of glutamate (as low as at the nanomolar range – up to 20 μM) (Conn and Pin, 1997). AMPARs mediate most of the fast excitatory transmission in the central nervous system and an AMPAR-peak response requires higher concentrations for activation (at least 100 μM ; Raman and Trussell, 1992). However, the dose-response curve for AMPAR steady-state currents is biphasic and bell-shaped, due to AMPAR desensitization. The current rises until the concentration of glutamate reaches 70-100 μM , and decreases rapidly due to receptor desensitization (Raman and Trussell, 1992). Furthermore, based on the dose response curve measured by different groups (Raman and Trussell, 1992; Kinney *et al.*, 1997; Morimoto-Tomita *et al.*, 2009; Semenov *et al.*, 2012), the initial phase of the steady-state dose response curve rises rapidly until the glutamate concentration reaches about 10 μM . At this level, the bell-shaped curve continues to rise, but very little, until it reaches maximum and starts to rapidly decline as the glutamate concentration further increases (1-2 mM). Kinney *et al.* (1997) measured the AMPAR steady-state dose response curve in UBCs and granule cells and the relationship was indeed bell-shaped with maximum concentration at 50 μM . Their results support the hypothesis that after release (20-40 ms), the glutamate concentration in the synaptic cleft rises rapidly (>50 μM) reaching a quasi-steady state. This effect underlies the undershoot in the current of the biphasic EPSC of ON UBCs.

We observed that a fraction of AMPARs in UBCs are constitutively desensitized at baseline. Additionally, the quasi state-state undershoot is reached rapidly after release in ON UBCs, and we observed cells with ‘outward’ desensitizing AMPAR undershoot

currents, going above baseline in response to glutamate puff application. This result suggests that in these cells the steady-state component reached very high levels of glutamate, still close to baseline, which is thus likely in the macromolar range. We propose that the concentration of glutamate maintaining the standing current is less than the maximum reached at the dose response curve ($\sim 50 \mu\text{M}$), but likely close to maximum – around $10 \mu\text{M}$.

Possible impact of ambient glutamate on UBC synaptic physiology

Spontaneous firing in UBCs is critical for the up- or down-regulation of firing resulting from the characteristic ON and OFF responses, respectively. Additionally, due to high input resistance, small synaptic currents can have a large impact on postsynaptic responses (Chapter 1). However, also due to high input resistance, small changes in basal intrinsic activity, such as fluctuations in the firing rate are likely to significantly influence the magnitude of these ON and OFF synaptic responses in each subtype. We show in this study that, by pharmacologically manipulating different glutamate receptors constitutively active in basal conditions, a shift of a few pico-amperes in the baseline current can depolarize or hyperpolarize the cell according to the polarity of this shift. This change in baseline, consequently, changed the firing rate of the cell. Such changes could significantly interfere with the magnitude of the up- or down-regulation of firing from synaptic ON or OFF response in UBCs, and thus, how that signal could be propagated downstream.

Cerebellar mossy fibers have been shown to fire at very high frequencies (Rancz *et al.*, 2007, Ritzau-Jost *et al.*, 2014), and glutamate released during such activity may

lead to spillover mediating slow synaptic responses and standing current in UBCs. Thus, the rate of presynaptic activity, and consequently the amount of glutamate in the cleft, would likely influence UBC excitability. If there are fluctuations in the concentration levels of glutamate in the cleft, UBCs might depolarize or hyperpolarize accordingly, and thus the magnitude of the ON and OFF responses might be dependent on the history of presynaptic-activity. Consequently, synaptic transmission dynamics at this synapse could strongly influence how UBCs relay multisensory signals from mossy fibers to downstream granule cells.

Finally, the level of depolarization or hyperpolarization of UBCs can influence activation of voltage-sensitive conductance such as voltage-gated calcium channels (VGCC) and I_h . Both VGCC and I_h are present in UBCs and influence their physiology (Diana *et al.*, 2007; Russo *et al.*, 2007; Birnstiel *et al.*, 2009; Kim *et al.*, 2012; Locatelli *et al.*, 2013; Subramayniyam *et al.*, 2014), and could thus, also contribute to multisensory signals relayed by UBCs.

Acknowledgements

This study was funded by National Institutes of Health (N.I.H) Grants NS028901 and DC004450 (PI: L.O.T); NIH-National Institute on Deafness and Other Communication Disorders Fellowship F31 DC012454 and N.L. Tartar Trust Fellowship (PI: C.B.M); P30DC005983 (PI: Gillespie, Peter) and P30 NS061800 (PI: Aicher, Sue). We would like to thank Dr. Craig Jahr and members of the Trussell Lab for helpful discussions. The authors declare no competing financial interests.

Figure 2.1

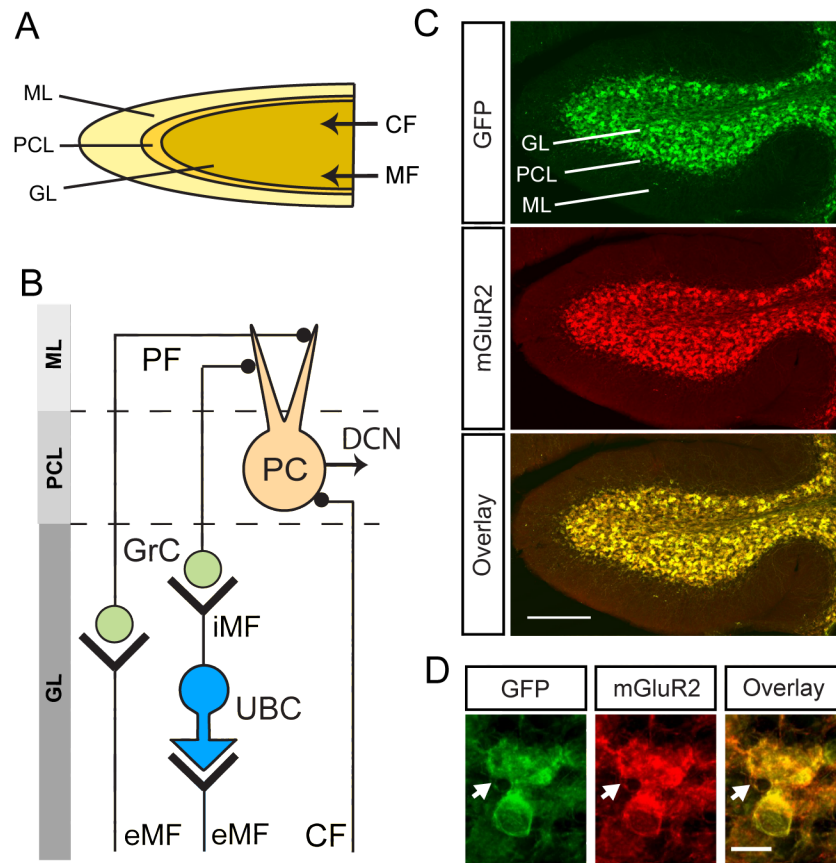


Figure 2.1. UBC identification in cerebellum. (A) Diagram of cerebellar lobe X, emphasizing the three layer components comprising the molecular layer (ML), Purkinje cell layer (PCL) and granule cell layer (GL), the latter receiving multisensory input via mossy fibers (MF) and inferior olive input via climbing fibers (CF). (B) The circuit organization of the cerebellum: CF fibers project to GL and contact the basal dendrites of Purkinje cells (PC), located in PCL and projecting to the deep cerebellar nucleus (DCN). Extrinsic glutamatergic mossy fibers (eMF) relaying multisensory input, terminate in GL, in large presynaptic terminals. eMF contact granule cells (GrC) and unipolar brush cells (UBC). UBCs contact GrCs via large glutamatergic intrinsic mossy fibers (iMF). GrC

axons project to the molecular layer as parallel fibers (PF) and contact the apical dendrites of PC, as well as other ML interneurons. Black circles indicate excitatory contacts. (C) Confocal immunofluorescence images of a sagittal section of cerebellar lobe X in a mouse expressing GFP under control of the mGluR2 promoter. Top panel shows GFP labeling with Alexa 488 secondary antibody, middle panel shows mGluR2 labeling with Cy3 secondary antibody, and bottom panel shows overlay of the two channels. UBCs are labeled in the GL. Scale bar: 200 μm . (D) High magnification of the image in panel C, shows GFP and mGluR2 co-localization of a labeled UBC. Scale bar: 10 μm . White arrow indicates the dendritic brush.

Figure 2.2

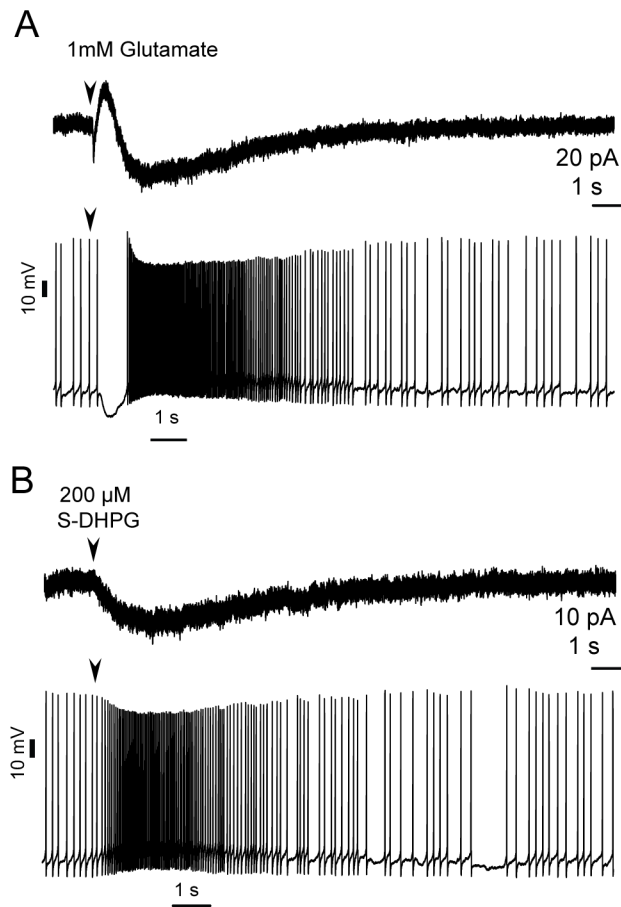


Figure 2.2. Outward current in ON UBCs. (A) Example trace of an ON UBC that displayed an outward current sag in response to a brief puff of glutamate (7-10 ms) (top panel), which lead to a pause in intrinsic firing (bottom panel) before prolonged excitation typical of ON UBCs. (B) Recordings from the same cell in A, showing the presence of an inward current in response to puff application of 200 μ M (S)-DHPG, and subsequent increase in spontaneous firing confirming the ON UBC subtype.

Figure 2.3

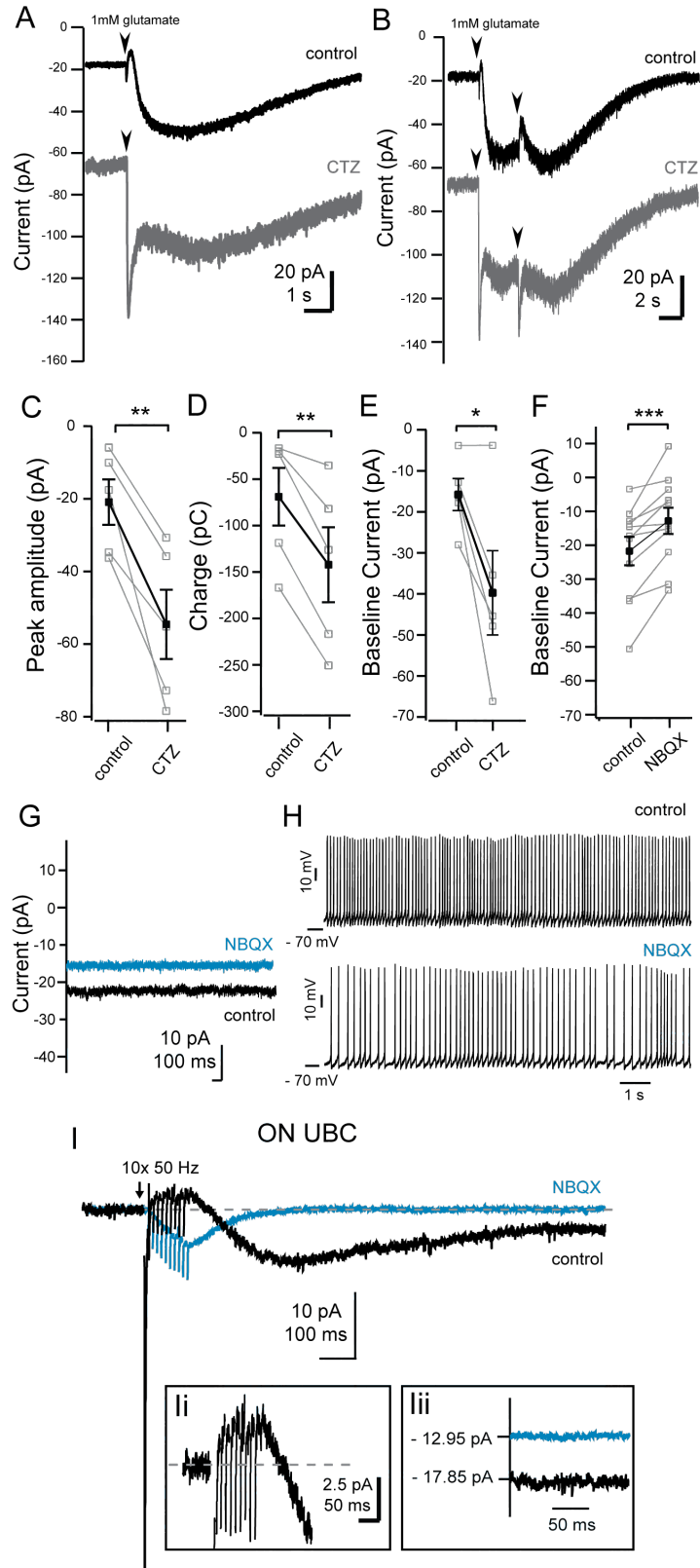


Figure 2.3. AMPAR-mediated standing current in ON UBCs (A) Example trace of an ON UBC with a outward current in response to glutamate puff (7-10 ms) in control (black) and in the presence of 100 μ M cyclothiazide (gray). (B) Same cell as in G, with application of a paired puff of glutamate (3 s inter-puff interval). (C) Measurements of the amplitude of inward current peaks of ON cells in response to a single glutamate puff application in control and in the presence of cyclothiazide (n=5; p=0.0099). (D) Charge measurements of ON UBC currents in response to puff application of glutamate in control and cyclothiazide (n=5; p=0.0091). (E) Baseline current of ON UBCs measured in control and in the presence of cyclothiazide (n=5; p=0.0091). (F) Baseline current of ON UBCs measured in control and in the presence of the AMPAR antagonist NBQX (5 μ M). (n=11; p=0.0010). (G) Example trace of the baseline current of an ON UBC in control (black) and in the presence of NBQX (blue). (H) Example traces of an ON UBC in current-clamp showing spontaneous firing in control (top) and in the presence of NBQX (bottom). (I) Traces of the single ON UBC in which an electrical stimulus elicited an outward current in control (black), sensitive to NBQX (blue). Inset Ii shows outward current at smaller scale and Iii shows the shift in baseline of 4.9 pA control (black) in the presence of NBQX (blue). In C-F graphs, gray squares show individual cells with data points in each treatment connected by a gray line. Mean is shown in black. Error bars show \pm SEM and significance level symbols are: ns, non-significant or (p>0.05), (*) (p \leq 0.05), (**) (p \leq 0.01), (***) (p \leq 0.001), (****) (p \leq 0.0001).

Figure 2.4

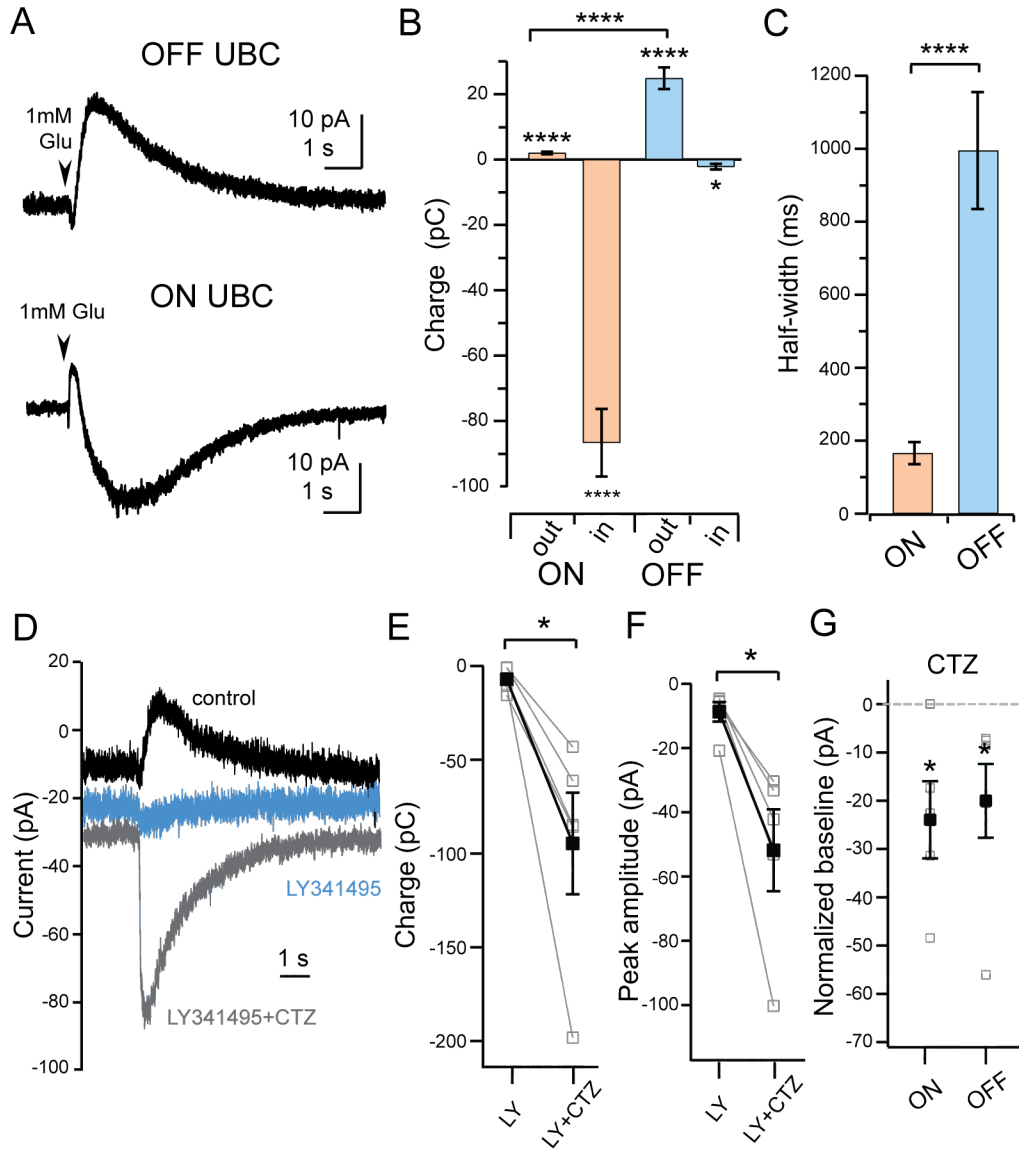


Figure 2.4. AMPAR-mediated standing current in OFF UBCs (A) Top panel shows OFF UBC example response to a brief (7-10 ms) glutamate puff application for comparison with an ON UBC example response to glutamate puff in the bottom panel, displaying an outward desensitizing sag. (B) Charge measurements for both outward (out) and inward (in) components of glutamate puff responses of ON (n=24) and OFF UBCs (n=24). (C)

Half-width measurements of the outward peak response of OFF UBCs (n=24) and of ON UBCs (n=24) of an outward desensitizing sag. (D) Example recording from an OFF UBC in control (black trace), followed by wash-in of 1 μ M of the mGluR2 antagonist LY341495 (blue), followed by wash-in of 100 μ M cyclothiazide (CTZ) (gray). (E) Charge measurements of the inward current of OFF UBCs in the presence of LY351595 (LY) alone and together with cyclothiazide (LY+CTZ) (n=5; p=0.0271). (F) Inward peak amplitude measurements of the inward current of OFF UBCs in the presence of LY341495 (LY) alone and together with cyclothiazide (LY+CTZ) (n=5; p=0.0111). (G) Comparison of the change in baseline (normalized to control) in the presence of cyclothiazide (CTZ) in ON and OFF UBCs (ON cells n=5, p=0.04; OFF cells n=6, p=0.47). In E-G graphs, gray squares show individual cells with data points in each treatment, with same cells connected by a gray line. Mean is shown in black. Error bars show \pm SEM and significance level symbols are: ns, non-significant or (p>0.05), (*) (p \leq 0.05), (**) (p \leq 0.01), (***) (p \leq 0.001), (****) (p \leq 0.0001).

Figure 2.5

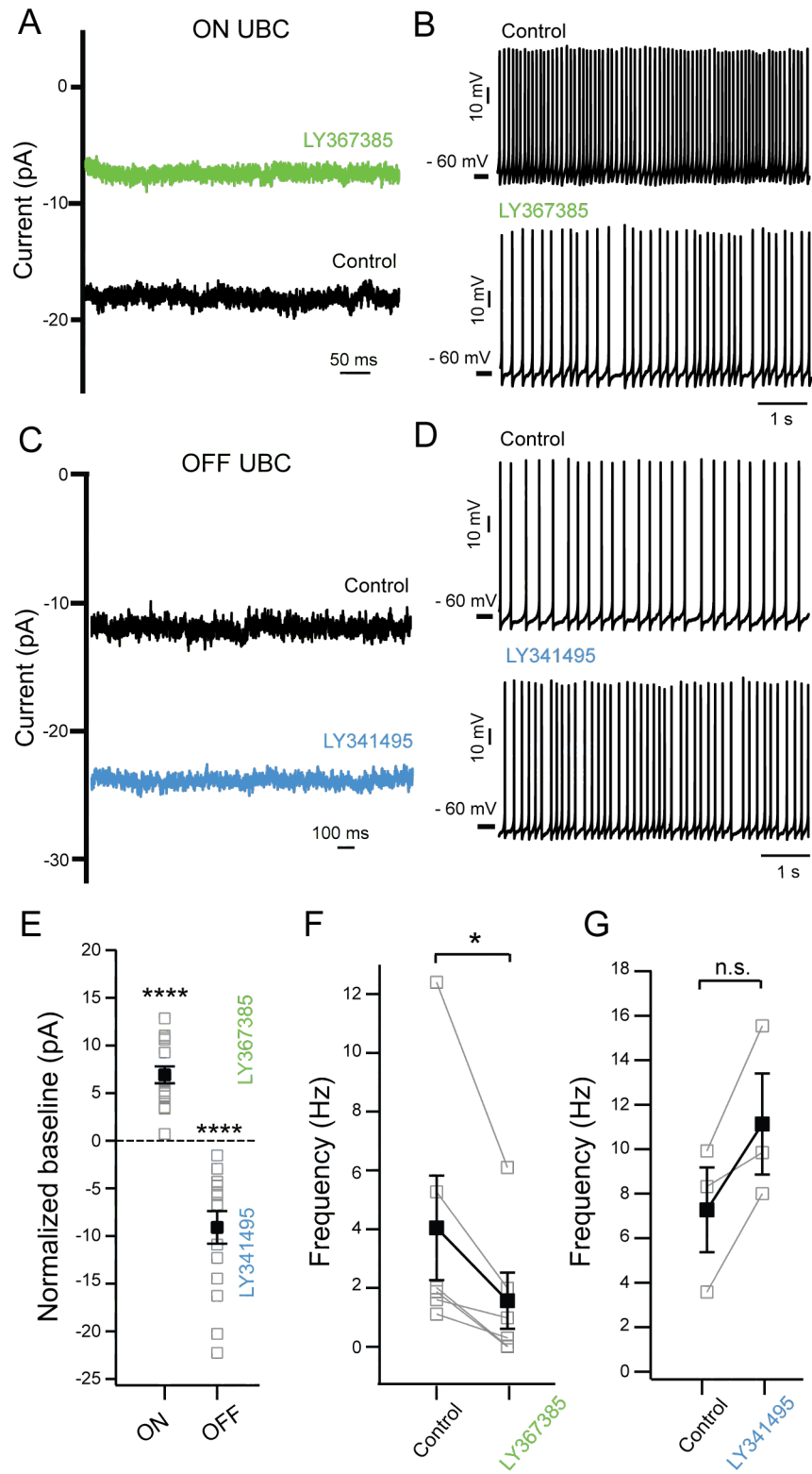


Figure 2.5. mGluR mediated standing currents. (A) Example baseline trace of an ON UBC in control (black) and in the presence of 150 μ M of the mGluR1 α antagonist LY367385 (green). (B) Example recordings of an ON UBC in current-clamp showing spontaneous firing in control (top) and in the presence of LY367385 (bottom). (C) Example baseline trace of an OFF UBC in control (black) and in the presence of 1 μ M LY341495 (blue). (D) Example recordings of an OFF UBC in current-clamp showing spontaneous firing in control (top) and in the presence of LY341495 (bottom). (E) Comparison of the change in baseline (normalized to control) for ON UBCs in the presence of LY367385 (n=16, p<0.0001) and for OFF UBCs in the presence of LY341495 (n=15, p<0.0001). (F) Change of firing frequency in ON UBCs from control to LY367385. (G) Change of firing frequency in OFF UBCs from control to LY341495. In E-G graphs, gray squares show individual cells with data points in each treatment, in F-G same cells are connected by a gray line. Mean is shown in black. Error bars show \pm SEM and significance level symbols are: ns, non-significant or (p>0.05), (*) (p \leq 0.05), (**) (p \leq 0.01), (***) (p \leq 0.001), (****) (p \leq 0.0001).

Figure 2.6. ON and OFF responses are intact in cell-attached recordings. (A) Top panel shows cell-attached recordings of OFF UBC with regular spontaneous firing; bottom panel shows a prolonged pause in firing in response to brief (15-40 ms) puff application of glutamate. (B) Graphic representation of the firing frequency of OFF UBCs before and during the 2-second period immediately following glutamate puff. (C) Top three panels show the irregularity of spontaneous firing of ON UBCs; bottom panel shows a prolonged increase in firing in response to brief application of glutamate. (D) Graphic representation of firing frequency of ON UBCs and the increase in frequency during the 2-second period following glutamate application. (E) To show the difference in regularity of firing, inter-spike interval (ISI) data of all N's for ON (light gray) and OFF (dark gray) cells were pooled and normalized to maximum number of events. OFF cells show a narrow peak, while ON cells display a broad distribution indicative of a larger variation in ISIs. (F) Graphic representation of the mean ISI of each subtype (OFF cells n=8; ON cells n=6) and (G) Graphic representation of the coefficient of variation of both ON and OFF cells. Black arrows in A and C show puff of 1 mM glutamate. Error bars show \pm SEM and significance level symbols are: ns, non-significant or ($p>0.05$), (*) ($p\leq 0.05$), (**) ($p\leq 0.01$), (***) ($p\leq 0.001$), (****) ($p\leq 0.0001$).

Figure 2.7

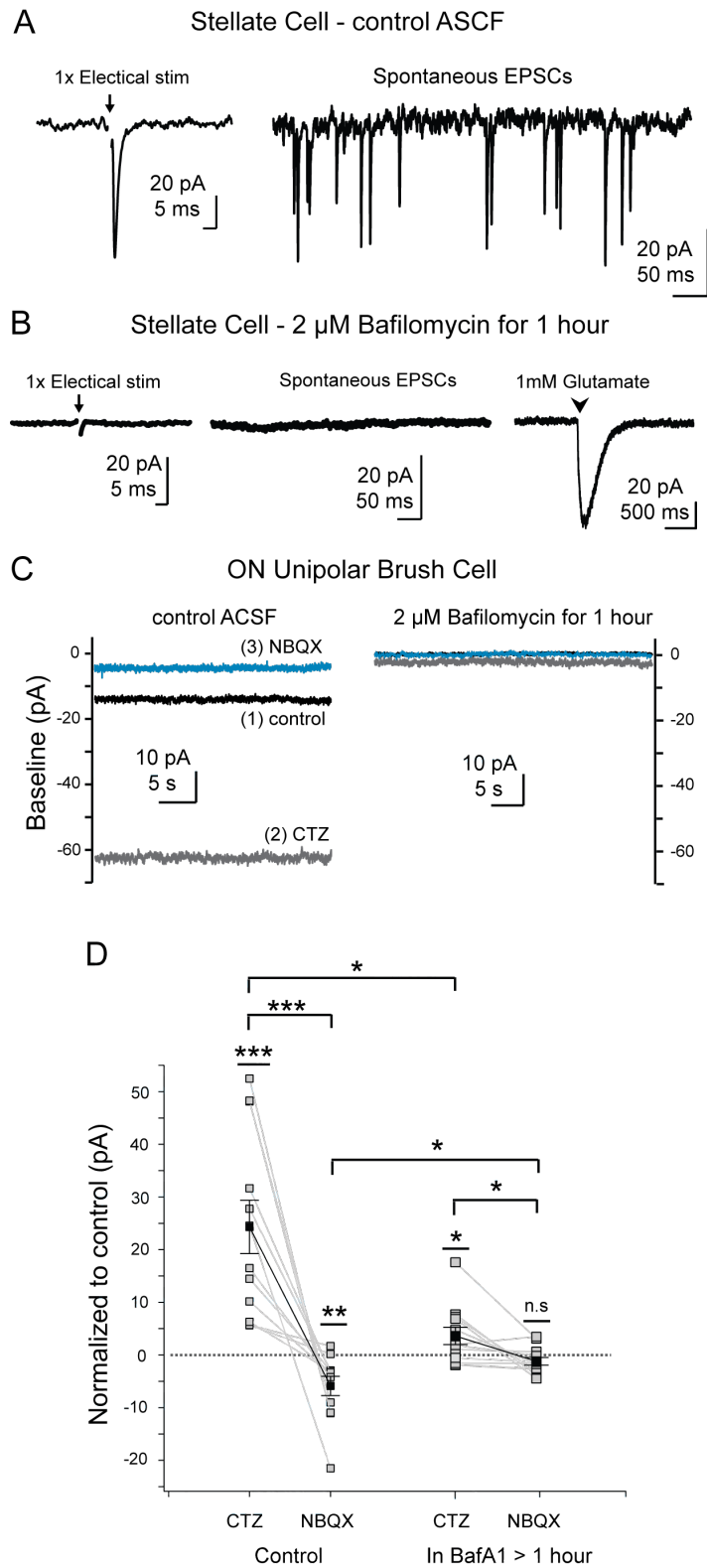


Figure 2.7. Decrease of vesicular glutamate concentration decreases standing current.

(A) Example traces of evoked EPSC in a control stellate cell and right panel shows spontaneous EPSCs. (B) Example traces from a stellate cell after BafA1 treatment. Evoked EPSCs and spontaneous EPSCs were absent. Far right trace shows a reliable response to puff application of glutamate. Stellate cells were filled with Alexa 488 and the dendrites locations were easily identified by fluorescence for targeted puff. (C) Example recordings of an ON UBC in control and of an ON UBC after BafA1 treatment, showing the decrease in the current revealed by 100 μ M CTZ with subsequent block by 5 μ M NBQX. (D) Graphic summary of all ON UBCs in control slices and in slices incubated in Baf1A for at least 1 hour. Measurements were normalized to control baseline, within each cell. Black arrows in A and B show onset of a single electrical stimulus and in B black arrowhead indicates onset of a brief puff (10-15 ms) of glutamate. Error bars show \pm SEM and significance level symbols are: ns, non-significant or ($p > 0.05$), (*) ($p \leq 0.05$), (**) ($p \leq 0.01$), (***) ($p \leq 0.001$), (****) ($p \leq 0.0001$).

SUMMARY AND CONCLUSIONS

The general goal of the work presented in this dissertation was to elucidate the importance of glutamate receptor mediated currents for UBC function and how they could influence the processing of multisensory signals in cerebellum-like networks.

In Chapter 1, I investigated mossy fiber glutamatergic input to DCN UBCs. Immunohistochemical studies previously revealed two distinct UBC populations: calretinin⁺ UBCs and mGluR1 α ⁺ UBCs (Nunzi *et al.*, 2002; Diño and Mugnaini, 2008; Sekerková *et al.*, 2014). Although they had been distinguished by molecular markers and a more recent study had shown differences in intrinsic properties (Kim *et al.*, 2012), whether UBC subtypes have different roles in processing multisensory input from mossy fibers was unknown. I made the striking discovery that UBC subtypes may function as ON and OFF cells with respect to their response to glutamatergic input. These opposing responses are due to differential levels of glutamate receptor types expressed in each subtype. mGluR1 α positive UBCs had an excitatory (ON) response to glutamate, due to high expression of AMPARs and mGluR1 α , and small GIRK currents elicited by mGluR2 activation. mGluR1 α negative UBCs had an inhibitory (OFF) response to glutamate resulting from small AMPAR-mediated currents and large outward K⁺ currents activated by mGluR2. This finding was interesting in several aspects.

Firstly, aside from UBCs, subtypes of neurons characterized by opposing responses to the same glutamatergic input in the brain are uncommon in vertebrates. The best-known examples are the ON and OFF retinal bipolar cells, which utilize metabotropic and ionotropic receptors, respectively. ON bipolar cells depolarize in response to light: in low light intensity, glutamate activates mGluR6 receptors, which

through intracellular signaling closes a cation channel and hyperpolarizes ON cells. With increase in light intensity, less glutamate leads to decrease in activation of the inhibitory mGluR6 and thus depolarizes ON cells (Nawy and Jahr, 1990a; Nawy and Jahr, 1990b; Shiells and Falk, 1990). Conversely, OFF bipolar cells hyperpolarize in response to light: AMPA/KA receptors mediate glutamatergic transmission – glutamate activates these channels in low intensity light depolarizing OFF cells and with decrease in glutamate release with increase in light intensity, OFF bipolar cells hyperpolarize (Slaughter and Miller, 1983a; Slaughter and Miller, 1983b; Sasaki and Kaneko, 1996; Devries and Schwartz, 1999). Additionally, there are examples of glutamate mediating inhibition in invertebrates, for instance in the *Drosophila* olfactory system (Liu and Wilson, 2013). However, except for the case of the ON retinal bipolar cell, we are unaware of another vertebrate synapse in which glutamate almost entirely mediates inhibition.

This differential response splits the visual signals into separate pathways based on the dual mode of action of glutamate receptors expressed by each subtype. Since UBCs relay feedforward input from mossy fibers, and their ON and OFF responses also have opposing polarities, establishing the sources of mossy input to ON versus OFF UBCs, in both DCN and cerebellum will aid in predicting the impact of multisensory input to sound localization and vestibular function.

In Chapter 2, I investigated the contribution of ambient glutamate to maintenance of intrinsic firing of UBCs. I found that a fraction of AMPARs, in ON and OFF UBCs, are desensitized at baseline, due to exposure to ambient glutamate. Additionally, blockade of AMPARs leads to a significant decrease in the baseline current and a fraction of both mGluR1 α in ON UBCs and mGluR2 in OFF UBCs are also constitutively active

and blockade of these receptors either decrease or increase spontaneous firing respectively. The ON and OFF responses characterized in chapter 1, either up- or down-regulate firing, respectively. In the context of UBC physiology, high input resistance renders these cells with the ability to respond strongly to small changes in conductance, either inhibitory or excitatory. Since extracellular glutamate influences UBC excitability and can modulate spontaneous firing, it could consequently also modulate the magnitude of these ON/OFF responses, and thus, synaptic transmission dynamics and UBC output at this synapse.

I also found that the extracellular glutamate mediating this standing current in ON and OFF UBCs is in large proportion of vesicular origin. Slow diffusion of glutamate from the glomerular synaptic structure has been shown to influence post-synaptic responses not only in UBCs with slow AMPAR and mGluR currents (Chapter 1; Rossi *et al.*, 1995; Kinney *et al.*, 1997) but also in granule cells with spillover currents and AMPAR desensitization (Overstreet *et al.*, 1999; DiGregorio *et al.* 2002; Sargent *et al.*, 2005; Xu-Friedman and Regehr, 2003; DiGregorio, 2007).

Physiological and morphological studies support the hypothesis that a large amount of glutamate is released from the presynaptic terminal, with slow diffusion from the restricted synaptic cleft and limited uptake by transporter. For instance, cerebellar mossy fibers fire at very high frequencies (Rancz *et al.*, 2007, Ritzau-Jost *et al.*, 2014), and a mossy fiber terminal could form large numbers of synaptic contacts (>150) with postsynaptic densities (Jakab and Hámori, 1988; Jakab, 1989). Consequently, glutamate released during such activity may lead to prolonged spillover currents. Glial cells are positioned near by, but have limited access to the glomerulus, with slow clearance of

glutamate. (Rossi *et al.*, 1995; Mugnaini *et al.*, 1997; Xu-Friedman and Regehr, 2003).

There is very little known about distribution and location of glutamate reuptake transporters within this synapse, however impairment of glutamate transport does prolong AMPAR EPSCs in UBCs (Kinney *et al.*, 1997). In granule cells, restricted glutamate uptake leads to spillover currents, which are an important element to synaptic transmission dynamics at this synapse (Sargent *et al.*, 2005; DiGregorio *et al.*, 2002), and transporters have been shown to play an important role in limiting the extent of these glutamate spillover currents (Overstreet *et al.*, 1999). Further studies on the location and density of transporters at this synapse would elucidate their role in shaping glutamate transients and their influence to granule cells and UBCs physiology. For instance, based on what is known about synaptic physiology and morphology, could these prolonged glutamate transients and limited clearance from the cleft lead to ambient micromolar levels of glutamate in the glomerulus? Since the ultrastructure of the synaptic contacts between granule cells and mossy terminals versus UBCs and mossy terminals and their corresponding postsynaptic densities are drastically different, UBCs are more vulnerable to such prolonged glutamate spillover. Based on my findings in Chapter 2, I propose that UBC dendrites are likely exposed to spillover glutamate constitutively at basal levels. In turn, this 'ambient' level of glutamate in the cleft could thus maintain a fraction of receptors in UBCs constitutively active. Consequently, fluctuations on baseline could lead to fluctuations on spontaneous firing rate and affect the magnitude of ON and OFF responses in UBCs.

The opposing ON and OFF responses of UBCs, and the magnitude of these responses modulated by ambient glutamate, may be highly influential to how signals are

relayed in cerebellum-like circuits. Granule cell dendrites arise from the soma as 3-4 different short branches and terminate in dendritic claws that form synaptic glomeruli with mossy fiber terminals. Additionally, granule cells are multimodal (Arenz *et al.*, 2008; Sawtell, 2010; Huang *et al.*, 2013), their dendritic claws receive input from different origins and thus integrate different modalities of signals and sensory information. Ascending projections relaying multisensory input as mossy fibers likely have different patterns of activity. Thus, depending on the timing of arrival of converging mossy fibers onto a granule cell from functionally distinct inputs, an ON or an OFF UBC response may highly influence how this granule cell will integrate and relay information in cerebellum and DCN (Fig 1). Further studies to identify whether UBCs receive input from different origins, whether they diverge the same input modality and what subset of granule cells they contact might shed light on the function of UBCs in cerebellum-like structures – integrating proprioceptive and vestibular streams with sound localization and direction of motion.

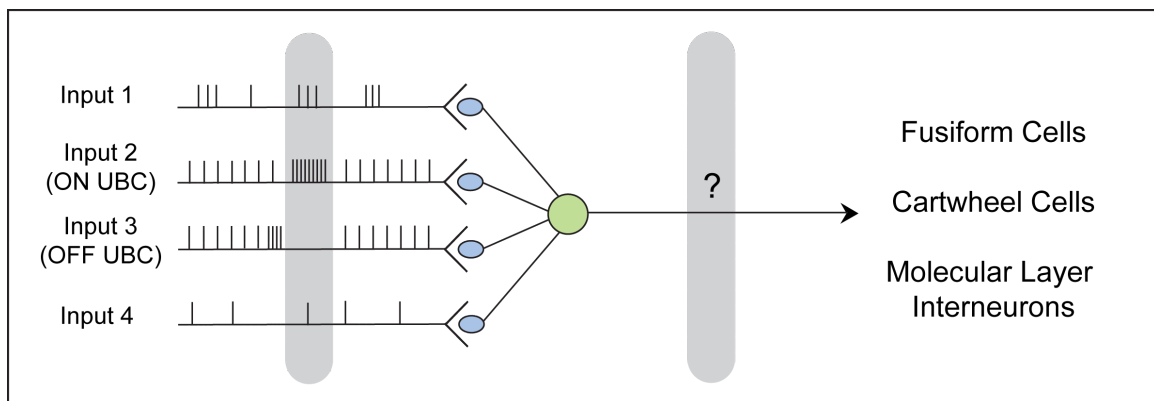


Figure 1: Diagram of a hypothetical granule cell receiving 4 different input modalities through mossy fibers, with different pattern of activity.

REFERENCES

- Abbott, L.C., and Jacobowitz, D.M. (1995). Development of calretinin-immunoreactive unipolar brush-like cells and an afferent pathway to the embryonic and early postnatal mouse cerebellum. *Anat. Embryol.* *191* 541–59
- Alcami, P., Franconville, R., Llano, I., and Marty, A. (2012). Measuring the firing rate of high-resistance neurons with cell-attached recording. *J. Neurosci.* *32*, 3118–3130.
- Alvarez, M.-I., Lacruz, C., Toledano-Díaz, A., Monleón, E., Monzón, M., Badiola, J.-J., and Toledano, A. (2008). Calretinin-immunopositive cells and fibers in the cerebellar cortex of normal sheep. *Cerebellum* *7*, 417–429.
- Ando, M., Sawada, K., Sakata-Haga, H., Jeong, Y.-G., Takeda, N., and Fukui, Y. (2005). Regional difference in corticotropin-releasing factor immunoreactivity in mossy fiber terminals innervating calretinin-immunoreactive unipolar brush cells in vestibulocerebellum of rolling mouse Nagoya. *Brain Res.* *1063*, 96–101.
- Arenz, A., Bracey, E.F., and Margrie, T.W. (2009). Sensory representations in cerebellar granule cells. *Curr. Opin. Neurobiol.* *19*, 445–451.
- Arenz, A., Silver, R.A., Schaefer, A.T., and Margrie, T.W. (2008). The contribution of single synapses to sensory representation in vivo. *Science* *321*, 977–980.
- Bal, T., and McCormick, D.A. (1993). Mechanisms of oscillatory activity in guinea-pig nucleus reticularis thalami in vitro: a mammalian pacemaker. *J. Physiol. (Lond.)* *468*, 669–691.

Balakrishnan, V., and Trussell, L.O. (2008). Synaptic inputs to granule cells of the dorsal cochlear nucleus. *J. Neurophysiol.* *99*, 208–219.

Balakrishnan, V., Kuo, S.P., Roberts, P.D., and Trussell, L.O. (2009). Slow glycinergic transmission mediated by transmitter pooling. *Nat. Neurosci.* *12*, 286–294.

Barmack, N.H., and Yakhnitsa, V. (2008). Functions of interneurons in mouse cerebellum. *J. Neurosci.* *28*, 1140–1152.

Bazwinsky, I., Härtig, W., and RübSamen, R. (2008). Characterization of cochlear nucleus principal cells of *Meriones unguiculatus* and *Monodelphis domestica* by use of calcium-binding protein immunolabeling. *J. Chem. Neuroanat.* *35*, 158–174.

Bell, C.C., and Russell, C.J. (1978). Effect of electric organ discharge on ampullary receptors in a mormyrid. *Brain Res.* *145*, 85–96.

Bell, C.C., Han, V.Z., Sugawara, Y., and Grant, K. (1997). Synaptic plasticity in a cerebellum-like structure depends on temporal order. *Nature* *387*, 278–281.

Bell, C.C., Han, V., and Sawtell, N.B. (2008). Cerebellum-Like Structures and Their Implications for Cerebellar Function. *Annu. Rev. Neurosci.* *31*, 1–24.

Berthié, B., and Axelrad, H. (1994). Granular layer collaterals of the unipolar brush cell axon display rosette-like excrescences. A Golgi study in the rat cerebellar cortex. *Neurosci. Lett.* *167*, 161–165.

Bevan, M.D., and Wilson, C.J. (1999). Mechanisms underlying spontaneous oscillation and rhythmic firing in rat subthalamic neurons. *J. Neurosci.* *19*, 7617–7628.

- Billups, D., Liu, Y.-B., Birnstiel, S., and Slater, N.T. (2002). NMDA receptor-mediated currents in rat cerebellar granule and unipolar brush cells. *J. Neurophysiol.* *87*, 1948–1959.
- Birnstiel, S., Slater, N.T., McCrimmon, D.R., Mugnaini, E., and Hartell, N.A. (2009). Voltage-dependent calcium signaling in rat cerebellar unipolar brush cells. *Neuroscience* *162*, 702–712.
- Bischofberger, J., Engel, D., Li, L., Geiger, J.R.P., and Jonas, P. (2006). Patch-clamp recording from mossy fiber terminals in hippocampal slices. *Nat Protoc* *1*, 2075–2081.
- Borges-Merjane C. and Trussell L.O. (2015). ON and OFF unipolar brush cells transform multisensory inputs to the auditory system. *Neuron* *85*, 1029–42
- Bukowska, D. (2002). Morphological evidence for secondary vestibular afferent connections to the dorsal cochlear nucleus in the rabbit. *Cells Tissues Organs (Print)* *170*, 61–68.
- Burian, M., and Gstoettner, W. (1988). Projection of primary vestibular afferent fibres to the cochlear nucleus in the guinea pig. *Neurosci. Lett.* *84*, 13–17.
- Carter, A.G., and Regehr, W.G. (2002). Quantal events shape cerebellar interneuron firing. *Nat. Neurosci.* *5*, 1309–1318.
- Chadderton, P., Margrie, T.W., and Häusser, M. (2004). Integration of quanta in cerebellar granule cells during sensory processing. *Nature* *428*, 856–860.
- Chan-Palay, V., and Palay, S.L. (1971). The synapse en marron between golgi II neurons

and mossy fibers in the rat's cerebellar cortex. *Z Anat Entwicklungsgesch* 133, 274–287.

Chung, S.-H., Sillitoe, R.V., Croci, L., Badaloni, A., Consalez, G., and Hawkes, R. (2009a). Purkinje cell phenotype restricts the distribution of unipolar brush cells. *Neuroscience* 164, 1496–1508.

Chung, S.-H., Marzban, H., Watanabe, M., and Hawkes, R. (2009b). Phospholipase C β 4 expression identifies a novel subset of unipolar brush cells in the adult mouse cerebellum. *Cerebellum* 8, 267–276.

Clements, J.D., Lester, R.A., Tong, G., Jahr, C.E., and Westbrook, G.L. (1992). The time course of glutamate in the synaptic cleft. *Science* 258, 1498–1501.

Conn P.J. and Pin J.P. (1997). Pharmacology and functions of metabotropic glutamate receptors. *Annu Rev Pharmacol Toxicol.* 37 205-37

DeVries S.H. and Schwartz E.A. (1999). Kainate receptors mediate synaptic transmission between cones and ‘Off’ bipolar cells in a mammalian retina. *Nature* 397 157-60

Diana, M.A., Otsu, Y., Maton, G., Collin, T., Chat, M., and Dieudonné, S. (2007). T-type and L-type Ca²⁺ conductances define and encode the bimodal firing pattern of vestibulocerebellar unipolar brush cells. *J. Neurosci.* 27, 3823–3838.

DiGregorio, D.A., Nusser, Z., and Silver, R.A. (2002). Spillover of glutamate onto synaptic AMPA receptors enhances fast transmission at a cerebellar synapse. *Neuron* 35, 521–533.

DiGregorio, D.A., Rothman, J.S., Nielsen, T.A., and Silver, R.A. (2007). Desensitization

properties of AMPA receptors at the cerebellar mossy fiber granule cell synapse. *J. Neurosci.* 27, 8344–8357.

Diño, M.R., and Mugnaini, E. (2000). Postsynaptic actin filaments at the giant mossy fiber-unipolar brush cell synapse. *Synapse* 38, 499–510.

Diño, M.R., and Mugnaini, E. (2008). Distribution and phenotypes of unipolar brush cells in relation to the granule cell system of the rat cochlear nucleus. *Neuroscience* 154, 29–50.

Diño, M.R., Nunzi, M.G., Anelli, R., and Mugnaini, E. (2000). Unipolar brush cells of the vestibulocerebellum: afferents and targets. *Prog. Brain Res.* 124, 123–137.

Diño, M.R., Perachio, A.A., and Mugnaini, E. (2001). Cerebellar unipolar brush cells are targets of primary vestibular afferents: an experimental study in the gerbil. *Exp Brain Res* 140, 162–170.

Diño, M.R., Willard, F.H., and Mugnaini, E. (1999). Distribution of unipolar brush cells and other calretinin immunoreactive components in the mammalian cerebellar cortex. *J. Neurocytol.* 28, 99–123.

Do, M.T.H., and Bean, B.P. (2003). Subthreshold sodium currents and pacemaking of subthalamic neurons: modulation by slow inactivation. *Neuron* 39, 109–120.

Dotd, H.-U., Eder, M., Schierloh, A., and Zieglgänsberger, W. (2008). Infrared-guided laser stimulation of neurons in brain slices. *CSH Protoc* 2008, pdb.prot4851.

Dugué, G.P., Dumoulin, A., Triller, A., and Dieudonné, S. (2005). Target-dependent use

of co-released inhibitory transmitters at central synapses. *J. Neurosci.* 25, 6490–6498.

Eccles, J.C., Ito, M., and Szentágothai, J. (1967). *The Cerebellum as a Neuronal Machine* (Springer).

Floris, A., Diño, M., Jacobowitz, D.M., and Mugnaini, E. (1994). The unipolar brush cells of the rat cerebellar cortex and cochlear nucleus are calretinin-positive: a study by light and electron microscopic immunocytochemistry. *Anat. Embryol.* 189, 495–520.

Forti, L., Cesana, E., Mapelli, J., and D'Angelo, E. (2006). Ionic mechanisms of autorhythmic firing in rat cerebellar Golgi cells. *J. Physiol. (Lond.)* 574, 711–729.

Haenggeli, C.-A., Pongstaporn, T., Doucet, J.R., and Ryugo, D.K. (2005). Projections from the spinal trigeminal nucleus to the cochlear nucleus in the rat. *J. Comp. Neurol.* 484, 191–205.

Harashima, C., Jacobowitz, D.M., Stoffel, M., Chakrabarti, L., Haydar, T.F., Siarey, R.J., and Galdzicki, Z. (2006). Elevated expression of the G-protein-activated inwardly rectifying potassium channel 2 (GIRK2) in cerebellar unipolar brush cells of a Down syndrome mouse model. *Cell. Mol. Neurobiol.* 26, 719–734.

Harris, J., Moreno, S., Shaw, G., and Mugnaini, E. (1993). Unusual neurofilament composition in cerebellar unipolar brush neurons. *J. Neurocytol.* 22, 1039–1059.

Hámori, J., and Somogyi, J. (1983). Differentiation of cerebellar mossy fiber synapses in the rat: a quantitative electron microscope study. *J. Comp. Neurol.* 220, 365–377.

Hámori, J., and Szentágothai, J. (1966). Participation of Golgi neuron processes in the

cerebellar glomeruli: an electron microscope study. *Exp Brain Res* 2, 35–48.

Häusser, M., and Clark, B.A. (1997). Tonic synaptic inhibition modulates neuronal output pattern and spatiotemporal synaptic integration. *Neuron* 19, 665–678.

Holtzman, T., Sivam, V., Zhao, T., Frey, O., van der Wal, P.D., de Rooij, N.F., Dalley, J.W., and Edgley, S.A. (2011). Multiple extra-synaptic spillover mechanisms regulate prolonged activity in cerebellar Golgi cell-granule cell loops. *J. Physiol. (Lond.)* 589, 3837–3854.

Huang, C.-C., Sugino, K., Shima, Y., Guo, C., Bai, S., Mensh, B.D., Nelson, S.B., and Hantman, A.W. (2013). Convergence of pontine and proprioceptive streams onto multimodal cerebellar granule cells. *Elife* 2, e00400.

Hull, C., and Regehr, W.G. (2012). Identification of an inhibitory circuit that regulates cerebellar Golgi cell activity. *Neuron* 73, 149–158.

Hutson, K.A., and Morest, D.K. (1996). Fine structure of the cell clusters in the cochlear nerve root: stellate, granule, and mitt cells offer insights into the synaptic organization of local circuit neurons. *J. Comp. Neurol.* 371, 397–414.

Ishikawa T., Sahara Y. and Takahashi T. (2002). A single packet of transmitter does not saturate postsynaptic glutamate receptors. *Neuron* 34 613-21.

Itoh, K., Kamiya, H., Mitani, A., Yasui, Y., Takada, M., and Mizuno, N. (1987). Direct projections from the dorsal column nuclei and the spinal trigeminal nuclei to the cochlear nuclei in the cat. *Brain Res.* 400, 145–150.

Itō, M. (1984). *The cerebellum and neural control* (Raven Pr).

Jaarsma, D., Diño, M.R., Ohishi, H., Shigemoto, R., and Mugnaini, E. (1998).

Metabotropic glutamate receptors are associated with non-synaptic appendages of unipolar brush cells in rat cerebellar cortex and cochlear nuclear complex. *J. Neurocytol.* 27, 303–327.

Jahnsen, H., and Llinás, R. (1984). Ionic basis for the electro-responsiveness and oscillatory properties of guinea-pig thalamic neurones in vitro. *J. Physiol. (Lond.)* 349, 227–247.

Jakab, R.L. (1989). Three-dimensional reconstruction and synaptic architecture of cerebellar glomeruli in the rat. *Acta Morphol Hung* 37, 11–20.

Jakab, R.L., and Hátori, J. (1988). Quantitative morphology and synaptology of cerebellar glomeruli in the rat. *Anat. Embryol.* 179, 81–88.

Josephson, E.M., and Morest, D.K. (2003). Synaptic nests lack glutamate transporters in the cochlear nucleus of the mouse. *Synapse* 49, 29–46.

Jörntell, H., and Ekerot, C.-F. (2006). Properties of somatosensory synaptic integration in cerebellar granule cells in vivo. *J. Neurosci.* 26, 11786–11797.

Kalinichenko, S.G., and Pushchin, I.I. (2008). Calcium-binding proteins in the cerebellar cortex of the bottlenose dolphin and harbour porpoise. *J. Chem. Neuroanat.* 35, 364–370.

Kanold, P.O., Davis, K.A., and Young, E.D. (2011). Somatosensory context alters auditory responses in the cochlear nucleus. *J. Neurophysiol.* 105, 1063–1070.

- Kennedy, A., Wayne, G., Kaifosh, P., Alviña, K., Abbott, L.F., and Sawtell, N.B. (2014). A temporal basis for predicting the sensory consequences of motor commands in an electric fish. *Nat. Neurosci.* *17*, 416–422.
- Kim, J.-A., Sekerková, G., Mugnaini, E., and Martina, M. (2012). Electrophysiological, morphological, and topological properties of two histochemically distinct subpopulations of cerebellar unipolar brush cells. *Cerebellum* *11*, 1012–1025.
- Kinney, G.A., Overstreet, L.S., and Slater, N.T. (1997). Prolonged physiological entrapment of glutamate in the synaptic cleft of cerebellar unipolar brush cells. *J. Neurophysiol.* *78*, 1320–1333.
- Knoflach, F., and Kemp, J.A. (1998). Metabotropic glutamate group II receptors activate a G protein-coupled inwardly rectifying K⁺ current in neurones of the rat cerebellum. *J. Physiol. (Lond.)* *509* (Pt 2), 347–354.
- Koehler, S.D., Pradhan, S., Manis, P.B., and Shore, S.E. (2011). Somatosensory inputs modify auditory spike timing in dorsal cochlear nucleus principal cells. *Eur. J. Neurosci.* *33*, 409–420.
- Li, H., and Mizuno, N. (1997). Single neurons in the spinal trigeminal and dorsal column nuclei project to both the cochlear nucleus and the inferior colliculus by way of axon collaterals: a fluorescent retrograde double-labeling study in the rat. *Neurosci. Res.* *29*, 135–142.
- Liu, W.W., and Wilson, R.I. (2013). Glutamate is an inhibitory neurotransmitter in the *Drosophila* olfactory system. *Proc. Natl. Acad. Sci. U.S.a.* *110*, 10294–10299.

Llinás, R.R. (1988). The intrinsic electrophysiological properties of mammalian neurons: insights into central nervous system function. *Science* 242, 1654–1664.

Llinás, R.R. (2014). Intrinsic electrical properties of mammalian neurons and CNS function: a historical perspective. *Front Cell Neurosci* 8, 320.

Locatelli, F., Botta, L., Prestori, F., Masetto, S., and D'Angelo, E. (2013). Late-onset bursts evoked by mossy fibre bundle stimulation in unipolar brush cells: evidence for the involvement of H- and TRP-currents. *J. Physiol. (Lond.)* 591, 899–918.

McCormick, D.A., and Pape, H.C. (1990). Properties of a hyperpolarization-activated cation current and its role in rhythmic oscillation in thalamic relay neurones. *J. Physiol. (Lond.)* 431, 291–318.

Meek, J., Yang, J.Y., Han, V.Z., and Bell, C.C. (2008). Morphological analysis of the mormyrid cerebellum using immunohistochemistry, with emphasis on the unusual neuronal organization of the valvula. *J. Comp. Neurol.* 510, 396–421.

Monteiro, R.A. (1986). Critical analysis on the nature of synapses en marron of cerebellar cortex. *J Hirnforsch* 27, 567–576.

Morimoto-Tomita, M., Zhang, W., Straub, C., Cho, C.-H., Kim, K.S., Howe, J.R., and Tomita, S. (2009). Autoinactivation of neuronal AMPA receptors via glutamate-regulated TARP interaction. *Neuron* 61, 101–112.

Morin, F., Diño, M.R., and Mugnaini, E. (2001). Postnatal differentiation of unipolar brush cells and mossy fiber-unipolar brush cell synapses in rat cerebellum. *Neuroscience*

104, 1127–1139.

Mugnaini, E. (1970) Neurons as synaptic targets. In: Andersen, P. and Jansen, J.K.S (Eds.), *Excitatory Synaptic Mechanisms*. Universitets Forlaget 149-169

Mugnaini, E. (1972) The histology and cytology of the cerebellar cortex. In: Larsell, O. and Jansen, J. (Eds.), *The Comparative Anatomy and Histology of the Cerebellum: The Human Cerebellum, Cerebellar Connections, and Cerebellar Cortex*. The University of Minnesota Press 210-264.

Mugnaini, E., and Floris, A. (1994). The unipolar brush cell: a neglected neuron of the mammalian cerebellar cortex. *J. Comp. Neurol.* 339, 174–180.

Mugnaini, E., Diño, M.R., and Jaarsma, D. (1997). The unipolar brush cells of the mammalian cerebellum and cochlear nucleus: cytology and microcircuitry. *Prog. Brain Res.* 114, 131–150.

Mugnaini, E., Floris, A., and Wright-Goss, M. (1994). Extraordinary synapses of the unipolar brush cell: an electron microscopic study in the rat cerebellum. *Synapse* 16, 284–311.

Mugnaini, E., Osen, K.K., Dahl, A.L., Friedrich, V.L., and Korte, G. (1980). Fine structure of granule cells and related interneurons (termed Golgi cells) in the cochlear nuclear complex of cat, rat and mouse. *J. Neurocytol.* 9, 537–570.

Mugnaini, E., Sekerková, G., and Martina, M. (2011). The unipolar brush cell: a remarkable neuron finally receiving deserved attention. *Brain Res Rev* 66, 220–245.

- Müller, A., Kukley M., Stausberg P., Beck H., Müller W. and Dietrich D. (2005). Endogenous Ca²⁺ Buffer Concentration and Ca²⁺ Microdomains in Hippocampal Neurons. *J. Neurosci.* 25, 558–565
- Nakamura, M., Sato, K., Fukaya, M., Araishi, K., Aiba, A., Kano, M., and Watanabe, M. (2004). Signaling complex formation of phospholipase C β 4 with metabotropic glutamate receptor type 1 α and 1,4,5-trisphosphate receptor at the perisynapse and endoplasmic reticulum in the mouse brain. *Eur. J. Neurosci.* 20, 2929–2944.
- Nawy, S., and Jahr, C.E. (1990a). Suppression by glutamate of cGMP-activated conductance in retinal bipolar cells. *Nature* 346, 269–271.
- Nawy, S., and Jahr, C.E. (1990b). Time-dependent reduction of glutamate current in retinal bipolar cells. *Neurosci. Lett.* 108, 279–283.
- Neuhoff, H., Neu, A., Liss, B., and Roeper, J. (2002). I(h) channels contribute to the different functional properties of identified dopaminergic subpopulations in the midbrain. *J. Neurosci.* 22, 1290–1302.
- Nielsen, T.A., DiGregorio, D.A., and Silver, R.A. (2004). Modulation of glutamate mobility reveals the mechanism underlying slow-rising AMPAR EPSCs and the diffusion coefficient in the synaptic cleft. *Neuron* 42, 757–771.
- Nunzi, M.G., and Mugnaini, E. (2000). Unipolar brush cell axons form a large system of intrinsic mossy fibers in the postnatal vestibulocerebellum. *J. Comp. Neurol.* 422, 55–65.
- Nunzi, M.G., Birnstiel, S., Bhattacharyya, B.J., Slater, N.T., and Mugnaini, E. (2001).

Unipolar brush cells form a glutamatergic projection system within the mouse cerebellar cortex. *J. Comp. Neurol.* *434*, 329–341.

Nunzi, M.-G., Shigemoto, R., and Mugnaini, E. (2002). Differential expression of calretinin and metabotropic glutamate receptor mGluR1alpha defines subsets of unipolar brush cells in mouse cerebellum. *J. Comp. Neurol.* *451*, 189–199.

Oertel, D., and Young, E.D. (2004). What's a cerebellar circuit doing in the auditory system? *Trends Neurosci.* *27*, 104–110.

Ohishi, H., Neki, A., and Mizuno, N. (1998). Distribution of a metabotropic glutamate receptor, mGluR2, in the central nervous system of the rat and mouse: an immunohistochemical study with a monoclonal antibody. *Neurosci. Res.* *30*, 65–82.

Overstreet, L.S., Kinney, G.A., Liu, Y.B., Billups, D., and Slater, N.T. (1999). Glutamate transporters contribute to the time course of synaptic transmission in cerebellar granule cells. *J. Neurosci.* *19*, 9663–9673.

Perkins, K.L. (2006). Cell-attached voltage-clamp and current-clamp recording and stimulation techniques in brain slices. *J. Neurosci. Methods* *154*, 1–18.

Petralia, R.S., Rubio, M.E., Wang, Y.X., and Wenthold, R.J. (2000). Differential distribution of glutamate receptors in the cochlear nuclei. *Hear. Res.* *147*, 59–69.

Puopolo, M., Bean, B.P., and Raviola, E. (2005). Spontaneous activity of isolated dopaminergic periglomerular cells of the main olfactory bulb. *J. Neurophysiol.* *94*, 3618–3627.

- Raman, I.M., and Bean, B.P. (1999). Ionic currents underlying spontaneous action potentials in isolated cerebellar Purkinje neurons. *J. Neurosci.* *19*, 1663–1674.
- Raman, I.M., and Trussell, L.O. (1992). The kinetics of the response to glutamate and kainate in neurons of the avian cochlear nucleus. *Neuron* *9*, 173–186.
- Raman, I.M., Gustafson, A.E., and Padgett, D. (2000). Ionic currents and spontaneous firing in neurons isolated from the cerebellar nuclei. *J. Neurosci.* *20*, 9004–9016.
- Rancz, E.A., Ishikawa, T., Duguid, I., Chadderton, P., Mahon, S., and Häusser, M. (2007). High-fidelity transmission of sensory information by single cerebellar mossy fibre boutons. *Nature* *450*, 1245–1248.
- Ritzau-Jost, A., Delvendahl, I., Rings, A., Byczkowicz, N., Harada, H., Shigemoto, R., Hirrlinger, J., Eilers, J., and Hallermann, S. (2014). Ultrafast Action Potentials Mediate Kilohertz Signaling at a Central Synapse. *Neuron* *84*, 152–163.
- Roberts, P.D., and Portfors, C.V. (2008). Design principles of sensory processing in cerebellum-like structures. Early stage processing of electrosensory and auditory objects. *Biol Cybern* *98*, 491–507.
- Rossi, D.J., Alford, S., Mugnaini, E., and Slater, N.T. (1995). Properties of transmission at a giant glutamatergic synapse in cerebellum: the mossy fiber-unipolar brush cell synapse. *J. Neurophysiol.* *74*, 24–42.
- Rousseau, C.V., Dugué, G.P., Dumoulin, A., Mugnaini, E., Dieudonné, S., and Diana, M.A. (2012). Mixed inhibitory synaptic balance correlates with glutamatergic synaptic

phenotype in cerebellar unipolar brush cells. *J. Neurosci.* *32*, 4632–4644.

Ruigrok, T.J.H., Hensbroek, R.A., and Simpson, J.I. (2011). Spontaneous activity signatures of morphologically identified interneurons in the vestibulocerebellum. *J. Neurosci.* *31*, 712–724.

Russo, M.J., Mugnaini, E., and Martina, M. (2007). Intrinsic properties and mechanisms of spontaneous firing in mouse cerebellar unipolar brush cells. *J. Physiol. (Lond.)* *581*, 709–724.

Russo, M.J., Yau, H.-J., Nunzi, M.-G., Mugnaini, E., and Martina, M. (2008). Dynamic metabotropic control of intrinsic firing in cerebellar unipolar brush cells. *J. Neurophysiol.* *100*, 3351–3360.

Safo, P., and Regehr, W.G. (2008). Timing dependence of the induction of cerebellar LTD. *Neuropharmacology* *54*, 213–218.

Sargent, P.B., Saviane, C., Nielsen, T.A., DiGregorio, D.A., and Silver, R.A. (2005). Rapid vesicular release, quantal variability, and spillover contribute to the precision and reliability of transmission at a glomerular synapse. *J. Neurosci.* *25*, 8173–8187.

Sasaki, T., and Kaneko, A. (1996). L-Glutamate-induced responses in OFF-type bipolar cells of the cat retina. *Vision Res.* *36*, 787–795.

Sawtell, N.B. (2010). Multimodal integration in granule cells as a basis for associative plasticity and sensory prediction in a cerebellum-like circuit. *Neuron* *66*, 573–584.

Schwartz, E.J., Rothman, J.S., Dugué, G.P., Diana, M., Rousseau, C., Silver, R.A., and

- Dieudonné, S. (2012). NMDA receptors with incomplete Mg^{2+} block enable low-frequency transmission through the cerebellar cortex. *J. Neurosci.* 32, 6878–6893.
- Sekerková, G., Ilijic, E., Mugnaini, E., and Baker, J.F. (2005). Otolith organ or semicircular canal stimulation induces c-fos expression in unipolar brush cells and granule cells of cat and squirrel monkey. *Exp Brain Res* 164, 286–300.
- Sekerková, G., Watanabe, M., Martina, M., and Mugnaini, E. (2014). Differential distribution of phospholipase C beta isoforms and diacylglycerol kinase-beta in rodent cerebella corroborates the division of unipolar brush cells into two major subtypes. *Brain Struct Funct* 219, 719–749.
- Semenov, A., Möykkynen, T., Coleman, S.K., Korpi, E.R., and Keinänen, K. (2012). Autoinactivation of the stargazin-AMPA receptor complex: subunit-dependency and independence from physical dissociation. *PLoS ONE* 7, e49282.
- Shiells, R.A., and Falk, G. (1990). Glutamate receptors of rod bipolar cells are linked to a cyclic GMP cascade via a G-protein. *Proc. Biol. Sci.* 242, 91–94.
- Shimazaki H. and Shinomoto S. (2007) A method for selecting the bin size of a time histogram. *Neural Comput* 19 1503–27
- Shore, S.E. (2005). Multisensory integration in the dorsal cochlear nucleus: unit responses to acoustic and trigeminal ganglion stimulation. *Eur. J. Neurosci.* 21, 3334–3348.
- Shore, S.E., and Moore, J.K. (1998). Sources of input to the cochlear granule cell region in the guinea pig. *Hear. Res.* 116, 33–42.

- Shore, S.E., Helfert, R.H., Bledsoe, S.C., Altschuler, R.A., and Godfrey, D.A. (1991). Descending projections to the dorsal and ventral divisions of the cochlear nucleus in guinea pig. *Hear. Res.* *52*, 255–268.
- Shore, S.E., Vass, Z., Wys, N.L., and Altschuler, R.A. (2000). Trigeminal ganglion innervates the auditory brainstem. *J. Comp. Neurol.* *419*, 271–285.
- Shore, S., Zhou, J., and Koehler, S. (2007). Neural mechanisms underlying somatic tinnitus. *Prog. Brain Res.* *166*, 107–123.
- Simpson, J.I., Hulscher, H.C., Sabel-Goedknecht, E., and Ruigrok, T.J.H. (2005). Between in and out: linking morphology and physiology of cerebellar cortical interneurons. *Prog. Brain Res.* *148*, 329–340.
- Slaughter, M.M., and Miller, R.F. (1983a). Bipolar cells in the mudpuppy retina use an excitatory amino acid neurotransmitter. *Nature* *303*, 537–538.
- Slaughter, M.M., and Miller, R.F. (1983b). An excitatory amino acid antagonist blocks cone input to sign-conserving second-order retinal neurons. *Science* *219*, 1230–1232.
- Spatz, W.B. (1999). Unipolar brush cells in the cochlear nuclei of a primate (*Callithrix jacchus*). *Neurosci. Lett.* *270*, 141–144.
- Spatz, W.B. (2000). Unipolar brush cells in marmoset cerebellum and cochlear nuclei express calbindin. *Neuroreport* *11*, 1–4.
- Spatz, W.B. (2001). Unipolar brush cells in the human cochlear nuclei identified by their expression of a metabotropic glutamate receptor (mGluR2/3). *Neurosci. Lett.* *316*, 161–

164.

Subramaniam S., Solinas S., Perin P., Locatelli F., Masetto S. and D'Angelo E (2014). Computational modeling predicts the ionic mechanism of late-onset responses in unipolar brush cells. *Front Cell Neurosci* **8**:237. doi: 10.3389/fncel.2014.00237

Taddese, A., and Bean, B.P. (2002). Subthreshold sodium current from rapidly inactivating sodium channels drives spontaneous firing of tuberomammillary neurons. *Neuron* **33**, 587–600.

Takács, J., Markova, L., Borostyánkői, Z., Görcs, T.J., and Hámori, J. (1999). Metabotropic glutamate receptor type 1a expressing unipolar brush cells in the cerebellar cortex of different species: a comparative quantitative study. *J. Neurosci. Res.* **55**, 733–748.

Toledano, A., Alvarez, M.-I., Monleón, E., Toledano-Díaz, A., Badiola, J.-J., and Monzón, M. (2012). Changes induced by natural scrapie in the calretinin-immunopositive cells and fibres of the sheep cerebellar cortex. *Cerebellum* **11**, 593–604.

Tzounopoulos, T., Kim, Y., Oertel, D., and Trussell, L.O. (2004). Cell-specific, spike timing-dependent plasticities in the dorsal cochlear nucleus. *Nat. Neurosci.* **7**, 719–725.

van Dorp, S., and De Zeeuw, C.I. (2014). Variable timing of synaptic transmission in cerebellar unipolar brush cells. *Proc. Natl. Acad. Sci. U.S.A.* **111**, 5403–5408.

Víg, J., Takács, J., Abrahám, H., Kovács, G.G., and Hámori, J. (2005). Calretinin-immunoreactive unipolar brush cells in the developing human cerebellum. *Int. J. Dev. Neurosci.* **23**, 723–729.

Wang, S.S., Denk, W., and Häusser, M. (2000). Coincidence detection in single dendritic spines mediated by calcium release. *Nat. Neurosci.* 3, 1266–1273.

Watanabe, D., Inokawa, H., Hashimoto, K., Suzuki, N., Kano, M., Shigemoto, R., Hirano, T., Toyama, K., Kaneko, S., Yokoi, M., et al. (1998). Ablation of cerebellar Golgi cells disrupts synaptic integration involving GABA inhibition and NMDA receptor activation in motor coordination. *Cell* 95, 17–27.

Watanabe, D., and Nakanishi, S. (2003). mGluR2 postsynaptically senses granule cell inputs at Golgi cell synapses. *Neuron* 39, 821–829.

Weedman, D.L., Pongstaporn, T., and Ryugo, D.K. (1996). Ultrastructural study of the granule cell domain of the cochlear nucleus in rats: mossy fiber endings and their targets. *J. Comp. Neurol.* 369, 345–360.

Williams, J.T., North, R.A., Shefner, S.A., Nishi, S., and Egan, T.M. (1984). Membrane properties of rat locus coeruleus neurones. *Neuroscience* 13, 137–156.

Wright, D.D., Blackstone, C.D., Haganir, R.L., and Ryugo, D.K. (1996). Immunocytochemical localization of the mGluR1 alpha metabotropic glutamate receptor in the dorsal cochlear nucleus. *J. Comp. Neurol.* 364, 729–745.

Xu-Friedman, M.A., and Regehr, W.G. (2003). Ultrastructural contributions to desensitization at cerebellar mossy fiber to granule cell synapses. *J. Neurosci.* 23, 2182–2192.

Yan, X.X., and Garey, L.J. (1996). Calretinin immunoreactivity in the monkey and cat

cerebellum: cellular localisation and modular distribution. *J Hirnforsch* 37, 409–419.

Young, E.D., Nelken, I., and Conley, R.A. (1995). Somatosensory effects on neurons in dorsal cochlear nucleus. *J. Neurophysiol.* 73, 743–765.

Zhou, J., and Shore, S. (2004). Projections from the trigeminal nuclear complex to the cochlear nuclei: a retrograde and anterograde tracing study in the guinea pig. *J. Neurosci. Res.* 78, 901–907.